

SLAC-PUB-1528
January 1975
(T/E)

ELECTRON SCATTERING AT 4° WITH
ENERGIES OF 4.5 - 20 GeV*

S. Stein,** W. B. Atwood, E. D. Bloom, R. L. A. Cottrell, H. DeStaebler,
C. L. Jordan,† H. G. Piel, †† C. Y. Prescott, R. Siemann,‡ R. E. Taylor

Stanford Linear Accelerator Center
Stanford University, Stanford, California 94305

ABSTRACT

This paper presents the results of the analysis of a single-arm inelastic electron scattering experiment at an angle of 4° . We present data on the turnon of scaling in the low q^2 region $0.1 < q^2 < 1.8$, the neutron-proton comparison at large values of the scaling variable, ω , resonance excitation, and the shadowing in scattering from heavy nuclei.

(Submitted to Phys. Rev.)

*Work supported by the U.S. Atomic Energy Commission.

**Present address: CERN, 1211 Geneva 23, Switzerland.

†Present address: I. Physikalisches Institut, RWTH Aachen, Aachen,
West Germany.

††Present address: University of Wuppertal, Hofkamp 82-84, Wuppertal,
West Germany.

‡ Present address: Cornell University, Ithaca, New York.

From the time of Rutherford's analysis of α particle scattering, the scattering of charged particles has provided a probe with which we are still learning about the structure of matter. The experimental observation¹ of large, almost point-like, cross sections in electron scattering has prompted much discussion of constituent models of the nucleon, notably the parton model. The prediction of Bjorken² regarding scaling behavior for nucleon structure functions was also approximately verified, and at rather small values of q^2 , the four momentum transfer. The present experiment, which measures electron scattering at an angle of 4° for various incident energies, was designed to investigate the structure functions νW_2 for the proton and neutron for values of q^2 smaller than those for which scaling has already been observed. In addition to this study of the turnon of scaling, the study of the ratio of neutron and proton scattering at large values of the scaling variable $\omega = 2M\nu/q^2$ is of interest.

Inelastic scattering can be considered as photoproduction by "off-mass-shell" photons. The total photoproduction cross section is connected in a simple way with the inelastic scattering of electrons in the limit $q^2 \rightarrow 0$. In the present experiment, data for values of q^2 from 0.1 to 1.8 (GeV/c)² provide some opportunities to study how photoproduction is modified as q^2 increases. An interesting example is the phenomenon of shadowing in electron-nucleus scattering which has been observed³ in real photoproduction but not yet⁴ in electroproduction. Data were taken with heavy targets at selected kinematic points, attempting to detect shadowing effects at lower values of q^2 .

The production of resonances is a prominent feature of the photoproduction total cross section at low energy. Previous experiments have shown prominent bumps corresponding to production of resonances in inelastic electron scattering. At 4°, counting rates are high and by adopting experimental techniques

designed to minimize systematic errors as the energy loss in the inelastic scattering varies, we can carefully study the already observed enhancements and look for heretofore unobserved structure in inelastic scattering.

This paper reports the results of the analysis of this experiment. In Section I we discuss the experimental apparatus; Section II, the data analysis procedures; Section III, some kinematics and definitions; and Section IV, the results of the experiment.

I. EXPERIMENTAL APPARATUS

This experiment was carried out at the Stanford Linear Accelerator Center in December of 1970 and March of 1971. Preliminary results were reported⁵ at the Electron-Photon Symposium held at Cornell in August of 1971.

A. Beam

The primary electron beam from the accelerator was used at energies of 4.5, 7, 10, 13, 16, 18, and 20 GeV. A momentum slit in the SLAC beam switchyard transport system defined the beam's energy spread to $\pm 0.1\%$ for almost all the running conditions. The absolute momentum calibration of the transport system was known to $\sim 0.1\%$ as defined by a flip coil in a duplicate magnet excited in series with the beam line bending magnets. The electron current was set to keep the rate of detected particles at an average of less than one per $1.6 \mu\text{sec}/\text{beam pulse}$ and varied from $3 \times 10^8 - 10^{11} \text{ e/pulse}$. The beam current was integrated using two nonintercepting toroid charge monitors⁶ which were intercalibrated with a Faraday cup and determined to have an accuracy better than 1%. The size of the beam at the target was typically 4 mm horizontally and 2 mm vertically, and the position and steering were checked by periodically inserting ZnS screens into the beam. After passing through the target, the beam was dumped outside the well-shielded experimental building.

B. Targets

During the experiment, we used a liquid hydrogen target, liquid deuterium target, and heavy targets of Be, Al, Cu, and Au. They were all mounted on a movable assembly, which enabled remote selection of the appropriate target.

Parameters for the various targets⁷ are given in Table I. The hydrogen and deuterium targets were vertical cylinders with 0.0076 cm aluminum walls.

The aluminum "empty" target was also constructed in a cylinder with walls six times thicker than the liquid target walls in order to achieve approximately the same target thickness in radiation lengths.⁸ The total amount of radiator for the targets is listed in Table II for reference.

C. Detector

The scattered electrons were detected in the SLAC 20-GeV spectrometer,⁹ shown in Figure 1, which was surveyed in place at a laboratory angle of 4.000 degrees. An electron first passes through the magnet transport system of the spectrometer, which disperses momentum in the vertical plane, and disperses the projected horizontal scattering angle in the horizontal plane. The first order optics are such that parallel rays from a horizontal line source are focused to a point. The detector arrangement in the hut of the spectrometer is shown in Figure 2. The particle traverses a Cerenkov counter (C) filled with nitrogen gas at atmospheric pressure, a scintillation counter TR1, five multiwire proportional chambers¹⁰ (three to measure the vertical position and two for the horizontal), two more scintillation counters (TR2 and TR3), three multiplicity counters (MULT) which sample the shower produced in one radiation length of lead, and a total absorption lead-lucite shower counter (TA). The event trigger was a coincidence between TR3 and TA (with a low discriminator threshold)

during the $1.6 \mu\text{sec}$ beam pulse. Counter and chamber dimensions are shown in Table III.

The vertical aperture of the spectrometer was restricted by slits which were set so as to pass particles with $\pm 4.25 \text{ mrad}$ in ϕ , the vertical projected scattering angle. Using the reconstructed tracks in the proportional chambers, we further restricted events to $\pm 3.5 \text{ mrad}$ in θ , the horizontal projected scattering angle, and to $\pm 1.6\%$ in $\Delta p/p$, the momentum acceptance of the spectrometer. Typical distributions for these quantities are shown in Fig. 3. These cuts on θ and $\Delta p/p$ are well within the full spectrometer aperture.

D. Data Acquisition

The data from each accelerator pulse was transmitted to an online SDS 9300 computer which sampled a fraction of the events and wrote all the events onto magnetic tape for subsequent offline analysis on the SLAC IBM 360/91 computer. The online electronics were designed to handle up to 3 events/pulse increasing our data acquisition rate appreciably and reducing corrections for lost events at high counting rates. Signals from each wire in the chambers were amplified and sent to the counting area on coaxial cables, where they were fed into CAMAC latches which could be sequentially gated up to three times before being read out. In addition, for up to 3 events in the pulse, we recorded the pulse heights in the Cerenkov counter, the three multiplicity counters, and the TA. Online histograms of these quantities as well as track reconstruction in the chambers, enabled us to monitor the performance of the hardware. The other quantities which would be needed to evaluate the cross section, such as charge and spectrometer momentum, were also written onto tape by the SDS 9300. In the two cycles of running, a total of 217 tapes were recorded. These were condensed offline yielding 108 tapes to be analyzed.

II. DATA ANALYSIS

The data taking was divided into two modes of running: discrete mode and scan mode. These were processed in a similar manner offline.

A. Discrete Mode

In this type of operation, the parameters for the run were entered, and data were taken at a single momentum setting. This procedure was followed for most of the structureless part of the data. In this region the spectrometer momentum was changed between runs by amounts much larger than the spectrometer's momentum bite. For each setting, the online computer set the currents in the magnets and recorded the quantities needed to calculate the cross section-scalers, charge monitors, magnet parameters, etc.

B. Scan Mode

In order to minimize the effect of nonuniform bin efficiencies that might exist in the wire chambers and which might cause erroneous bumps in the missing mass spectrum, we ran the spectrometer in the scan mode.¹¹ The computer automatically changed the spectrometer momentum setting by a small fraction of the momentum bite after a predetermined number of incident electrons had been obtained. Each momentum setting, called a mini-run, was analyzed offline as a separate run. By using this technique, each missing mass bin receives data averaged over all the wires, which also minimizes errors caused by any variation in the detector's solid angle. Since we were interested in looking for small or narrow bumps in the cross section, removing erroneous sources that might cause such effects was important. Typically, the momentum change per mini-run corresponded to one wire spacing or 0.07% in $\Delta p/p$, which is approximately the momentum resolution of the spectrometer. For

most scans, the number of events measured gave $\pm 2\%$ statistical error in bins that were $\approx 0.1\%$ of the incident energy.

C. Data Reduction

For each run, various cuts were applied to the data to select only events in which the detected particle was an electron. From all the runs, distributions of pulse height for the TA, MULT, and C counters were made. For the TA, the mean and standard deviation of the distribution were determined as a function of scattered energy, E' , and a cut placed for all the data at 3.5 standard deviations below the mean. This has an efficiency of 0.9998, assuming a Gaussian distribution for the low energy side of the data. Other reasonable assumptions about the spectrum shape that are consistent with the data also yield an efficiency of ≈ 1.0 with no appreciable systematic error. Sample TA distributions are shown in Fig. 4a for typical running conditions and 4b for one of the worst conditions.

The C counter was able to distinguish electrons from π 's when the momentum was less than 6 GeV/c. For all data below this energy, a cut was applied to the C pulse height that was 0.98 efficient for electrons. This efficiency was determined from runs where the TA cut alone was sufficient to eliminate almost all the π 's. Fig. 4b also shows the TA distribution with the C cut applied to eliminate the pion background.

For ten runs with the momentum between 6 and 10 GeV/c, the TA counter alone was inadequate to eliminate the pion background. For these runs, the multiplicity counter pulse height information was used to eliminate the remaining π 's. The efficiency of this cut depended on energy and was determined by looking at runs for which the TA and C counters were adequate. Fig. 5 shows the measured efficiency which varied from 0.945 at 6 GeV/c to 0.96 at 10 GeV/c.

Corrections were applied to the data for the C and MULT efficiencies. There were also electronics dead time counting rate corrections which were < 0.5%. During the data taking circuits were incorporated to measure this dead time and corrections were applied for it. In addition we made corrections for events lost due to computer dead time by comparing the number of events recorded on tape to the number seen by a fast hardware scaler. This varied from run to run and was about 0.5% on the average. There was also a correction for the proportional wire chamber's efficiency, which was about 95% averaged over the experiment.

The events were processed offline and a summary of each run and mini-run, including counter efficiencies, run parameters and cross sections, was written onto disk. There were approximately 10,000 runs and mini-runs recorded.

The data were divided into larger blocks, called lines, defined as containing all the runs (or mini-runs) with the same target and incident energy. These lines constitute the raw data spectra. A typical line is shown in Fig. 6.

The counts recorded in the hydrogen and deuterium running include target wall events which were subtracted using data from the dummy target. For all targets, some events arise from charge symmetric processes such as π^0 production, with subsequent conversion of the photon into $e^+ - e^-$ pairs. In order to obtain the cross section for only the scattered e^- events, measurements were taken with the spectrometer set to detect e^+ and the cross section from these runs was subtracted from the corresponding e^- run. This affects only the very low energy ends of the lines. Fig. 7 shows the worst case of such a subtraction on hydrogen. After these corrections were made, the data were ready for radiative corrections.

D. Radiative Corrections for Hydrogen

1. Elastic Tail

One of the processes contributing to the inelastic yield is the radiative tail from elastic scattering. We calculated the elastic tail cross section following the procedure given in the thesis of G. Miller.¹² Details of the calculations are given in Appendix I. The energy of the incident beam was used as an adjustable parameter in this calculation to match the theoretical tail with the data between the elastic peak and one-pion threshold. There was one adjustment for each line of data taken. In all cases the amount of change to the incident energy was less than 0.1%, which is smaller than the estimated error due to the energy defining slits in the accelerator. An example of the agreement between theory and experiment is shown in Fig. 8. This calculated elastic tail cross section was then subtracted from each point on the line and the resulting cross sections recorded to be used as input for the remaining radiative corrections. The errors were propagated as though there were no error on the calculated tail. The subtraction was as much as 50% for the lowest E' point on each line. We estimate the systematic error in the calculated tail as $\pm 5\%$, which contributes an error of 5% to the subtracted cross sections for the worst case. For most of the data the error in the subtracted cross section is much smaller than this figure.

2. Inelastic Corrections

To calculate the inelastic radiative corrections for a measured cross section at incident energy E_0 and scattered energy E' , a knowledge of the cross sections for all lower values of E_0 and for all higher values of E' is required. Since only some of these are measured experimentally, the usual procedure¹³ has been to use the measured points and interpolate in order to determine the

cross section for any desired value of (E_0, E') . Numerous interpolations make it difficult to assign errors to the final values of cross sections as this procedure tends to mix systematic and statistical errors and to correlate the errors among the data points. Further, using the peaking approximation (see Appendix I), the separation of the two-dimensional integral into two one-dimensional integrals plus one single function makes the errors depend somewhat upon the choice of an arbitrary parameter, ΔE , used to split the integration region.

In this paper we have adopted a new approach to the radiative corrections which is briefly described here. Cross sections obtained by applying the radiative corrections procedure of Mo and Tsai¹³ are represented by an approximate expression containing 30 parameters. Using this fit and the formulae of ref. 13 and Appendix I, we calculated a ratio of cross sections with and without radiative corrections. Each measured cross section was then corrected by this ratio. The statistical errors are obtained by multiplying the uncorrected data errors by the same ratio. The newly corrected data were then refitted and the process iterated to obtain the final answers. The use of a smooth model eliminates the spurious amplifications of point-to-point statistical fluctuations in the data. We estimate a possible systematic uncertainty in the corrected data varying from $\pm 3\%$ near inelastic threshold to $\pm 5\%$ at the low E' end of the lines. A major contribution to this estimate arises from uncertainties in the calculations of the multiple photon emission.

E. Radiative Corrections for Deuterium and Higher Z Targets

Three radiative processes contributing to the observed cross section for heavy targets are: the radiative tail from elastic nucleus scattering, tails from quasi-elastic electron nucleon scattering and processes in the inelastic continuum.

1. Elastic Tail

The elastic form factor is a rapid function of q^2 , so this process affects mainly the very low E' region of each line where hard photons can be radiated yielding an effective q^2 ($\approx 4 E'^2 \sin^2 \theta/2$, for small angles) that is small. The formulae used for the elastic radiative tail are the same as those for hydrogen, with the structure functions replaced by their counterpart for each target (see Appendix I). We caution that the one-photon exchange approximation has been used and the corrected cross section for the high Z elements is suspect where the calculated elastic tails are large.

2. Quasi-elastic Tail

For most of the data, a larger contribution to the observed cross section is that from the quasi-elastic tail. This tail arises from elastic scattering from individual nucleons in the nucleus. To account for the bound nature of the nucleons we have used the technique suggested by Atwood and West.¹⁴ The exact formulae will be found in Appendix I. An example of this calculation is shown in Fig. 9, which shows the observed scattering cross section for the deuterium data at 4.5 GeV and the calculated quasi-elastic and elastic peaks with radiative effects and resolution included.

One modification must be made to the impulse approximation calculation when the quasi-elastic cross section is calculated for the low q^2 data. As is known from low energy electron-deuteron scattering,¹⁵ the inelastic cross sections are suppressed from their simple incoherent sum due to the probability of coherent, i. e., elastic, scattering. This introduces a factor $(1 - F_{el}^2(q^2))$ into the quasi-elastic electric form factor, where $F_{el}(q^2)$ is the nuclear elastic form factor. For the lowest energy line at q^2 of $0.1(\text{GeV}/c)^2$, this is a 15% correction to the quasi-elastic peak on deuterium.

These elastic and quasi-elastic tails were calculated as described in Appendix I and subtracted from the data. The inelastic radiative correction for deuterium was performed as for hydrogen. No inelastic radiative corrections were made on the nuclei heavier than deuterium.

For all the hydrogen and deuterium data, the final cross sections are shown in Fig. 10 for values of W up to 3 GeV and a complete table may be found in SLAC-PUB-1528 (1975), which is available from the authors of this paper. Fig. 11 displays the $q^2-\nu$ kinematic plane and shows the region covered by this experiment.

F. Errors

The cross sections in Appendix II are shown with statistical errors only except for the ten values of E' at which the multiplicity counters were used for electron identification. For these runs, we have included a measure of their relative systematic error by adding 1% linearly to the statistical error.

For almost all the data, the systematic errors are greater than the statistical errors. We consider the following sources of systematic error:

- 1) Number of target nuclei - for each run and mini-run and approximately every minute in the long runs, we recorded the liquid target temperatures using four hydrogen vapor pressure thermometers. Measurements were taken both above and below the target volume on both hydrogen and deuterium. The results for the four values of pressure are shown as the first line in Table IV. The largest contribution to the errors in these pressures are from the absolute calibration of the digital voltmeter and reference voltage source. This pressure is then converted to temperature¹⁶ with negligible additional error (< .1%). The density is calculated for each of the four values of temperature,¹⁷ which adds an error of $\pm 0.1\%$ for hydrogen and $\pm 0.6\%$ for deuterium to the propagated error from the vapor pressures. A systematic error was assigned

to the target density, based on the overall spread of the observed temperature distributions. Combining these results with the measurement of the target lengths and its error yields a systematic uncertainty in the average target density of $\pm 0.94\%$ for hydrogen and $\pm 1.26\%$ for deuterium.

2) Number of electrons - the estimated systematic error in the toroid charge monitor is $\pm 1\%$. Both the toroids were calibrated using pulsers to simulate the beam by discharging capacitors through single turns on the toroid cores.⁶ The stability of these calibrations was checked frequently during the data taking. In addition the toroids were compared against a Faraday cup. Consideration of the results of these various calibrations plus estimates of the expected levels of absolute accuracy leads us to assign $\pm 1\%$ as the estimated systematic error in the incident beam charge.

3) Solid angle - optics measurements made on the 20-GeV spectrometer in 1967 and 1968 yield an estimate of the systematic error of $\pm 2\%$ for the solid angle. We reanalyzed the optics measurements, taking account of the restricted aperture and small effective transverse target size appropriate to this experiment. In addition, for this experiment, we made checks on the optics coefficients used in reconstructing events by changing the cuts on ϕ (the vertical projected scattering angle), θ (the horizontal projected scattering angle), and $\Delta p/p$. The cross section shows no variation outside of statistical errors. We also looked at the cross sections for a given E' as the spectrometer momentum was changed during the scanning procedure; the distributions are also consistent with statistical errors. Based on these studies, we estimate $\pm 2\%$ as the systematic error in solid angle.

4) Track reconstruction efficiency - each event with a signal from TR1 should have a reconstructed track hitting both TR1 and TR3. The track

reconstruction efficiency was calculated, run (mini-run) by run (mini-run), by comparing the number of events with reconstructed tracks hitting the counters TR1 and TR3 (taking into account the measurement resolution) to the number of events with a signal from TR1. The average for all runs was 95%. This includes the intrinsic wire chamber inefficiency and effects of multiple tracks. The FWHM of the distribution of the efficiencies is 2%, and we estimate the systematic error as $\pm 1\%$ from this source.

In Table V we summarize these sources of systematic error. Combining in quadrature yields an overall uncertainty of $\pm 2.62\%$ in hydrogen and $\pm 2.75\%$ for deuterium. In ratios of deuterium to hydrogen, the overall uncertainty is estimated to be only $\pm 1.57\%$, since some of the above-mentioned errors cancel.

Systematic errors also arise from the corrections made for radiative processes. For the hydrogen cross sections errors arise in subtracting the elastic scattering tail and in the inelastic continuum corrections. The error on the elastic tail is estimated to be $\pm 5\%$; this results in an error of $\lesssim \pm 1\%$ for $E' > 5$ GeV growing to $\pm 5\%$ at our lowest value of $E' = 2.6$ GeV. Over most of the range of the hydrogen data the error in the cross section from the inelastic radiative corrections is $\pm 3\%$. The error from this source is estimated to increase to $\pm 5\%$ for $W \geq 5$ GeV.

For deuterium cross sections three radiative processes contribute (see Sec. E) but only two of these processes contribute significant errors to the final cross sections, since the elastic scattering falls off rapidly even for small values of q^2 . The calculation of the quasi-elastic scattering tails depends on knowledge of both the proton and neutron form factors. The latter are not known as well as those for the proton, so the error on the quasi-elastic tail is estimated to be $\pm 7.5\%$, somewhat larger than for the hydrogen case. This

error in the tail results in an error in the final deuterium cross sections of $\lesssim \pm 1.5\%$ for $E' \geq 5$ GeV growing to $\pm 7.5\%$ at $E' = 2.6$ GeV. The error arising from inelastic corrections is assumed to be the same as in the case of hydrogen.

In the ratio of D/H, errors from radiative corrections tend to cancel, but the uncertainty in the neutron form factors generates some uncertainty in the relative values of the quasi-elastic tail in deuteron when compared with the elastic tail in hydrogen. We estimate that an error of $\pm 5\%$ might persist in the deuteron quasi-elastic tail calculation. For our final n/p ratio this leads to an estimated error due to radiative corrections of $\lesssim \pm 1\%$ for $E' \gtrsim 5$ GeV growing to $\pm 5\%$ at $E' = 2.6$ GeV.

The above estimates of systematic error due to radiative corrections should be combined with the other sources of systematic errors enumerated in Table V.

G. Deuterium Analysis

1. Extraction of Neutron Information

The scattering from deuterium is approximately the sum of scattering from the proton and the neutron. Our purpose in measuring deuterium cross sections was to learn about the neutron, so the contribution from the proton must be accounted for. We have used the same formalism (Atwood and West)¹⁴ as for the quasi-elastic scattering to calculate the cross section for the proton in the deuteron, the "smeared" cross section.

We first fitted all the hydrogen data to the same function as used in the radiative correction procedure. This model, σ_H^M , is used to perform the smearing integral¹⁴ and gives us σ_H^{MS} , the smeared model, from which we calculate the smearing ratio σ_H^M/σ_H^{MS} . In Fig. 12 we plot these ratios as a function of

W for the different lines of data. Since we will restrict the analysis to values of $W > 2$ GeV, this correction is small, $\lesssim 2\%$. Using the smearing ratio we calculate a smeared proton cross section as $\sigma_P^S = \sigma_H^M / (\sigma_H^M / \sigma_H^{MS})$ where σ_H is the experimentally measured hydrogen cross section. Subtraction yields the smeared neutron cross section:

$$\sigma_N^S = \sigma_D - \sigma_P^S.$$

Since the smearing correction is small, we assign no additional systematic error to the neutron data and just consider the deuterium and hydrogen errors.

2. Glauber Correction

Based upon the strength of the electromagnetic interaction, the mean free path of a photon in nuclear matter is quite large. However, theories like vector meson dominance have predicted¹⁸ that shadowing in electron scattering should occur and that a correction for this effect would have to be made. Since experimental measurements of the scattering on heavy nuclei by electrons show no significant shadowing (see ref. 4 and Sec. IV.F) we have made no Glauber corrections to our deuterium data.

III. KINEMATICS AND DEFINITIONS

Let us consider the process shown in Fig. 13. An electron of energy E_0 in the laboratory is incident upon a nucleon of mass M . We assume that one photon exchange is adequate for describing this process. The momentum (energy) E' and angle θ of the scattered electron are measured, completely defining the virtual photon. We then define:

$$q^2 = 4E_0 E' \sin^2 \theta/2$$

$$\nu = E_0 - E'$$

$$W^2 = M^2 + 2M\nu - q^2$$

W is the missing mass, or effective mass, of the unobserved particles produced in the reaction. In terms of these, two common scaling variables¹⁹ are:

$$\omega = 1/x = 2M\nu/q^2$$

$$\omega' = 1/x' = (2M\nu + M^2)/q^2 = 1 + W^2/q^2$$

The cross section can be written as:

$$\frac{d^2\sigma}{d\Omega dE'} = \frac{\alpha^2 \cos^2 \theta/2}{4E_0^2 \sin^4 \theta/2} \left[W_2(q^2, \nu) + 2 \tan^2 \theta/2 W_1(q^2, \nu) \right]$$

where α is the fine structure constant $\alpha = 1/137.036$.

The structure functions W_1 and W_2 are functions of the Lorentz invariants, q^2 and ν . This form for the cross section is valid for one photon exchange and for an unpolarized beam and target²⁰ assuming conservation of parity, Lorentz and gauge invariance. Because the photon is virtual, it can have both longitudinal and transverse polarizations. The value of the polarization parameter, ϵ , is defined as follows:

$$\epsilon = \left[1 + 2 \tan^2 \theta/2 (1 + \nu^2/q^2) \right]^{-1}$$

In analogy with photoproduction, we can also write the cross section in the form:²¹

$$\frac{d^2\sigma}{d\Omega dE'} = \Gamma_T(\sigma_T + \epsilon \sigma_L)$$

where the "flux" of virtual photons is given by:

$$\Gamma_T = \frac{\alpha}{2\pi^2} \frac{K}{q^2} \frac{E'}{E_0} \frac{1}{1-\epsilon}, \quad K = \frac{W^2 - M^2}{2M}$$

K is the photon energy needed to produce the mass W in photoproduction. The transverse and longitudinal cross sections, σ_T and σ_L , are related to W_1 and W_2 by

$$W_1 = \frac{K}{4\pi^2 \alpha} \sigma_T$$

$$W_2 = \frac{K}{4\pi^2 \alpha} \frac{q^2}{q^2 + \nu^2} (\sigma_T + \sigma_L)$$

and have the limiting property,

$$\lim_{q^2 \rightarrow 0} \sigma_T(q^2, \nu) = \sigma_{\gamma p}(K), \quad \lim_{q^2 \rightarrow 0} \sigma_L(q^2, \nu) = 0.$$

We define the variable $R = \sigma_L/\sigma_T$, and write the relation between W_1 and W_2 as:

$$\frac{W_2}{W_1} = \frac{1+R}{1+\nu^2/q^2}$$

The relative contribution to the measured cross section of W_1 and W_2 is then given by

$$\frac{2W_1 \tan^2 \theta/2}{W_2} = \frac{2 \tan^2 \theta/2 (1 + \nu^2/q^2)}{1+R} = \frac{1-\epsilon}{\epsilon(1+R)}$$

For most of the kinematic range covered by this experiment, the W_1 contribution to the cross section is considerably smaller than that of W_2 .

IV. RESULTS

A. Elastic Electron-Proton Scattering

The elastic scattering cross section was determined for each of the seven incident energies. An example of the data at one of the energies is shown in Fig. 14. We have plotted the measured cross section, $d^2\sigma/d\Omega dE'$ versus the "missing energy", calculated as follows. For each event, the energy of an elastically scattered electron is calculated corresponding to the measured scattering angle. Then, the measured energy is subtracted from this quantity.

Thus, elastic scattering corresponds to missing energy of zero. The width of the raw data peak is due to instrumental resolution and radiative processes. Using the formulas from ref. 12, we have corrected the data for soft-photon radiation. This unfolded spectrum is also shown in the figure. The remaining width is due to resolution and has as its main contribution the FWHM of the incident beam, which corresponds to 24 MeV in missing energy in this example. The instrumental resolutions in the spectrometer of $\pm 0.07\%$ in $\Delta p/p$ and ± 0.05 mrad in θ are negligible when added in quadrature. We determined the total cross section by integrating over the scattered electron's energy. The results for $d\sigma/d\Omega$ for each of the energies are listed in Table VI, along with the corresponding values of q^2 and the errors of each measurement.

In order to compare these measurements with other experiments, we have calculated the expected 4° cross sections using data²² in the range of q^2 from 0 to 2 $(\text{GeV}/c)^2$ for which more than one angle has been measured at each q^2 . In Fig. 15, we plot as a function of $\sqrt{q^2}$ our data and the extrapolated data from other experiments, both divided by the dipole calculation. We conclude that our data agree with the other available measurements within our systematic errors.

B. Neutron-Proton Comparison

Previous results²⁴ have shown that the deuteron exhibits scaling behavior similar to that of the proton. The neutron structure function is quite different from that of the proton at large x' . Previously published electroproduction data have not covered the very low x' region in detail and in this experiment we are able to extend into this region for small values of q^2 . Using the method described in Sec. II. G, we extract the smeared neutron cross section σ_N^S . We present results in terms of σ_N^S/σ_P^S . This quantity is essentially the same as

σ_N/σ_P for our data, since the smearing ratios for the proton and neutron are small and the effects of this correction tend to cancel in the ratio.

We first look at the quantity $\sigma_D^S/\sigma_P^S = 1 + \sigma_N^S/\sigma_P^S$ as a function of q^2 for different regions of x' . Plots of this quantity are shown in Fig. 16. We see that "scaling" of σ_D^S/σ_P^S (that is, no dependence upon q^2) begins at low values of q^2 . Using the "closure approximation" to take into account the nuclear elastic scattering (see ref. 15 and Appendix II) suggests a q^2 variation in the cross section of the form $\sigma_D^S \propto 1 - |F_D(q^2)|^2$ where F_D is the deuteron elastic form factor.²⁵ For the lower x' bins, where the data extend to low q^2 , there is a variation consistent with this behavior. We fitted the ratio σ_D^S/σ_P^S for each x' bin to the form $A(1 - |F_D(q^2)|^2)$ and these fits are shown on the graphs. We point out that only data for $W > 2.1$ GeV have been used in these fits to avoid the resonance region. From each of these fits, we have extracted a value of A and its error and listed the quantities (A-1) in Table VII. These values represent the neutron-proton ratio σ_N^S/σ_P^S for each bin, since, except for the two lowest ranges of x' , A is essentially the average of the measurements in that bin. These two values for the two lowest ranges of x' are obtained from extrapolation into the scaling region from data measured at $q^2 \leq 0.75(\text{GeV}/c)^2$. These extracted values for σ_N^S/σ_P^S are plotted in Fig. 17 along with results from larger angles.^{24,26} The differences in σ_N^S/σ_P^S between the three experiments correspond to $\approx 3\%$ differences in the σ_D^S/σ_H^S measurements and are comparable with the estimated systematic errors in the three experiments. Assuming that $R = \sigma_L/\sigma_T$ is the same for the neutron and proton, then for large ω' (where the smearing ratio is near unity)

$$\frac{\sigma_D^S}{\sigma_P^S} - 1 = \frac{\sigma_N^S}{\sigma_P^S} = \frac{W_{2N}^S}{W_{2P}^S} = \frac{W_{2N}}{W_{2P}}$$

It is expected that purely diffractive processes should dominate as $\omega' \rightarrow \infty$ so that σ_N/σ_P should approach 1. In these data the ratio obtained from the two extrapolated points at lowest x' are consistent with 1. It is of some interest that the ratio is significantly below 1 for $x' \gtrsim 0.05$ ($\omega' \sim 20$). Recall that there is an estimated uncertainty of $\pm 1.57\%$ in σ_D/σ_H which becomes $\sim 3\%$ in σ_N/σ_P . Systematic errors from the radiative corrections tend to cancel in this ratio and have an appreciable effect in only the two lowest ranges of x' . These two points are in a kinematic region where there are no measurements of A dependence (see Sec. IVF) and further uncertainty can arise from our neglect of shadowing corrections.

C. νW_2 for the Proton and the Approach to Scaling

The experimental observation of scaling of the structure function νW_2 has been observed¹ for some region of q^2 and W . The original scaling variable of Bjorken, ω , has been supplemented by several others to extend the range of kinematic variables where scaling works. We use the variable $\omega' = 1 + W^2/q^2$ where $\nu W_2(\omega')$ has previously been shown to exhibit scaling behavior for values of $q^2 \geq 2(\text{GeV}/c)^2$ and outside the resonance region of $W \geq 2$ GeV. Since W_2 vanishes at $q^2 = 0$, it is an interesting question to see how νW_2 approaches its scaling behavior. In Fig. 18 we show νW_2 versus q^2 for $\omega' > 6$. Only data for $W > 2$ GeV are used, and we have assumed $R = \sigma_L/\sigma_T = 0.18$. As stated earlier, the largest effect due to uncertainties in R occurs for the largest ω' values (lowest q^2). These data suggest that the turnon to scaling depends mostly on q^2 . Vector meson dominance is expected to apply for large values of ω' (small values of q^2 in this experiment) and in this region will predict that νW_2 depends mainly on q^2 .

By analogy with the situation in deuterium where the inelastic cross section is suppressed by the coherent nuclear elastic scattering, we parametrize the inelastic structure function, W_2 , for the proton as a product:

$$\nu W_{2P}(q^2, \nu) = [1 - W_2^{el}(q^2)] F_{2P}(\omega')$$

where $F_{2P}(\omega')$ is the scaling limit structure function and

$$W_2^{el}(q^2) = \frac{G_E^2(q^2) + \tau G_M^2(q^2)}{1 + \tau} ; \quad \tau = q^2/4M^2$$

is the counterpart of W_2 for elastic scattering (see Appendix III), where G_E and G_M are, respectively, the elastic electric and magnetic form factors for the proton. This form satisfies the constraint that W_2 vanish at $q^2 = 0$. Integrating W_{2P} over all values of ν yields:

$$\int_{inelastic} d\nu W_{2P}(q^2, \nu) = [1 - W_2^{el}(q^2)] \int_{inelastic} \frac{d\nu}{\nu} F_{2P}(\omega')$$

But this is the Gottfried sum rule²⁷ for the proton, where

$$\int_{inelastic} \frac{d\nu}{\nu} F_{2P}(\omega') = \sum_i q_i^2$$

is the sum of the parton charges squared.

In order to examine the factorization parametrization, we have separated the data into equal bins of ω' and included some earlier measurements²⁴ at 6° and 10°. The data in each bin are plotted as a function of q^2 in Fig. 19. The curves shown are fits to:

$$\nu W_{2P}(q^2, \text{fixed } \omega') = D(\omega') [1 - W_2^{el}(q^2)]$$

where D was determined for each bin of ω' separately. The values of D with the errors from the fit and an estimate of the systematic errors are listed in Table VIII. Thus we see that the turnon to scaling is adequately accounted for

by the factorization parametrization. Using the results of the fits for each ω' bin we estimate the values of $F_{2P}(\omega')$ for larger values of ω' than previously available. In Fig. 20 we have plotted νW_{2P} vs ω' obtained this way. The region at low $\omega' < 5$ is obtained from a larger angle experiment.¹² The values obtained from the various fits in the present experiment are shown starting at $\omega' = 8$. We should point out that for $\omega' > 32$ the results of the fit will depend upon the factorization parametrization more and more strongly as ω' gets larger, since the range of q^2 for the data gets quite limited. We can then refit both the small and large ω' regions to the form

$$F_{2P}(\omega') = \sum_{n=3}^7 a_n (1 - 1/\omega')^n$$

and obtain the values

$$\begin{aligned} a_3 &= 1.0621 \\ a_4 &= -2.2594 \\ a_5 &= 10.5400 \\ a_6 &= -15.8277 \\ a_7 &= 6.7931 \end{aligned}$$

with $F_{2P}(\infty) = 0.308$. We emphasize that the systematic uncertainties may be as large as 20% by the highest ω' bin, so the results for these parameters must be used with caution.

D. Resonances in Electron-Proton Scattering

Perhaps the most obvious feature of the data in this range of q^2 is the production of the nucleon resonances (see Fig. 10a). There are four enhancements in the scattering cross sections which will be referred to as the first, second, third, and fourth resonance regions. If we look at results from photoproduction,²⁸ we know that these regions, except for the first, contain several resonances each.

There is no obvious evidence of enhancements above $W = 2$ GeV. We have fitted the data between $W = 2$ and 3 GeV to quadratics in W for each of five energies. Fig. 21 shows the residuals of the fits. These data are consistent with no enhancements. At an incident energy of 13 GeV, a resonance with a strength of 3% of the first resonance and a similar width would be easily observed in the graph of the residuals. The sensitivity decreases rapidly with increasing q^2 .

To study the four prominent enhancements between $W = 1.07$ GeV and 2 GeV, we have adopted the following procedure. The measured cross sections were first converted to a virtual photo absorption cross section

$$\sigma_{\text{tot}}(q^2, W) = \frac{1}{\Gamma_T} \frac{d^2\sigma}{d\Omega dE} = \sigma_T + \epsilon \sigma_L = \sigma_R(q^2, W) + \sigma_{\text{BKD}}(q^2, W)$$

where σ_R and σ_{BKD} are the resonance and background contributions to the cross sections. In order to remove some of the known kinematic variations, we write the structure function νW_2 as

$$\nu W_2(q^2, W) = \left[1 - W_2^{el}(q^2) \right] F_2(\omega') \cdot B(q^2, W) \left[4\pi^2 \alpha F_2(\infty) \lim_{q^2 \rightarrow 0} \left(\frac{1 - W_2^{el}(q^2)}{q^2} \right) \right]^{-1}$$

where the term in the braces is included so that

$$\lim_{q^2 \rightarrow 0} B(q^2, W) = \sigma_{\gamma p}(W)$$

and $\sigma_{\gamma p}(W)$ is the total photoproduction cross section. This makes

$$\begin{aligned} B(q^2, W) &= \left[\left(\frac{q^2}{1 - W_2^{el}(q^2)} \right) \cdot \lim_{q^2 \rightarrow 0} \left(\frac{1 - W_2^{el}(q^2)}{q^2} \right) \right] \times \left[\frac{\nu K}{q^2 + \nu^2} \right] \times \left[\frac{1+R}{1+\epsilon R} \right] \times \\ &\quad \times \left[\frac{F_2(\infty)}{F_2(\omega')} \right] \times \sigma_{\text{tot}}(q^2, W) \end{aligned}$$

where we have used $R = 0.23 q^2$ which has the correct limit as $q^2 \rightarrow 0$ and is consistent with electroproduction data²⁹ for $q^2 < 2(\text{GeV}/c)^2$.

We then fitted the values of B for each of the lines separately to the sum of four resonances and a polynomial background, only including data for $W \leq 2.1$ GeV:

$$B(q^2, W) = \sum_{i=1}^4 \text{Res}_i(q^2, W) + \sum_{j=1}^4 c_j q^{*j}$$

where

$$q^* = \left\{ \left[(W^2 + M^2 - m_\pi^2)/2W \right]^2 - M^2 \right\}^{\frac{1}{2}}$$

For single pion production, q^* is the momentum of the pion in the πN cm system. The resonance forms used were the same as in Walker's analysis of photoproduction.²⁸

$$\text{Res}_i(q^2, W) = A_R \left(\frac{k_R^*}{k^*} \right)^2 W_R^2 \frac{\Gamma \Gamma_\gamma}{(W_R^2 - W^2)^2 + W_R^2 \Gamma^2}$$

where

$$k^* = \left\{ \left[(W^2 + M^2 + q^2)/2W \right]^2 - M^2 \right\}^{\frac{1}{2}}$$

is the momentum of the virtual photon in the same πN cm system.

$$k_R^* = k^* \text{ at } W = W_R$$

$$\Gamma = \Gamma_R \left(\frac{q^*}{q_R^*} \right)^{2L+1} \left(\frac{q_R^{*2} + X^2}{q^{*2} + X^2} \right)^L$$

$$\Gamma_\gamma = \Gamma_R \left(\frac{k^*}{k_R^*} \right)^{2J} \left(\frac{k_R^{*2} + X^2}{k^{*2} + X^2} \right)^J$$

The parameters that were fitted for each resonance region were the amplitude, A_R , mass, W_R , and width, Γ_R . The other parameters L , J , and X , were taken from Walker and are shown in Table IX. For some lines, the fourth resonance enhancement was omitted from the fit, and for others, some parameters were held fixed to stabilize the fit. Table X lists the results of the fits for each line. In addition, we have fitted the total photoproduction data³⁰ to the same form. In Fig. 22 we show the data and the fitted functions.

We recognize that assigning only one Breit-Wigner resonant shape to each of the four obvious enhancement regions may be an oversimplified representation of the actual physics underlying the enhancements. For example, in Fig. 22 it is evident that in the third resonance region the mass at the peak of the enhancement increases as the incident energy increases. This is borne out by the fits given in Table X, where W_R increases continuously from 1675 to 1713 MeV as q^2 increases from 0.08 to 1.8 GeV². Fits with two, instead of one, Breit-Wigners in the third resonance region are consistent, not surprisingly, with a lower mass resonance (around 1670 MeV) decreasing in amplitude as q^2 increases plus a higher mass resonance (around 1710 MeV) increasing as q^2 increases. However, considering the various arbitrary aspects of the parametrization used in the fitting we have not pursued a more detailed breakdown of the total cross section into its constituent reactions. In deuterium there is an extra complication due to smearing, and we are not presenting an analysis of the resonant structures for this target.

After the parameters were determined from the fits, the amplitudes, A_R , were converted to values of $\sigma_{\text{RES}} = \sigma_R (W = W_R)$ for each resonance separately. These values are listed with their corresponding values of q^2 in Table XI. In addition, for the first resonance we have calculated the expected value of σ_{RES} ,

assuming the form used by Bartel et al.,³¹ in analyzing the first resonance data. This predicts that, at the resonant mass, the cross section is

$$\sigma_{\text{RES}} = \frac{4\alpha\pi(\nu^2 + q^2)}{\Gamma_0 W_R (W_R^2 - M^2)} \left[\frac{G_M^*(q^2)}{G_D(q^2)} \right]^2 \cdot G_D^2(q^2)$$

where

$$\Gamma_0 = 115 \text{ MeV}$$

and

$$G_D(q^2) = 3/(1 + q^2/.71)^2$$

This determines the ratio $(G_M^*/G_D)^2$ and these values are listed in Table XII for the first resonance. In Fig. 23 we plot this ratio for our data and the previous DESY experiment. Our results are consistent with the others that show this form factor definitely falls off faster than the dipole expression in this q^2 range.

The results for σ_{RES} for each of the resonance regions are shown in Fig. 24. The slope of a line through the data is clearly greater for the first resonance than for any of the others. The second, third, and fourth regions exhibit similar behavior as q^2 increases, whereas the first resonance amplitude is decreasing more rapidly. In Fig. 25, we have also plotted the ratio of the resonance peak height to the amount of background at the peak as determined from the fit. This shows that, whereas the first resonance becomes smaller compared with the background as q^2 increases, the higher mass resonances show less dependence on q^2 .

As can be observed in the photoproduction data (see Fig. 22), there is some evidence for an enhancement in the region of $W = 1435$. This can be attributed to the $P_{11}(1470)$ and is normally included in fits to photoproduction data.³⁰ In our electroproduction data satisfactory fits can be obtained without assuming any resonance in this mass region.

E. Sum Rules

Over the ranges of the experimental data we calculate integrals occurring in certain sum rules.

First, there is the Callan-Gross³² integral:

$$I_{1P} = \int_1^{\infty} \frac{d\omega}{\omega^2} \nu W_2 = \int_0^1 dx F_{2P}(x)$$

In the parton model, I_{1P} represents the mean square charge per parton. We also calculate the Gottfried integral:²⁷

$$I_{2P} = \int_1^{\infty} \frac{d\omega}{\omega} \nu W_2 = \int_0^1 \frac{dx}{x} F_{2P}(x)$$

In the parton model, this represents the sum of the squares of the parton charges in the proton.

In Table XIII we list the measured values of these integrals and their expected values in the three-quark model and in a simple parton model.³³ For convenience we evaluated the integrals using the fit to $F_{2P}(x')$ given in Sec. IV.C and shown in Fig. 20. Since the variable x' is observed to be a better scaling variable for the finite q^2 where data are available, we have used $F_{2P}(x')$ as an estimate of the asymptotic scaling function $F_{2P}(x)$ and have calculated all the integrals in terms of x' . By combining the results of the fit for $F_{2P}(x')$ with the measured σ_N/σ_P ratio, we calculate the corresponding integrals for the difference between proton and neutron. For values of $x' > 0.28$, we have used the data from ref. 26. Remember that there are no data for $x' < 0.02$ and also no data in the scaling region for $x' < 0.05$, and that these regions may be important for the I_{2P} and I_{2N} integrals. Note that the errors given in Table XIII are the estimated systematic errors. Propagation of the statistical errors yields

values much smaller than the errors shown. An interesting discussion of the significance of these sum rules is given in ref. 34.

F. A-Dependence

The phenomenon of "shadowing", in which the scattering probability per nucleon decreases in heavy nuclei, has been observed³⁵ in purely hadronic processes, such as πA scattering, and also in photoproduction. The usual explanation relies on the fact that the mean free path for hadronic interactions is of the same order as the nuclear sizes, so the incident particle is only able to see the surface of the nucleus. This would give a cross section of $\sigma_A = \sigma_0 A^{2/3}$. In photoproduction, where a naive estimate gives a mean free path large compared to the nuclear size, models like vector dominance, in which the photon spends some of the time as a hadron, can be used to account for the observed shadowing. However, previous experiments in electroproduction have failed to show any shadowing effect.⁴

In this experiment, we took data on targets of hydrogen, deuterium, beryllium, aluminum, copper, and gold at energies of 13 and 20 GeV in order to see if any A-dependence could be observed for low q^2 electroproduction. The analysis for the targets heavier than deuterium was done in the same way as for deuterium, except that no smearing correction and no inelastic radiative corrections were made. In Table XIV we list all the cross sections used for this analysis. The data with and without the elastic and quasi-elastic tails subtracted are plotted in Fig. 26. We have omitted points from further analysis when the radiative tail subtractions were greater than 25%, and we have made no inelastic radiative corrections for any of the targets. We should point out, however, that applying our procedure for calculating the inelastic radiative corrections to the data does not change the results of the comparison of cross

sections between nuclei. In models such as vector dominance that show decreasing shadowing for small ω' , the effects of the radiation process tend to dilute the possible shadowing when looking at data which are not radiatively corrected.³⁶ Comparisons with theoretical predictions, therefore, require the calculation of the expected results including the effects of the radiation process.

We calculate the "shadowing factor"

$$F = \frac{\sigma(A)}{N\sigma(D) - (N-Z)\sigma(H)}$$

where $\sigma(D)$, $\sigma(H)$ are the deuterium and hydrogen cross sections, N is the average number of neutrons, and Z the number of protons in the nucleus. No corrections for proton smearing were made to $\sigma(H)$, since it affects the value of F by $\lesssim 0.5\%$. In Fig. 27, F is plotted vs. A for each of the kinematic points. The results for each (q^2, W) point were fitted to the expression

$$F = a_0 A^\epsilon$$

determining the parameters a_0 and ϵ . (Note that in this section ϵ is not the photon polarization defined in Sec. III.) The results are listed in Table XV and ϵ plotted as a function of x' in Fig. 28.

Systematic errors are difficult to estimate. Many sources of systematic error cause shifts in ϵ at all values of x' and are, therefore, "normalization" errors in ϵ . We estimate these kinds of errors as $\pm .02$ in the value of ϵ .

The subtraction of elastic radiative tails introduces errors which would depend on x' (though the dependence is also a function of E_0). We are, therefore, reluctant to interpret the observed falloff at low x' as definitive evidence for the observation of shadowing in electroproduction.

V. Conclusion

The results of this experiment can be briefly summarized as follows:

- 1) The turnon of scaling behavior for the proton appears to take a remarkably simple form in q^2 , which is independent of the value of ω' chosen and is consistent with the closure approximation. The lack of q^2 dependence in the ratio σ_D/σ_P^S suggest that the turnon of scaling in the neutron is similar to that observed for the proton.
- 2) The ratio of $\nu W_{2N}/\nu W_{2P}$ is less than unity even for ω' as large as 20, suggesting a sizable nondiffractive component to the scattering.
- 3) We observe no significant resonance enhancements between $W = 2$ GeV and $W = 3$ GeV.
- 4) For our range of $q^2 = 0.1$ to 1.8 (GeV/c)^2 the first resonance decreases in size relative to its underlying background. For the higher lying resonance enhancements the ratio of peak to background remains relatively constant, varying no more than 30% from $q^2 = 0$ to $q^2 = 1.8 \text{ (GeV/c)}^2$.

- 5) Electroproduction shadowing in heavy nuclei is significantly smaller than in photoproduction.

We would like to thank the operating crew of the SLAC accelerator for putting up with our requests for a very well-defined beam and producing one of the finest beams available. We also want to thank the Spectrometer Facilities Group, C. Sinclair and D. Sherden in particular, for assistance with the spectrometer magnet control and the detectors. The Cryogenics Group under J. Mark is also thanked for construction and keeping a watchful eye on the targets. We also thank R. Haley for programming assistance during the early stages of the run and analysis. Special appreciation is given to Connie Logg, who provided many of the programs for the final analysis, which will be useful for

future electroproduction experiments at SLAC. For technical help and construction of the apparatus, we thank G. Johnson, K. Doty and W. Weeks. And, for the preparation of this paper, our appreciation to M. L. Arnold for typing and S. Sund for the computer plots.

APPENDIX I

RADIATIVE CORRECTION FORMULAE

In this appendix we present the expressions used in the radiative corrections for this experiment. The corrections consisted of: the radiative tail from elastic scattering, σ_{eltail} ; the tail from quasi-elastic scattering in the case of targets other than hydrogen, σ_{qtail} ; and the inelastic radiative corrections. We are able to calculate exact radiative tails under the assumption of one-photon exchange and for single photon emission.³⁷ This we call σ_{extail} . We also can use the angle-peaking approximation to calculate σ_{pktail} , which is a faster calculation and is used where speed is more important than accuracy. In the case of the quasi-elastic scattering, we must include the smearing due to the motion of the nucleons within the nucleus. Because of speed limitations we use the peaking approximation for radiation when the smearing calculation is done to get σ_{qt} . This is then corrected by comparing an unsmeared, but exact, radiation calculation to the unsmeared peaking approximation result. In both elastic and quasi-elastic cases, we correct for the finite solid angle of the detector using the peaking approximation to average over the acceptance to get σ_{finite} . By putting all these factors together, we obtain the following for the total elastic and quasi-elastic tails:

$$\sigma_{\text{eltail}} = \sigma_{\text{extail}} \cdot \frac{\sigma_{\text{finite}}}{\sigma_{\text{pktail}}}$$

$$\sigma_{\text{qtail}} = \sigma_{\text{qt}} \cdot \frac{\sigma_{\text{extail}}}{\sigma_{\text{pktail}}} \cdot \frac{\sigma_{\text{finite}}}{\sigma_{\text{pktail}}}$$

In the case of the inelastic correction, we use the peaking approximation and a model for the inelastic cross sections as described in the text. The following are the formulae as used in the analysis.

A. General Definitions

We first consider the cross section for elastic electron scattering from a target of mass M_T . This will define the structure functions $W_1^{el}(q^2)$ and $W_2^{el}(q^2)$:

$$\sigma_{el} \equiv \left(\frac{d\sigma}{d\Omega} \right)_{el} = \frac{\alpha^2 \cos^2 \theta/2}{4E_0^2 \sin^4 \theta/2} \frac{E'_{el}}{E_0} \left\{ W_2^{el} + 2 \tan^2 \theta/2 W_1^{el} \right\}$$

where E_0 is the incident energy

θ is the laboratory scattering angle

and $E'_{el} = E_0 / \left(1 + \frac{2E_0}{M_T} \sin^2 \theta/2 \right)$

α = fine structure constant = 1/137.03604 .

We consider three cases: elastic proton scattering, elastic nucleus scattering and quasi-elastic scattering and define the parameters needed for the calculation:

1) Elastic electron-proton scattering

$$M_T = M_P = .938256 \text{ GeV}$$

$$W_1^{el} = \tau G_{MP}^2 , \quad W_2^{el} = \frac{G_{EP}^2 + \tau G_{MP}^2}{1 + \tau}$$

where $\tau = q^2 / 4M_P^2$

$$G_{MP} = (1 + K_P) G_{EP}, \quad K_P = 1.7927$$

and $G_{EP} = P(q^2) / (1 + q^2 / .71)^2$

where $P(q^2)$ takes into account the deviation of the measured form factors from the dipole expression,¹² and is given by:

$$P(q^2) = \sum_{i=0}^5 \left[H_i \prod_{\substack{j=0 \\ (j \neq i)}}^5 \left\{ (\sqrt{q^2} - j) / (i - j) \right\} \right]$$

and $H_0 = 1.0007$, $H_1 = 1.01807$, $H_2 = 1.05584$, $H_3 = 0.836380$, $H_4 = 0.6864584$,
 $H_5 = -0.672830$.

2) Deuterium elastic

$$M_T = 1.87537 \text{ GeV}$$

$$W_1^{el} = F_D^2 \cdot \frac{2}{3} \tau G_S^2, \quad W_2^{el} = F_D^2 \cdot \left[G_P^2 + \frac{2}{3} \tau G_S^2 \right]$$

where²⁵ $F_D = F(q) = \frac{1.580}{q} \left(\tan^{-1} \frac{q}{0.930} - 2 \tan^{-1} \frac{q}{3.19} + \tan^{-1} \frac{q}{5.45} \right)$,

and $q = \sqrt{q^2} \text{ in fm}^{-1}$,

and³⁸

$$G_P = F_{1N} + F_{1P}$$

$$G_S = F_{1N} + F_{1P} + K_N F_{2N} + K_P F_{2P}$$

$$F_{1N} = \tau G_{MN}/(1+\tau)$$

$$F_{1P} = (G_{EP} + \tau G_{MP})/(1+\tau)$$

$$F_{2N} = G_{MN}/K_N(1+\tau)$$

$$F_{2P} = (G_{MP} - G_{EP})/\left[K_P(1+\tau)\right]$$

$$G_{MN} = K_N G_{EP}$$

and

$$K_N = -1.91348$$

3) Beryllium elastic

$$M_T = (.938256/1.00797) \cdot 9.012 = 8.38871 \text{ GeV}$$

$$W_1^{el} = 0$$

$$W_2^{el} = [Z \cdot F(q)]^2$$

where³⁹ $F(q) = 1 - ax^2/[2k(2+3a)] e^{-x^2/4k}$

and $k = 3(2+5a)/2(2+3a)$

$$a = (Z-2)/3$$

$$x = q \cdot 1.07 A^{1/3}$$

q in fm^{-1} ; Z = atomic charge number of the nucleus and is

given in Table I.

4) Aluminum, Copper and Gold Elastic

$$M_T = (.938256/1.00797) \cdot 26.98, 63.54, 197$$

$$= 25.1140 \text{ GeV}, 59.1454 \text{ GeV}, 183.375 \text{ GeV}$$

$$W_1^{el} = 0$$

$$W_2^{el} = [Z \cdot F(q)]^2$$

where $F(q) = e^{-(qb)^2/6}/(1+q^2c^2/6)$

$$b = 2.4 \text{ fm}$$

$$c = 1.07 A^{1/3} \text{ fm}$$

and q is in fm^{-1}

5) Quasi-elastic

$$M_T = .938256 \text{ GeV}$$

$$W_1^{el} = \tau G_M'^2, \quad W_2^{el} = \frac{G_E'^2 + \tau G_M'^2}{1+\tau}$$

where¹⁵ $G_E'^2 = Z \left[1 - F^2(q) \right] G_{EP}^2$

$$G_M'^2 = \left[Z(1+K_P)^2 + NK_N^2 \right] G_{EP}^2$$

and the appropriate $F(q)$ is chosen according to the target,

and N = number of neutrons in the target and is given in Table I.

B. "Exact" Radiative Tail

The cross section σ_{ex} for the radiative tail from a state of definite mass M_f can be calculated exactly under the assumption of one-photon exchange and for single photon emission. It depends upon knowledge of the structure functions $W_1^{\text{el}}(q^2)$ and $W_2^{\text{el}}(q^2)$ and is given by Tsai.¹³ We have changed the notation in the following sections from that used in the previous part of this paper, in order to follow more closely that used by Tsai. This means that now

$s(E_s, \vec{s})$: four momentum of the incident electron ($E_s = E_0$)

$p(E_p, \vec{p})$: four momentum of the outgoing electron ($E_p = E'$)

$t(M_T, 0)$: four momentum of the target particle

$k(\omega, \vec{k})$: four momentum of the real photon emitted

and in addition we define the four vectors

$$u = s + t - p$$

$$p_f = u - k$$

where $p_f \cdot p_f = M_f^2$.

For the radiative tail from elastic scattering $M_f = M_T$.

Then following Tsai we obtain:

$$\begin{aligned}
 \tilde{\sigma}_{\text{ex}} = & \left(\frac{d^2\sigma}{d\Omega dE_p} \right)_{\text{ex}} = \frac{\alpha^3}{(2\pi)} \left(\frac{E_p}{E_s} \right) \int_{-1}^1 \frac{2M_T \omega d(\cos \theta_k)}{q^4 (u_0 - |\vec{u}| \cos \theta_k)} \\
 & \left(\tilde{W}_2(q^2) \left\{ \frac{-am^2}{x^3} \left[2E_s(E_p + \omega) + \frac{q^2}{2} \right] - \frac{a'm^2}{y^3} \left[2E_p(E_s - \omega) + \frac{q^2}{2} \right] \right. \right. \\
 & - 2 + 2\nu(x^{-1} - y^{-1}) \left\{ m^2(s \cdot p - \omega^2) + (s \cdot p) \left[2E_s E_p - (s \cdot p) + \omega(E_s - E_p) \right] \right\} \\
 & + x^{-1} \left[2(E_s E_p + E_s \omega + E_p^2) + \frac{q^2}{2} - (s \cdot p) - m^2 \right] \\
 & - y^{-1} \left[2(E_s E_p - E_p \omega + E_s^2) + \frac{q^2}{2} - (s \cdot p) - m^2 \right] \left. \right\} \\
 & + \tilde{W}_1(q^2) \left[\left(\frac{a}{x^3} + \frac{a'}{y^3} \right) m^2 (2m^2 + q^2) + 4 \right. \\
 & \left. \left. + 4\nu(x^{-1} - y^{-1})(s \cdot p)(s \cdot p - 2m^2) + (x^{-1} - y^{-1})(2s \cdot p + 2m^2 - q^2) \right] \right)
 \end{aligned}$$

where ω is the photon energy in the lab system

$$\omega = \frac{1}{2} (u^2 - M_f^2) / (u_0 - |\vec{u}| \cos \theta_k)$$

$$s \cdot p = E_s E_p - |\vec{p}| |\vec{s}| \cos \theta$$

$$u_0 = E_s + M_T - E_p$$

$$|\vec{u}| = (u_0^2 - u^2)^{1/2}$$

$$u^2 = 2m^2 + M_T^2 - 2(s \cdot p) + 2M_T(E_s - E_p)$$

$$q^2 = 2m^2 - 2(s \cdot p) - 2\omega(E_s - E_p) + 2\omega|\vec{u}| \cos \theta_k$$

$$a = \omega(E_p - |\vec{p}| \cos \theta_p \cos \theta_k)$$

$$a' = \omega(E_s - |\vec{s}| \cos \theta_s \cos \theta_k)$$

$$b' = -\omega |\vec{p}| \sin \theta_p \sin \theta_k$$

$$\nu = (a' - a)^{-1}$$

$$\cos \theta_p = \frac{|\vec{s}| \cos \theta - |\vec{p}|}{|\vec{u}|} .$$

$$\cos \theta_s = \frac{|\vec{s}| - |\vec{p}| \cos \theta}{|\vec{u}|}$$

$$x = (a^2 - b^2)^{1/2}$$

$$y = (a'^2 - b'^2)^{1/2}$$

m = electron mass = 0.511 MeV

θ = scattering angle

θ_k = angle between \vec{u} and \vec{k}

and

$$\tilde{W}_1(q^2) = \tilde{F}(q^2) W_1^{el}(q^2)$$

$$\tilde{W}_2(q^2) = \tilde{F}(q^2) W_2^{el}(q^2)$$

$$\begin{aligned} \tilde{F}(q^2) = & 1 + 0.5772 bT + \frac{2\alpha}{\pi} \left[\frac{-14}{9} + \frac{13}{12} \ln \frac{-q^2}{m^2} \right] - \frac{\alpha}{2\pi} \ln^2 \left(\frac{E_s}{E_p} \right) \\ & + \frac{\alpha}{\pi} \left[\frac{1}{6} \pi^2 - \Phi \left(\cos^2 \frac{\theta}{2} \right) \right] . \end{aligned}$$

$$b = \frac{4}{3} \left\{ 1 + \frac{1}{9} \left[(Z+1)/(Z+\eta) \right] \left[\ln (183 Z^{-1/3})^{-1} \right] \right\} \approx 1.357$$

$$\eta = \ln (1440 Z^{-2/3}) / \ln (183 Z^{-1/3}) ,$$

$$T = t_a + t_b$$

and t_b and t_a = total path length in units of radiation length of the electron in the target before and after the scattering respectively (see Table II).

The Spence function is defined as

$$\Phi(x) = \int_0^x \frac{-\ln |1-y|}{y} dy$$

C. Real Bremsstrahlung and Ionization Loss in Target

The straggling caused by target bremsstrahlung and ionization loss also contributes to the radiative tail and can be written:

$$\sigma_b \equiv \left(\frac{d^2\sigma}{d\Omega dE_p} \right)_b = \frac{M_T + 2(E_s - \omega_s) \sin^2 \theta/2}{M_T - 2E_p \sin^2 \theta/2} \tilde{\sigma}_{el}(E_s - \omega_s) \left\{ \frac{bt_b}{\omega_s} \phi(v_s) + \frac{\xi}{2\omega_s^2} \right\}$$

$$+ \tilde{\sigma}_{el}(E_s) \left\{ \frac{bt_a}{\omega_p} \phi(v_p) + \frac{\xi}{2\omega_p^2} \right\}$$

$$\omega_s = E_s - E_p / \left(1 - \frac{2E_p}{M_T} \sin^2 \theta/2 \right)$$

$$\omega_p = E_s / \left(1 + \frac{2E_s}{M_T} \sin^2 \theta/2 \right) - E_p$$

$$\xi = \frac{\pi m}{2\alpha} \frac{t_a + t_b}{(Z + \eta) \ln(183/Z^{1/3})}$$

$$v_s = \omega_s/E_s$$

$$v_p = \omega_p/(E_p + \omega_p)$$

$$\phi(v) = 1 - v + 3/4 v^2$$

$$\text{and } \tilde{\sigma}_{el}(E) = \tilde{F}(q^2) \sigma_{el}(E)$$

D. Peaking Approximation

It is also possible to develop an angle-peaking approximation for the exact radiative tail which looks very similar to the expression for target straggling:

$$\sigma_p \equiv \left(\frac{d^2\sigma}{d\Omega dE_p} \right)_{\substack{\text{peak} \\ \text{approx.}}} = \frac{M_T + 2(E_s - \omega_s) \sin^2 \theta/2}{M_T - 2E_p \sin^2 \theta/2} \tilde{\sigma}_{el}(E_s - \omega_s) \left[\frac{bt_r \phi(v_s)}{\omega_s} \right] + \tilde{\sigma}_{el}(E_s) \left[\frac{bt_r \phi(v_p)}{\omega_p} \right]$$

$$\text{where } t_r = b^{-1}(\alpha/\pi) \left[\ln(-q^2/m^2) - 1 \right].$$

E. Multiple Photon Correction

The cross section for single photon emission is corrected for multiple soft photon radiation by multiplying by the factor:

$$F_{\text{soft}} = \left(\frac{\omega_s}{E_s} \right)^{b(t_b + t_r)} \left(\frac{\omega_p}{E_p + \omega_p} \right)^{b(t_a + t_r)}$$

F. Target Radiation

In an attempt to take into account radiation from the target, we have used the approach in Ref. 12. We calculate the quantity

$$t = \sum_{i,j} \frac{\alpha}{\pi} \int \frac{k^2 d\Omega_k}{4\pi} Z_i Z_j \theta_i \theta_j \frac{(p_i p_j)}{(p_i^k)(p_j^k)}$$

where	for	$i = 1$	$Z_i = -1$	$\theta_i = +1$	$p_i = s$
		2	+1	+1	t
		3	-1	-1	p
		4	+1	-1	p_f

and compare this to t_{el} , which is obtained by summing over only terms with i or $j = 1$ and 3. This results in a correction:

$$R_t = t/t_{el}$$

G. Complete Elastic Radiative Tail

By putting all the above expressions together, we arrive at two expressions for the elastic tail: σ_{extail} , using the exact one-photon formula and σ_{pktail} , using the peaking approximation:

$$\sigma_{\text{extail}} = [\sigma_{\text{ex}} \cdot R_t + \sigma_b] F_{\text{soft}}$$

$$\sigma_{\text{pktail}} = [\sigma_p + \sigma_b] F_{\text{soft}}$$

We also evaluate one other cross section using the peaking approximation, but averaging over the finite $\Delta\Omega$ acceptance of the spectrometer. This is done by summing over the individual θ and ϕ bins of the spectrometer:

$$\sigma_{\text{finite}} = \frac{1}{(2n_\theta+1)(2n_\phi+1)} \sum_{i=-n_\theta}^{n_\theta} \sum_{j=-n_\phi}^{n_\phi} \sigma_{\text{pktail}}(E_s, E_1, \sin^2 \theta/2)$$

where

$$\sin^2 \theta/2 = \sin^2 \left(\frac{\theta_0 + i\Delta\theta}{2} \right) + \sin^2 \left(\frac{j\Delta\phi}{2} \right) - 2 \sin^2 \left(\frac{\theta_0 + i\Delta\theta}{2} \right) \sin^2 \left(\frac{j\Delta\phi}{2} \right)$$

and

$$E_1 = E_s / \left(1 + 2 \frac{E_s}{M_T} \sin^2 \frac{\theta_0}{2} \right) - E_s / \left(1 + 2 \frac{E_s}{M_T} \sin^2 \frac{\theta_0 + i\Delta\theta}{2} \right) + E_p$$

θ = scattering angle corresponding to the center of the $\theta - \phi$ bin

$\Delta\theta$ = width of θ bin

$(2n_\theta + 1)$ = number of θ bins summed over

θ_0 = central horizontal projected angle of the spectrometer

$\Delta\phi$ = width of ϕ bin

$(2n_\phi + 1)$ = number of ϕ bins summed over

The final expression we have used for the complete elastic tail is then

$$\sigma_{\text{eltail}} = \sigma_{\text{extail}} \cdot \frac{\sigma_{\text{finite}}}{\sigma_{\text{pktail}}}$$

H. Quasi-elastic Scattering

The quasi-elastic scattering cross section in Section A does not take into account the motion of the nucleons within the nucleus. It represents a δ -function scattering with the correct total strength, but without the shape which is a result of smearing by the nuclear motion. Following the treatment by Atwood and

West,¹⁴ we calculate the quasi-elastic peak cross section as:

$$\begin{aligned} \hat{\sigma}_q &\equiv \left(\frac{d^2\sigma}{d\Omega dE_p} \right)_{\text{quasi}} \equiv \frac{\alpha^2 \cos^2 \theta/2}{4E_s^2 \sin^4 \theta/2} M_p \frac{P_{cm}}{2W_t} \\ &\quad \left[W_2^{el} \int_{-1}^{+1} \left(\mathcal{F} + \frac{P_x^2}{M_p^2} 2 \tan^2 \theta/2 \right) F_p E_{sp} d(\cos \theta_{cm}) \right. \\ &\quad \left. + 2 \tan^2 \theta/2 W_1^{el} \int_{-1}^{+1} F_p E_{sp} d(\cos \theta_{cm}) \right] \end{aligned}$$

where W_1^{el} and W_2^{el} are the nucleon form factors as in Section A.

cm = center of mass of photon-deuteron system

$$P_{cm} = (E_{cm}^2 - M_N^2)^{1/2}$$

$$E_{cm} = (S_t + M_N^2 - M_D^2)/2W_t$$

$$W_t = S_t^{1/2}$$

$$S_t = M_D^2 + 2M_D\nu - q^2, \quad \nu = E_s - E_p; \quad |q^2| = q^2 + \nu^2$$

M_p = proton rest mass, M_N = neutron rest mass, M_D = deuteron rest mass

$$\mathcal{F} = \frac{1}{M_p^2} \left[\left(P^0 - \frac{\nu}{|q|} P_z \right)^2 + \left(1 - \frac{\nu^2}{|q|^2} \right) P_x^2 \right],$$

and F_p = the probability that the nucleons have the momentum \vec{P}_{sp} inside the deuteron. We use $F_p = |\psi(\vec{P}_{sp})|^2$ where $\psi(\vec{P}_{sp})$ is the Fourier transform of the non-relativistic spatial wave function.⁴⁰

$$P_{sp}^2 = (E_{cm} |q| - (M_D - \nu) P_{cm} \cos \theta_{cm})^2 / S_t$$

$$E_{sp}^2 = P_{sp}^2 + (M_p^2 \text{ or } M_N^2)$$

$$P^0 = M_D - E_{sp}$$

$$P_x^2 = \frac{1}{2} P_{cm}^2 (1 - \cos^2 \theta_{cm})$$

$$P_z^2 = P_{sp}^2 - 2P_x^2$$

I. Quasi-elastic Radiative Tail

The radiative tail associated with this quasi-elastic scattering is then calculated using the peaking approximation as given in the following formula:

$$\begin{aligned} \sigma_{qt} &\equiv \left(\frac{d^2\sigma}{d\Omega dE_p} \right)_q = \left(\frac{R \Delta E}{E_s} \right)^{b(t_b+t_r)} \left(\frac{\Delta E}{E_p} \right)^{b(t_a+t_r)} \left(1 - \frac{\xi/\Delta E}{[1 - b(t_a+t_b+2t_r)]} \right) \tilde{\sigma}_q(E_s, E_p) \\ &+ \int_{E_s \min(E_p)}^{E_s - R \Delta E} \tilde{\sigma}_q(E'_s, E_p) \left(\frac{E_s - E'_s}{E_p R} \right)^{b(t_a+t_r)} \left(\frac{E_s - E'_s}{E_s} \right)^{b(t_b+t_r)} \\ &\times \left[\frac{b(t_b+t_r)}{E_s - E'_s} \phi \left(\frac{E_s - E'_s}{E_s} \right) + \frac{\xi}{2(E_s - E'_s)^2} \right] dE'_s \\ &+ \int_{E_p + \Delta E}^{E_p \max} \tilde{\sigma}_q(E_s, E'_p) \left(\frac{E'_p - E_p}{E'_p} \right)^{b(t_a+t_r)} \left(\frac{(E'_p - E_p)R}{E_s} \right)^{b(t_b+t_r)} \\ &\times \left[\frac{b(t_a+t_r)}{E'_p - E_p} \phi \left(\frac{E'_p - E_p}{E'_p} \right) + \frac{\xi}{2(E'_p - E_p)^2} \right] dE'_p \end{aligned}$$

where

$$R = \frac{M_T + 2E_s \sin^2 \theta/2}{M_T - 2E_p \sin^2 \theta/2}$$

$$\Delta E = 5 \text{ MeV}$$

$$\phi(v) = 1 - v + 3/4 v^2$$

$$\tilde{\sigma}(E_s, E_p) = \tilde{F}(q^2) \sigma_q(E_s, E_p)$$

J. Inelastic Radiative Corrections

The corrections for radiation from the inelastic states is done in the peaking approximation.

By replacing σ_q in Section I by a model for the inelastic cross section σ^M , we obtain the cross section with radiative effects included σ^M (radiated). The measured cross sections are corrected by the ratio σ^M (radiated) / σ^M .

APPENDIX II

NON-RELATIVISTIC DERIVATION OF CLOSURE

A. General

We write the cross section $d\sigma/d\Omega$ for the scattering of a spinless particle interacting solely by Coulomb interaction as

$$d\sigma/d\Omega = \sigma_M G(q^2)$$

where σ_M is the Mott cross section. We will not worry about recoil factors. If the target is made up of N constituents with charge e_i each, then the "form-factor" for the transition to a particular final state $|f\rangle$ is given in the non-relativistic Born approximation by

$$G_{0 \rightarrow f}(q^2) = \left| \sum_{i=1}^N e_i \langle f | e^{i\vec{q} \cdot \vec{R}_i} | 0 \rangle \right|^2$$

where \vec{R}_i is the position of the i th constituent. We shall distinguish the case where f is the same as the initial state (elastic scattering) from all others (inelastic scattering) and write

$$G_{\text{tot}}(q^2) = \sum_f G_{0 \rightarrow f}(q^2) = G_{\text{el}}(q^2) + G_{\text{inel}}(q^2)$$

For the case of elastic scattering, $\langle f | = \langle 0 |$, so

$$G_{\text{el}}(q^2) \equiv G_{0 \rightarrow 0}(q^2) = \left| \sum_{i=1}^N e_i \langle 0 | e^{i\vec{q} \cdot \vec{R}_i} | 0 \rangle \right|^2$$

For simplicity we assume that the ground state expectation value is independent of the index i , that is, each constituent has the same momentum distribution inside the target, and define

$$F_{\text{el}}(q^2) = \langle 0 | e^{i\vec{q} \cdot \vec{R}} | 0 \rangle$$

Then, we get

$$G_{el}(q^2) = \left| \sum_{i=1}^N e_i \right|^2 \left| F_{el}(q^2) \right|^2$$

Now, we evaluate the form-factor for the total cross section:

$$G_{tot}(q^2) = \sum_f G_{0 \rightarrow f}(q^2) = \sum_f \left| \sum_{i=1}^N e_i \langle f | e^{i\vec{q} \cdot \vec{R}_i} | 0 \rangle \right|^2$$

Expanding the squared matrix element,

$$G_{tot}(q^2) = \sum_f \sum_{i,j=1}^N e_i e_j \langle 0 | e^{-i\vec{q} \cdot \vec{R}_j} | f \rangle \langle f | e^{i\vec{q} \cdot \vec{R}_i} | 0 \rangle$$

We now make the closure approximation, that $\sum_f |f\rangle \langle f| = 1$. This assumes that all possible final states can be excited. So,

$$G_{tot}(q^2) = \sum_{i,j=1}^N e_i e_j \langle 0 | e^{i\vec{q} \cdot (\vec{R}_i - \vec{R}_j)} | 0 \rangle$$

Separating out the diagonal terms and using the normalization $\langle 0 | 0 \rangle = 1$, yields

$$G_{tot}(q^2) = \sum_{i=1}^N e_i^2 + \sum_{i \neq j}^N e_i e_j \langle 0 | e^{i\vec{q} \cdot (\vec{R}_i - \vec{R}_j)} | 0 \rangle$$

Next, we separate out a contribution, $C(q^2)$, which vanishes if there are no two particle correlations in the ground state, and which we assume to be independent of the constituents' indices i and j so that

$$\langle 0 | e^{i\vec{q} \cdot (\vec{R}_i - \vec{R}_j)} | 0 \rangle = |F_{el}(q^2)|^2 + C(q^2)$$

So,

$$G_{tot}(q^2) = \sum_{i=1}^N e_i^2 + \sum_{i \neq j}^N e_i e_j |F_{el}(q^2)|^2 + C(q^2) \sum_{i \neq j}^N e_i e_j$$

Now, we can subtract the elastic contribution to get just the inelastic form-

factor:

$$G_{inel}(q^2) = \sum_{i=1}^N e_i^2 + \sum_{i \neq j}^N e_i e_j |F_{el}(q^2)|^2 - \left| \sum_{i=1}^N e_i \right|^2 |F_{el}(q^2)|^2 + C(q^2) \sum_{i \neq j}^N e_i e_j$$

Rewriting the second term containing F_{el} as $\sum_{ij}^N e_i e_j |F_{el}(q^2)|^2$ yields

$$G_{inel}(q^2) = \sum_{i=1}^N e_i^2 - \sum_{i=1}^N e_i^2 |F_{el}(q^2)|^2 + C(q^2) \sum_{i \neq j}^N e_i e_j$$

or, summarizing the results:

$$G_{el}(q^2) = \left| \sum_{i=1}^N e_i \right|^2 |F_{el}(q^2)|^2$$

$$G_{inel}(q^2) = \sum_{i=1}^N e_i^2 \left[1 - |F_{el}(q^2)|^2 \right] + C(q^2) \sum_{i \neq j}^N e_i e_j$$

B. Application

We can now apply these results to the proton and neutron if we consider them as being made of constituents. These yield immediately

$$\int_{inel} d\nu W_{2P}(q^2, \nu) = \left(\sum_{i=1}^N e_i^2 \right)_P \left[1 - |F_{el}^P(q^2)|^2 \right] + C_P(q^2) \left(\sum_{i \neq j}^N e_i e_j \right)_P$$

$$\int_{inel} d\nu W_{2N}(q^2, \nu) = \left(\sum_{i=1}^N e_i^2 \right)_N \left[1 - |F_{el}^N(q^2)|^2 \right] + C_N(q^2) \left(\sum_{i \neq j}^N e_i e_j \right)_N$$

F_{el}^P and F_{el}^N would be equal if the momentum distributions of the constituents were the same in the proton and neutron, so if the correlation terms were

negligible, one might expect W_{2N}/W_{2P} to scale to lower values of q^2 than either W_{2P} or W_{2N} alone. Gottfried noted that in the simple quark model the charge sum in the correlation contribution vanishes for the proton, but not for the neutron.²⁷

For the case of particles with spin, magnetic moments, and more realistic ground states, the results get much more complicated. There are several more detailed accounts in the case of nuclear scattering in the literature.⁴¹ However, the simple approach stated here agrees with the spirit of the more complex analyses.

REFERENCES

1. E. D. Bloom et al., Phys. Rev. Letters 23, 930 (1969) and M. Breidenbach et al., Phys. Rev. Letters 23, 935 (1969).
2. J. D. Bjorken, Phys. Rev. 179, 1547 (1969).
3. D. O. Caldwell et al., Phys. Rev. D 7, 1362 (1973); V. Heynen et al., Phys. Letters 34B, 651 (1971); G. R. Brookes et al., Phys. Rev. D 8, 2826 (1973).
4. W. R. Ditzler, MIT Thesis, 1971 (unpublished);
see also H. Kendall in Proceedings of the 1971 International Symposium on Electron and Photon Interactions at High Energies, edited by N. B. Mistry (Laboratory of Nuclear Studies, Cornell University, Ithaca, New York, 1972), p. 254; and
J. Bailey et al., Paper No. 295, submitted to XVII International Conference on High Energy Physics, London, England, July 1-10, 1974.
5. See H. Kendall, p. 250 and R. Wilson, p. 106 in Proceedings of the 1971 International Symposium on Electron and Photon Interactions at High Energies, edited by N. B. Mistry (Laboratory of Nuclear Studies, Cornell University, Ithaca, New York, 1971).
See also Bloom et al., Phys. Rev. Letters 30, 1186 (1973).
6. R. S. Larsen and D. Horelick, "A Precision Toroidal Charge Monitor for SLAC," Report No. SLAC-PUB-398, Stanford Linear Accelerator Center (1968).
7. Densities and radiation lengths were taken from "Review of Particle Properties," Particle Data Group, LBL-100.
8. A. Bodek, Nucl. Instr. and Methods 109, 603 (1973).

9. W. K. H. Panofsky, "Magnetic Spectrometers," Report No. SLAC-PUB-798, Review talk presented at the High Energy Physics Instrumentation Conference, Dubna, USSR (1970).
10. E. Bloom et al., Nucl. Instr. and Methods 99, 255 (1972).
11. A. Boyarski et al., Phys. Rev. Letters 25, 695 (1970).
12. G. Miller, Thesis, Stanford University (1970), available as Report No. SLAC-129 (unpublished).
13. L. W. Mo and Y. S. Tsai, Rev. Mod. Phys. 41, 205 (1969); Y. S. Tsai, "Radiative Correction to Electron Scatterings," Report No. SLAC-PUB-848, Stanford Linear Accelerator Center (1971).
14. W. B. Atwood and G. B. West, Phys. Rev. D 7, 773 (1973).
15. V. Z. Jankus, Phys. Rev. 102, 1586 (1956).
16. L. A. Weber et al., Cryogenics 2, 236 (1962).
17. A. M. Roder et al., Cryogenics 2, 16 (1963); BNL Cryogenic Data Handbook.
18. S. J. Brodsky and J. Pumplin, Phys. Rev. 182, 5 (1969).
19. E. D. Bloom and F. J. Gilman, Phys. Rev. Letters 25, 1140 (1970).
20. S. D. Drell and J. D. Walecka, Ann. Phys. (N. Y.) 28, 18 (1964).
21. L. N. Hand, Phys. Rev. 129, 1834 (1963).
22. B. Dudelzak, Orsay Thesis (1965, unpublished); Ch. Berger et al., Phys. Letters 35B, 87 (1971); W. Bartel et al., Nucl. Phys. B58, 429 (1973).
23. M. N. Rosenbluth, Phys. Rev. 79, 615 (1950).
24. J. S. Poucher et al., Phys. Rev. Letters 32, 118 (1974).
25. J. A. McIntyre, Phys. Rev. 103, 1464 (1956).

26. A. Bodek, Ph. D. Thesis, Massachusetts Institute of Technology, MIT Laboratory for Nuclear Science Report No. COO-3069-116 (1972, unpublished).
27. K. Gottfried, Phys. Rev. Letters 18, 1174 (1967).
28. R. L. Walker, Phys. Rev. 182, 1729 (1969)..
29. E. M. Riordan, Ph. D. Thesis, Massachusetts Institute of Technology, MIT Laboratory for Nuclear Science Report No. COO-3069-176 (1973, unpublished).
30. H. Meyer et al., Phys. Letters 33B, 189 (1970);
D. O. Caldwell et al., Phys. Rev. Letters 25, 609 (1970);
T. A. Armstrong et al., Phys. Rev. D 5, 1640 (1972).
31. W. Bartel et al., Phys. Letters 28B, 148 (1968).
32. C. Callan and D. Gross, Phys. Rev. Letters 21, 311 (1968).
33. J. D. Bjorken and E. A. Paschos, Phys. Rev. 185, 1975 (1969).
34. E. D. Bloom in Proceedings of the 6th International Symposium on Electron and Photon Interactions at High Energies, edited by H. Rollnik and W. Pfeil (North Holland Publishing Co., Amsterdam, 1974), p. 227.
35. G. Bellettini et al., Nucl. Phys. 79, 609 (1966).
36. Private communication, D. Yennie.
37. Y. S. Tsai in Proceedings of the International Conference on Nuclear Structure, 1963 (Stanford University Press, Stanford, California 1964), p. 221.
38. N. K. Glendenning and G. Kramer, Phys. Rev. 126, 2159 (1962).
39. This and the other heavy target form-factors are taken from R. Hofstadter, Ann. Rev. Nucl. Sci. 7, 231 (1957).
40. R. V. Reid, Jr., Ann. Phys. (N.Y.) 50, 411 (1968).
41. For more detailed treatment of closure, see, for example, O. Kofoed-Hanson and C. Wilkin, Ann. Phys. (N.Y.) 63, 309 (1971);
K. W. McVoy and L. Van Hove, Phys. Rev. 125, 1034 (1962).

TABLE I
TARGET PARAMETERS

Target	Density (10^{20} nucleons/cm. ²)	Length (cm.)	Z	N	A
H (liquid)	2921.5 ± 0.94%	6.952 ± 0.4%	1	0	1.00797
D (liquid)	3605.8 ± 1.26%	7.117 ± 0.4%	1	1	2.01471
Al ("empty")	55.1 ± 2%	0.0914	13	14	26.98
Be	418.1 ± 2%	0.344	4	5	9.012
Cu	11.88 ± 3%	0.0145	29	34.62	63.54
Au	1.241±10%	0.0021	79	118	197.

The length of the heavy target foils is the average thickness based on the measured weight and area. The indicated error is an estimate of possible non-uniformity in the region where the beam went through.

TABLE II
TARGET RADIATION LENGTHS

	t_b (10^{-3} radiation lengths)	t_a (10^{-3} radiation lengths)
Hydrogen (liquid)	5.459	11.129
Deuterium (liquid)	6.348	12.018
Be	5.64	11.451
Al	5.30	11.111
Cu	5.382	11.193
Au	3.682	9.493

The quantity t_b is the thickness in radiation lengths of all material upbeam of the target plus one-half of the thickness of the target. The quantity t_a is the thickness of all material between the target and the spectrometer vacuum, including one-half the target thickness.

TABLE III
COUNTER AND CHAMBER DIMENSIONS (in cm)

	Horizontal	Vertical	Thickness	No. of wires
TR1	14.8	13.5	0.32	
TR2	11.2	11.2	0.64	
TR3	15.2	16.9	1.27	
TA	29.2	36.8	(16 radiation lengths)	
MULT 1,2,3	20	20	0.64	
C	20	20	285. N ₂ at 1 atm. .0685 Al .0127 Mylar	
Chamber 1(Y)	18.8	14.0		70
Chamber 2(X)	16.4	18.8		82
Chamber 3(Y)	18.8	15.6		78
Chamber 4(Y)	18.8	18.0		90
Chamber 5(X)	16.0	18.8		80

TABLE IV
HYDROGEN AND DEUTERIUM DENSITY

	Hydrogen		Deuterium	
	Lower	Upper	Lower	Upper
Vapor Pressure (atm.)	1.0897 ± 4.9%	1.1480 ± 5.2%	1.0970 ± 5.2%	1.1029 ± 5.3%
Temperature (°K)	20.560 ± 0.83%	20.741 ± 0.88%	20.582 ± 0.88%	20.601 ± 0.89%
Density (g-mole/cm ³)	0.03495 ± 0.38%	0.03484 ± 0.40%	0.04218 ± 0.84%	0.04217 ± 0.85%
Av. Density (g-mole/cm ³)	0.03489 ± 0.54%		0.04218 ± 0.86%	

Measured values of the vapor pressure below and above the target volume and the calculated average density which is the mean of the extreme values of the two measurements for each target. The errors are estimates of the systematic uncertainty arising from the measurements and the known temperature-density relationship.

TABLE V

SOURCES OF SYSTEMATIC UNCERTAINTIES
IN THE ABSOLUTE CROSS SECTIONS

	Hydrogen	Deuterium
No. of target nuclei	$\pm 0.94\%$	$\pm 1.26\%$
No. of incident electrons	$\pm 1\%$	
Solid angle	$\pm 2\%$	
Reconstruction efficiency	$\pm 1\%$	
Total	$\pm 2.62\%$	$\pm 2.75\%$

Estimates of the systematic errors contributing to the absolute cross section measurements. Errors due to the following sources were smaller and were neglected: rate effects, incomplete π -e separation, errors in the E_0 and θ measurements, purity of the gases used to fill the liquid targets. In addition to these systematic errors there are also errors due to radiative corrections which are discussed in the text.

TABLE VI
ELASTIC ELECTRON-PROTON CROSS SECTIONS

E_0 (GeV)	q^2 (GeV/c) ²	$d\sigma/d\Omega$ (μ b/sr)	Systematic Error (μ b/sr)
4.500	0.098	110.80 \pm 0.49	\pm 3.10
7.001	0.235	30.164 \pm 0.065	\pm 0.846
9.993	0.474	7.641 \pm 0.025	\pm 0.214
13.000	0.797	2.2151 \pm 0.0046	\pm 0.0620
16.000	1.198	0.7136 \pm 0.0041	\pm 0.020
18.010	1.510	0.3473 \pm 0.0028	\pm 0.0097
20.005	1.853	0.1778 \pm 0.0011	\pm 0.0050

Both the statistical errors and the estimated systematic errors are shown. The systematic errors are obtained by adding in quadrature the 2.62% error estimated in Table V to a 1% error estimated in the radiative correction procedure.

TABLE VII
NEUTRON-PROTON RATIOS

Bin	(A-1)	Systematic Errors
0 < x' < 0.02	0.994 ± 0.0125	± 0.053
0.02 < x' < 0.04	0.949 ± 0.0096	± 0.036
0.04 < x' < 0.06	0.892 ± 0.0089	± 0.031
0.06 < x' < 0.08	0.862 ± 0.0074	± 0.030
0.08 < x' < 0.10	0.839 ± 0.0084	± 0.030
0.10 < x' < 0.12	0.822 ± 0.0089	± 0.030
0.12 < x' < 0.14	0.797 ± 0.0077	± 0.029
0.14 < x' < 0.16	0.781 ± 0.0096	± 0.029
0.16 < x' < 0.18	0.769 ± 0.0067	± 0.029
0.18 < x' < 0.20	0.724 ± 0.0089	± 0.028
0.20 < x' < 0.22	0.736 ± 0.0073	± 0.028
0.22 < x' < 0.24	0.692 ± 0.0077	± 0.028
0.24 < x' < 0.26	0.685 ± 0.0096	± 0.028
0.26 < x' < 0.28	0.672 ± 0.0121	± 0.027

A is determined from the fit to $\sigma_D/\sigma_P^S = A(1 - |F_D(q^2)|^2)$. The first error shown is from the fit. In the right-hand column we give estimates of the systematic errors. These are computed by combining in quadrature the ± 1.57% systematic error in σ_D/σ_P^S with the estimate of radiative corrections errors given in Sec. II F.

TABLE VIII
EXTRACTED STRUCTURE FUNCTION

Bin	D	ΔR	Extrapolation Error	Combined Error
$8 < \omega' < 12$	0.355 ± 0.0005	$\pm .004$	$\pm .001$	$\pm .0042$
$12 < \omega' < 16$	0.343 ± 0.0008	$\pm .005$	$\pm .002$	$\pm .0054$
$16 < \omega' < 20$	0.335 ± 0.0012	$\pm .006$	$\pm .003$	$\pm .0068$
$20 < \omega' < 24$	0.325 ± 0.0014	$\pm .009$	$\pm .006$	$\pm .0109$
$24 < \omega' < 28$	0.328 ± 0.0029	$\pm .010$	$\pm .011$	$\pm .0151$
$28 < \omega' < 32$	0.321 ± 0.0031	$\pm .011$	$\pm .018$	$\pm .0213$
$32 < \omega' < 36$	0.332 ± 0.0027	$\pm .009$	$\pm .017$	$\pm .0194$
$36 < \omega' < 40$	0.317 ± 0.0022	$\pm .013$	$\pm .023$	$\pm .0265$
$40 < \omega' < 44$	0.320 ± 0.0051	$\pm .018$	$\pm .031$	$\pm .0362$
$44 < \omega' < 48$	0.332 ± 0.0030	$\pm .011$	$\pm .024$	$\pm .0266$
$48 < \omega'$	0.319 ± 0.0014	$\pm .020$	$\pm .031$	$\pm .0369$

Values of D determined from the fits to νW_2 for each ω' bin. The first errors shown are from the fit. The errors listed under ΔR arise from uncertainties in R and are obtained by letting $R = 0$ and comparing to the results with $R = 0.18$. The extrapolation error assigned corresponds to 1/2 of the difference of the function evaluated at the asymptotic value and at the q^2 of the last measured data point for that bin. These three sources of error are then combined in quadrature and the result listed under combined error. There is also the overall $\pm 2.62\%$ systematic uncertainty (see Table VI). There is an additional systematic error from the radiative corrections of 3 - 7.5% which is larger for higher ω' .

TABLE IX
RESONANCE REGION ASSIGNMENTS

Resonance Region	L	J	X(GeV)	Identified with
1	1	1	0.160	$P_{33}(1236)$
2	2	1	0.350	$D_{13}(1520)$
3	3	2	0.350	$F_{15}(1688)$
4	3	2	0.350	$F_{37}(1950)$

Spin assignments are taken from Ref. 28. X is the parameter determining the mass variation of the width.

TABLE X
RESONANCE FIT PARAMETERS

	4.5 GeV	7 GeV	10 GeV	13 GeV	16 GeV	18 GeV	20 GeV	
<u>Region 1</u>								
A_R (μb)	289.7±4.05	221.3±1.50	167.1±1.51	137.7±0.75	118.8±1.82	104.5±2.32	93.79±1.87	
W_R (GeV)	1.227±0.0010	1.231±0.0005	1.225±0.0006	1.224±0.0004	1.226±0.0010	1.233±0.0015	1.236±0.0015	
Γ_R (GeV)	0.116±0.0040	0.123±0.0021	0.119±0.0027	0.119±0.0016	0.120±0.0046	0.124±0.0068	0.141±0.0071	
<u>Region 2</u>								
A_R (μb)	118.2±3.82	100.8±1.70	82.94±1.61	72.52±0.82	70.62±1.70	62.06±2.20	61.15±1.70	
W_R (GeV)	1.519±0.0025	1.516±0.0010	1.512±0.0010	1.509±0.0005	1.507±0.0009	1.511±0.0012	1.513±0.0009	
Γ_R (GeV)	0.144±0.010	0.130±0.0046	0.114±0.0043	0.097±0.0021	0.088±0.0040	0.077±0.0052	0.078±0.0042	
<u>Region 3</u>								
A_R (μb)	64.92±3.74	61.56±1.67	61.06±1.93	57.32±1.01	51.18±1.64	50.79±2.18	47.00±1.75	
W_R (GeV)	1.675±0.0031	1.681±0.0014	1.692±0.0016	1.696±0.0008	1.700±0.0013	1.705±0.0017	1.713±0.0014	
Γ_R (GeV)	0.113±0.014	0.102±0.0055	0.115±0.0071	0.105±0.0035	0.094±0.0061	0.092±0.0079	0.102±0.0072	
<u>Region 4</u>								
A_R (μb)	---	---	21.87±4.13	12.57±1.59	10.26±2.08	13.71±3.14	11.78±2.49	
W_R (GeV)	---	---	1.950	--	1.950	--	1.950	--
Γ_R (GeV)	---	---	0.200	--	0.200	--	0.200	--
BACKGROUND FIT PARAMETERS								
C_1 ($\mu b/\text{GeV}$)	351.2±36.8	187.2±13.4	186.2±14.3	164.6±8.07	185.3±19.5	54.0±24.8	94.6±21.0	
C_2 ($\mu b/\text{GeV}^2$)	-926.5±268.2	-364.3±98.7	-481.4±103.3	-316.4±53.14	-333.4±115.1	584.2±149.7	320.3±124.1	
C_3 ($\mu b/\text{GeV}^3$)	1857.6±623.5	1270.2±221.2	1323.5±247.1	912.1±122.1	879.5±236.5	-940.3±318.0	-482.9±264.9	
C_4 ($\mu b/\text{GeV}^4$)	-1191.0±440.4	-1017.1±147.7	-1011.9±175.5	-681.2±83.7	-651.6±150.4	446.1±206.8	204.4±173.0	

The errors shown are the results from the error matrix from the fit. If no error is shown, the parameter was held fixed.
If no value is shown, the parameter was omitted from the fit.

TABLE XI
RESONANCE AMPLITUDES

	q^2 (GeV/c) ²	σ_{RES} (μb)	Error From Fit Parametrization
First Resonance Region	0.09	505.0 \pm 7.06	\pm 8.75
	0.22	468.7 \pm 3.19	\pm 6.68
	0.46	327.2 \pm 2.95	\pm 5.82
	0.78	187.7 \pm 1.03	\pm 4.00
	1.17	98.02 \pm 1.50	\pm 2.72
	1.48	59.12 \pm 1.31	\pm 1.88
	1.82	36.48 \pm 0.73	\pm 1.32
Second Resonance Region	0.08	129.5 \pm 4.19	\pm 10.1
	0.21	113.8 \pm 1.92	\pm 8.63
	0.44	84.24 \pm 1.63	\pm 6.67
	0.75	57.07 \pm 0.65	\pm 5.11
	1.14	38.84 \pm 0.94	\pm 3.79
	1.44	25.89 \pm 0.92	\pm 3.14
	1.78	19.12 \pm 0.53	\pm 2.25
Third Resonance Region	0.08	65.87 \pm 3.79	\pm 11.8
	0.20	60.29 \pm 1.64	\pm 10.2
	0.43	51.52 \pm 1.63	\pm 7.50
	0.73	37.73 \pm 0.66	\pm 5.89
	1.12	24.47 \pm 0.78	\pm 4.46
	1.42	19.11 \pm 0.82	\pm 3.59
	1.75	13.74 \pm 0.51	\pm 2.72
Fourth Resonance Region	0.40	15.98 \pm 3.02	\pm 7.82
	0.70	7.18 \pm 0.91	\pm 6.51
	1.08	4.39 \pm 0.89	\pm 4.95
	1.38	4.76 \pm 1.09	\pm 3.91
	1.71	3.29 \pm 0.70	\pm 3.10

The amplitudes of each resonance region cross section σ_{RES} at the corresponding resonance mass. The first errors shown are the fit errors. We also estimate the error due to the particular parametrization used in the fit by assuming a different parametrization could result in the background varying by as much as $\pm 10\%$.

TABLE XII
FIRST RESONANCE TRANSITION FORM FACTOR

$q^2 \text{ (GeV/c)}^2$	$\left[G_M^*(q^2) / G_D(q^2) \right]^2$
0.09	0.950 ± 0.030
0.22	0.905 ± 0.019
0.46	0.828 ± 0.022
0.78	0.735 ± 0.020
1.17	0.633 ± 0.027
1.48	0.548 ± 0.030
1.82	0.475 ± 0.027

Values of the transition form factor G_M^* compared to a dipole form $G_D(q^2) = 3/(1+q^2/.71)^2$. The errors include the fit error added linearly to the fit parametrization error estimate.

TABLE XIII
ELECTROPRODUCTION SUM RULES

	Expected		Measured Values	
	3 quarks	Parton Model	This Experiment $0.02 < x' < 0.28$	Extended Range $0.02 < x' < 0.82$
I_{1P}	$\frac{1}{3}$	$\frac{2}{9} + \frac{1}{3 < N >}$	0.089 ± 0.005	0.152 ± 0.009
$I_{1P} - I_{1N}$	$\frac{1}{9}$	$\frac{1}{3 < N >}$	0.019 ± 0.003	0.045 ± 0.005
I_{2P}	1	$\frac{1}{3} + \frac{2 < N >}{9}$	0.895 ± 0.072	1.052 ± 0.085
$I_{2P} - I_{2N}$	$\frac{1}{3}$	$\frac{1}{3}$	0.139 ± 0.031	0.200 ± 0.040

Expected parton model values are from Ref. 33; $< N >$ is the average number of partons. The extended range of $0.02 < x' < 0.82$ includes data σ_N/σ_P from Ref. 26. The errors are an estimate of the systematic uncertainty from the data.

TABLE XIV
CROSS SECTIONS FOR A-DEPENDENCE ANALYSIS

$E_0 = 13 \text{ GeV}$

W (GeV)	Target	Raw ($\mu\text{b}/(\text{GeV}\cdot\text{sr})$)	Raw-Tails ($\mu\text{b}/(\text{GeV}\cdot\text{sr})$)	W (GeV)	Target	Raw ($\mu\text{b}/(\text{GeV}\cdot\text{sr})$)	Raw-Tails ($\mu\text{b}/(\text{GeV}\cdot\text{sr})$)
2.00	H	3.173 ± 0.028	3.027 ± 0.028	3.25	H	1.477 ± 0.015	1.339 ± 0.015
	D	5.697 ± 0.068	5.490 ± 0.068		D	2.628 ± 0.017	2.449 ± 0.017
	Be	25.24 ± 0.39	24.39 ± 0.39		Be	11.70 ± 0.18	10.92 ± 0.18
	Al	76.4 ± 1.2	73.7 ± 1.3		Al	34.82 ± 0.46	31.94 ± 0.46
	Cu	186.1 ± 3.9	180.0 ± 3.9		Cu	81.3 ± 1.5	74.1 ± 1.5
	Au	$554. \pm 20.$	$538 \pm 20.$		Au	270.1 ± 8.8	247.7 ± 8.8
2.25	H	2.651 ± 0.029	2.525 ± 0.029	3.50	H	1.307 ± 0.014	1.140 ± 0.014
	D	4.697 ± 0.039	4.523 ± 0.039		D	2.354 ± 0.017	2.141 ± 0.017
	Be	21.34 ± 0.28	20.62 ± 0.28		Be	10.28 ± 0.14	9.34 ± 0.14
	Al	64.32 ± 0.92	62.04 ± 0.92		Al	31.19 ± 0.50	27.43 ± 0.50
	Cu	156.8 ± 2.6	151.6 ± 2.6		Cu	73.7 ± 1.4	63.6 ± 1.4
	Au	$481. \pm 15.$	$467. \pm 15.$		Au	230.1 ± 7.0	195.7 ± 7.0
2.50	H	2.192 ± 0.024	2.076 ± 0.024	3.75	H	1.265 ± 0.020	1.045 ± 0.020
	D	3.946 ± 0.034	3.788 ± 0.034		D	2.185 ± 0.031	1.912 ± 0.031
	Be	18.11 ± 0.25	17.45 ± 0.25		Be	10.17 ± 0.20	8.70 ± 0.20
	Al	53.63 ± 0.77	51.50 ± 0.77		Al	29.66 ± 0.62	24.29 ± 0.62
	Cu	132.4 ± 2.4	127.6 ± 2.4		Cu	70.9 ± 2.0	55.4 ± 2.0
	Au	$414. \pm 13.$	$401. \pm 13.$		Au	223.1 ± 8.4	164.3 ± 8.4
2.75	H	1.890 ± 0.018	1.774 ± 0.018	4.00	H	1.221 ± 0.022	
	D	3.414 ± 0.021	3.259 ± 0.021		D	2.135 ± 0.035	
	Be	15.12 ± 0.17	14.47 ± 0.17		Be	9.35 ± 0.23	
	Al	45.71 ± 0.60	43.55 ± 0.60		Al	29.72 ± 0.72	
	Cu	106.2 ± 1.7	101.2 ± 1.7		Cu	74.3 ± 2.5	
	Au	345.8 ± 8.1	331.9 ± 8.1		Au	$241. \pm 11.$	
3.00	H	1.639 ± 0.016	1.517 ± 0.016				
	D	2.960 ± 0.018	2.798 ± 0.018				
	Be	13.21 ± 0.19	12.52 ± 0.19				
	Al	39.76 ± 0.52	37.36 ± 0.52				
	Cu	92.3 ± 1.7	86.6 ± 1.7				
	Au	286.0 ± 9.3	269.4 ± 9.3				

TABLE XIV (cont'd.)

$E_0 = 20$ GeV

W (GeV)	Target	Raw ($\mu\text{b}/(\text{GeV}\cdot\text{sr})$)	Raw-Tails ($\mu\text{b}/(\text{GeV}\cdot\text{sr})$)	W (GeV)	Target	Raw ($\mu\text{b}/(\text{GeV}\cdot\text{sr})$)	Raw-Tails ($\mu\text{b}/(\text{GeV}\cdot\text{sr})$)
2.50	H	0.762 \pm 0.007	0.753 \pm 0.007	4.25	H	0.431 \pm 0.005	0.408 \pm 0.005
	D	1.292 \pm 0.008	1.279 \pm 0.008		D	0.783 \pm 0.010	0.752 \pm 0.010
	Be	5.72 \pm 0.11	5.67 \pm 0.11		Be	3.428 \pm 0.072	3.275 \pm 0.072
	Al	17.66 \pm 0.34	17.48 \pm 0.34		Al	10.67 \pm 0.19	9.92 \pm 0.19
	Cu	42.44 \pm 0.95	42.03 \pm 0.95		Cu	26.32 \pm 0.80	24.19 \pm 0.80
	Au	123.5 \pm 5.5	122.3 \pm 5.5		Au	86.0 \pm 3.7	78.8 \pm 3.7
2.75	H	0.695 \pm 0.007	0.686 \pm 0.007	4.50	H	0.426 \pm 0.004	0.394 \pm 0.004
	D	1.205 \pm 0.006	1.192 \pm 0.006		D	0.777 \pm 0.006	0.735 \pm 0.006
	Be	5.39 \pm 0.11	5.34 \pm 0.11		Be	3.385 \pm 0.049	3.177 \pm 0.049
	Al	16.99 \pm 0.20	16.80 \pm 0.20		Al	10.44 \pm 0.17	9.42 \pm 0.17
	Cu	40.4 \pm 1.2	40.0 \pm 1.2		Cu	24.03 \pm 0.50	21.02 \pm 0.50
	Au	123.3 \pm 5.1	122.1 \pm 5.1		Au	69.8 \pm 2.3	58.9 \pm 2.3
3.00	H	0.634 \pm 0.007	0.625 \pm 0.007	4.75	H	0.424 \pm 0.004	
	D	1.125 \pm 0.007	1.112 \pm 0.007		D	0.765 \pm 0.006	
	Be	5.119 \pm 0.070	5.061 \pm 0.070		Be	3.392 \pm 0.072	
	Al	15.40 \pm 0.24	15.18 \pm 0.24		Al	10.23 \pm 0.16	
	Cu	36.51 \pm 0.79	36.02 \pm 0.79		Cu		
	Au	115.1 \pm 3.5	113.7 \pm 3.5		Au	76.6 \pm 3.5	
3.25	H	0.583 \pm 0.006	0.573 \pm 0.006	5.00	H	0.458 \pm 0.005	
	D	1.038 \pm 0.007	1.023 \pm 0.007		D	0.796 \pm 0.007	
	Be	4.731 \pm 0.094	4.666 \pm 0.094		Be	3.591 \pm 0.084	
	Al	14.70 \pm 0.22	14.43 \pm 0.22		Al	10.68 \pm 0.17	
	Cu	35.49 \pm 1.03	34.87 \pm 1.03		Cu	25.94 \pm 0.88	
	Au	112.7 \pm 4.5	111.0 \pm 4.5		Au	76.4 \pm 4.1	
3.50	H	0.532 \pm 0.006	0.521 \pm 0.006	5.25	H	0.497 \pm 0.007	
	D	0.956 \pm 0.006	0.940 \pm 0.006		D	0.903 \pm 0.010	
	Be	4.308 \pm 0.059	4.232 \pm 0.059		Be	4.16 \pm 0.11	
	Al	13.04 \pm 0.19	12.70 \pm 0.19		Al	12.87 \pm 0.25	
	Cu	31.44 \pm 0.67	30.60 \pm 0.67		Cu	31.5 \pm 1.2	
	Au	97.4 \pm 3.0	95.0 \pm 3.0		Au	117.1 \pm 5.9	
3.75	H	0.495 \pm 0.005	0.481 \pm 0.005	5.50	H	0.601 \pm 0.011	
	D	0.899 \pm 0.007	0.880 \pm 0.007		D	1.009 \pm 0.013	
	Be	4.001 \pm 0.080	3.908 \pm 0.080		Be	4.79 \pm 0.15	
	Al	12.49 \pm 0.19	12.06 \pm 0.19		Al	16.69 \pm 0.39	
	Cu	30.06 \pm 0.87	28.92 \pm 0.87		Cu	46.5 \pm 2.0	
	Au	90.7 \pm 3.7	87.3 \pm 3.7		Au	186. \pm 11.	
4.00	H	0.471 \pm 0.004	0.454 \pm 0.004				
	D	0.840 \pm 0.006	0.817 \pm 0.006				
	Be	3.796 \pm 0.036	3.679 \pm 0.036				
	Al	11.23 \pm 0.17	10.67 \pm 0.17				
	Cu	27.53 \pm 0.59	25.98 \pm 0.59				
	Au	86.2 \pm 2.6	81.3 \pm 2.6				

TABLE XV
A-DEPENDENCE RESULTS

E_0 (GeV)	W (GeV)	q^2 (GeV/c) ²	x^t	ν (GeV)	a_0	$\epsilon \times 1000$	χ^2 (4D. F.)
13	2.00	0.695	0.148	2.034	0.998 ± 0.008	3.8 ± 3.8	2.1
	2.25	0.660	0.115	2.581	0.994 ± 0.008	12.9 ± 3.5	2.5
	2.50	0.621	0.090	3.191	0.994 ± 0.008	13.2 ± 3.7	5.7
	2.75	0.578	0.071	3.870	0.998 ± 0.006	0.5 ± 3.1	5.4
	3.00	0.531	0.056	4.612	1.002 ± 0.007	-3.0 ± 3.5	0.6
	3.25	0.481	0.044	5.416	1.003 ± 0.007	-6.2 ± 3.7	6.5
	3.50	0.425	0.034	6.282	1.007 ± 0.008	-15.4 ± 4.0	0.8
	3.75	0.366	0.025	7.216	1.014 ± 0.014	-18.8 ± 6.2	5.6
20	2.50	1.588	0.203	3.707	0.997 ± 0.006	7.2 ± 4.1	1.7
	2.75	1.524	0.168	4.373	0.991 ± 0.006	16.0 ± 3.7	1.7
	3.00	1.453	0.139	5.095	0.996 ± 0.006	9.0 ± 3.6	1.4
	3.25	1.375	0.115	5.894	0.990 ± 0.007	18.8 ± 4.1	1.8
	3.50	1.292	0.095	6.750	0.997 ± 0.007	6.4 ± 3.6	1.3
	3.75	1.203	0.079	7.666	0.997 ± 0.007	6.4 ± 4.3	0.9
	4.00	1.107	0.065	8.647	1.001 ± 0.007	0.8 ± 3.6	6.2
	4.25	1.005	0.053	9.692	0.997 ± 0.009	0.3 ± 5.0	4.9
	4.50	0.897	0.042	10.800	1.012 ± 0.007	-24.6 ± 4.0	7.3

Results of the fits to the A-dependence of the form $F = a_0 A^\epsilon$. The errors shown are from the fit only.
Systematic errors can shift the values of ϵ by as much as ± 0.02 .

FIGURE CAPTIONS

1. Plan and elevation views of the SLAC 20-GeV spectrometer. The arrangement of magnets is shown at the bottom of the picture where B = bending magnet, Q = quadrupole, S = sextupole.
2. The detector arrangement in the hut of the 20-GeV spectrometer.
3. Distributions in the reconstructed scattering coordinates of all events satisfying the trigger at incident energy 13 GeV and spectrometer momentum 9.13 GeV/c:
 - a) the horizontal projected scattering angle θ . The shape of the distribution reflects the $1/\sin^4 \theta/2$ of the cross section; the cut at ± 3.5 mrad is shown;
 - b) the vertical projected scattering angle ϕ . The position of the vertical slits at ± 4.25 mrad is shown; and,
 - c) the fractional momentum $\Delta p/p$. The cut at $\pm 1.6\%$ is shown.
4. Event distribution in the pulse height from the TA counter. The arrow indicates the position of the TA pulse height cut. The lack of events below channel 50 is due to the discriminator threshold setting. Zero pulse height should typically appear near channel 40.
 - a) Typical running conditions, $E_0 = 13$ GeV, $E' = 9.13$ GeV. The peak shows the clean electron signal; a very small two-electron peak can be seen around channel 475.
 - b) One of the worst conditions, $E_0 = 20$ GeV, $E' = 4.14$ GeV. The shaded region shows the data after a cut on the pulse height from the Cerenkov counter is made.
5. Measured efficiency of the MULT pulse height cut as a function of detected particle energy. The curve is the function used to correct the data in the

region shown. The data points show the mean and standard deviation of all measurements from runs in each bin of E' .

6. The raw scattering cross section $d^2\sigma/d\Omega dE'$ for hydrogen at $E_0 = 13$ GeV. No dummy subtractions, positron subtraction or radiative corrections have been made. The elastic peak is reduced by 5.
7. Positron subtraction for the worst line, $E_0 = 20$ GeV and the hydrogen target. The open circles are the cross sections from all detected electrons; the closed circles are after the positron cross sections are subtracted. The solid line is the ratio of the cross sections before and after subtractions.
8. Experimental value of the cross section $d^2\sigma/d\Omega dE'$ vs. missing mass for the 13 GeV hydrogen data. The line is the calculated elastic tail contribution. The errors on the data points are smaller than the symbols.
9. Experimental values of the cross section $d^2\sigma/d\Omega dE'$ vs. missing mass for the 4.5 GeV deuterium data. The lines are the calculated elastic and quasi-elastic peaks and radiative tails with effects of momentum resolution included. The statistical errors on the data points are smaller than the symbols.
10. Experimental values of the cross section $d^2\sigma/d\Omega dE'$ vs. missing mass for all the data. The incident energy and q^2 range (q^2 increasing with decreasing W) for each line are shown. a) Hydrogen. b) Deuterium.
11. Kinematic (q^2, ν) plane showing the location of the measured 4° cross sections. The heavy lines represent "scanned" data, where the measurements from each run overlapped. Lines of constant missing mass, W , are shown dashed, and lines of constant $\omega = 2M\nu/q^2$ are indicated.
12. The smearing correction applied to the hydrogen measurements when analyzing deuterium. The different lines are the six incident energies with data above $W = 2$ GeV.

13. Feynman diagram for electron-proton scattering in the one photon approximation.
14. Experimental values of the cross section $d^2\sigma/d\Omega dE'$ for elastic electron-proton scattering at $E_0 = 13$ GeV. The open circles are the data before radiative corrections; the closed circles are after unfolding the spectrum to take into account radiative effects. The energy resolution at this energy is 24 MeV FWHM arising from the incident beam energy definition. The errors are smaller than the symbols. The data are plotted vs. missing energy, the difference between the electron energy corresponding to elastic scattering and the measured energy of the detected electron. The slight offset from zero is an example of the differences in calibration of the spectrometer momentum and incident beam energy.
15. The ratio of the measured elastic electron-proton cross section $d\sigma/d\Omega$ to the cross section calculated using the dipole approximation for the electric form factor $G_E = (1 + q^2/.71)^{-2}$, form factor scaling to yield the magnetic form factor $G_M = 2.793 G_E$, and the Rosenbluth²³ approximation to the elastic cross section. Statistical errors for this experiment are shown by the inner error bars. The extended lines show the estimated systematic errors. The other points are deduced from fits to the Rosenbluth cross section extrapolated to 4°. The inner error bars on these points represent the errors derived from the fits with statistical errors on the data. The extended lines show the systematic errors quoted by the authors added in quadrature with the statistical errors.
16. The ratio of the deuterium cross section to the smeared proton cross section vs. q^2 for different range of x' as shown. The curves are the

functions $A \left[1 - |F_D(q^2)|^2 \right]$, where values of A are determined from fits to each set of data, and F_D is the deuteron elastic form-factor from Ref. 25. For all points W is greater than 2.1 GeV.

17. Experimental measurements of the smeared neutron-proton ratio, σ_N^S/σ_P^S vs. x' . For this experiment, statistical errors are shown by the inner error bars. The extended lines represent estimates of the systematic errors. No corrections have been made for any possible A-dependence in deuterium. The other data are from Refs. 24 and 26, the error bars do not include estimated systematic errors of about $\pm 6\%$.
18. Extracted values of νW_2 for the proton vs. q^2 . Only data with $W > 2$ GeV and $\omega' > 6$ have been used and $R = \sigma_L/\sigma_T = 0.18$ has been assumed. The errors are statistical only.
19. Extracted values of νW_2 vs. q^2 for the proton assuming $R = 0.18$. The separate ω' ranges are shown. The open circles are 6° data and the dashes 10° data from Ref. 24. The curves are the functions $D \left[1 - W_2^{el}(q^2) \right]$ with values of D determined from fits to each set of data separately.
20. The points below $\omega' = 8$ are values of νW_2 for the proton from Ref. 12. The data above $\omega' = 8$ are the values of D shown in Table VIII. The solid line is a fit to all the data shown using statistical errors on the data only.
21. The residuals from the quadratic fits to the cross section for the range $2 \text{ GeV} < W < 3 \text{ GeV}$ for each energy. The $\chi^2/\text{degree of freedom}$ for each fit is shown.
22. Measured values of $B(q^2, W)$ (see text) vs. missing mass, W. The curves show the fit and typical contributions of the resonances and background.

Each lower energy line is offset upward by $30 \mu\text{b}$. The top line is photoproduction data of Ref. 30 offset by $210 \mu\text{b}$. The succeeding lines are the data from the current experiment for 4.5, 7, 10, 13, 16, 18, and 20 GeV. The curves along the bottom axis show the decomposition of the 20 GeV line into the contributions from the individual resonances and the background. production data of Ref. 30 offset by $210 \mu\text{b}$.

23. Measured values of the transition form factor for $\Delta(1238)$ production compared to the dipole $G_D(q^2) = 3/(1+q^2/.71)^2$ vs. q^2 . The open circle is from a fit to photoproduction data of Ref. 30. The other measurements are from Ref. 31.
24. Measured values of the cross section from the resonances evaluated at each resonance mass vs. q^2 . The open circles are from fits to photoproduction data of Ref. 30. Errors are statistical only.
25. Measured values of the ratio of resonance peak cross sections to the background at each peak as determined from the fits. The open circles are from fits to photoproduction (Ref. 30).
26. Measured values of the cross section $d^2\sigma/d\Omega dE'$ vs. W for each of the six targets as shown:
 - a) Incident energy, $E_0 = 13 \text{ GeV}$
 - b) Incident energy, $E_0 = 20 \text{ GeV}$ (note suppressed zeros)

The closed circles are before any radiative corrections; the open circles are after elastic and quasi-elastic tails are subtracted. Statistical errors are shown where they are larger than the plotted points. Data where the subtraction arising from radiative corrections exceeds 25% are not used in the subsequent analysis.

27. The shadowing factor F (see text) vs. A for each kinematic point. The lines are fits to the form $a_0 A^\epsilon$ for each plot. Only statistical errors are shown.
- Incident energy, $E_0 = 13$ GeV
 - Incident energy, $E_0 = 20$ GeV
28. The exponent, ϵ , from the fits to the shadowing factor $F = a_0 A^\epsilon$ vs. x' . The closed circles are from the 13-GeV data, open circles from the 20-GeV data. Only statistical errors are shown in the figure. Systematic errors can shift the values of ϵ by as much as ± 0.02 .

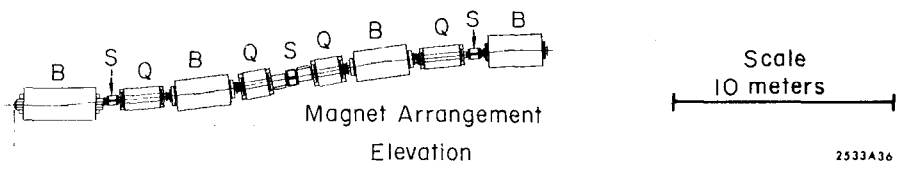
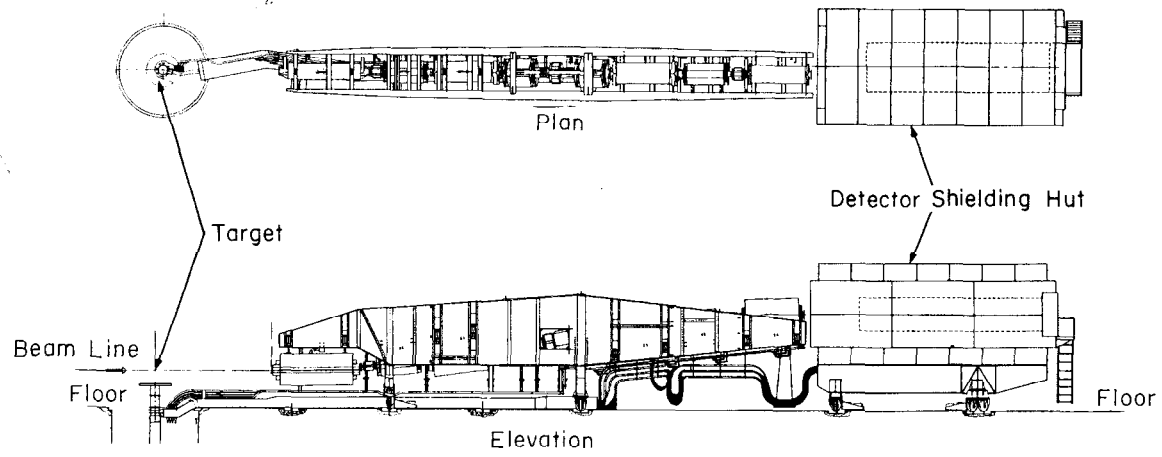


Fig. 1

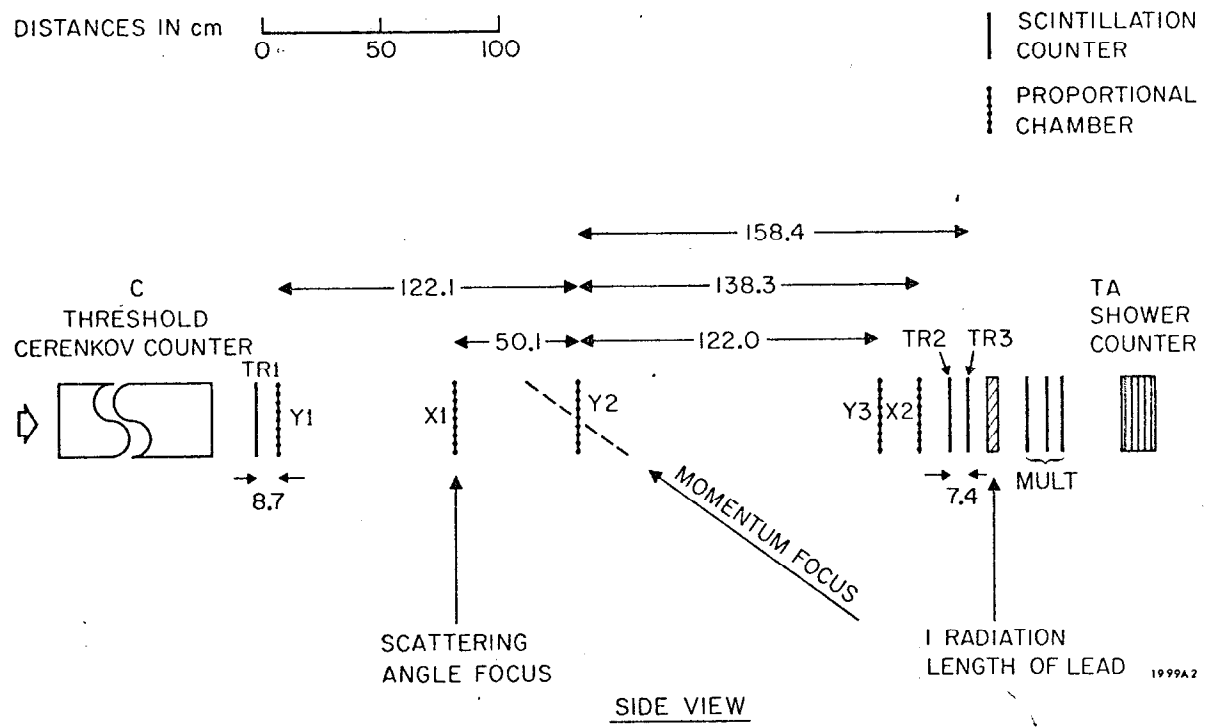


Fig. 2

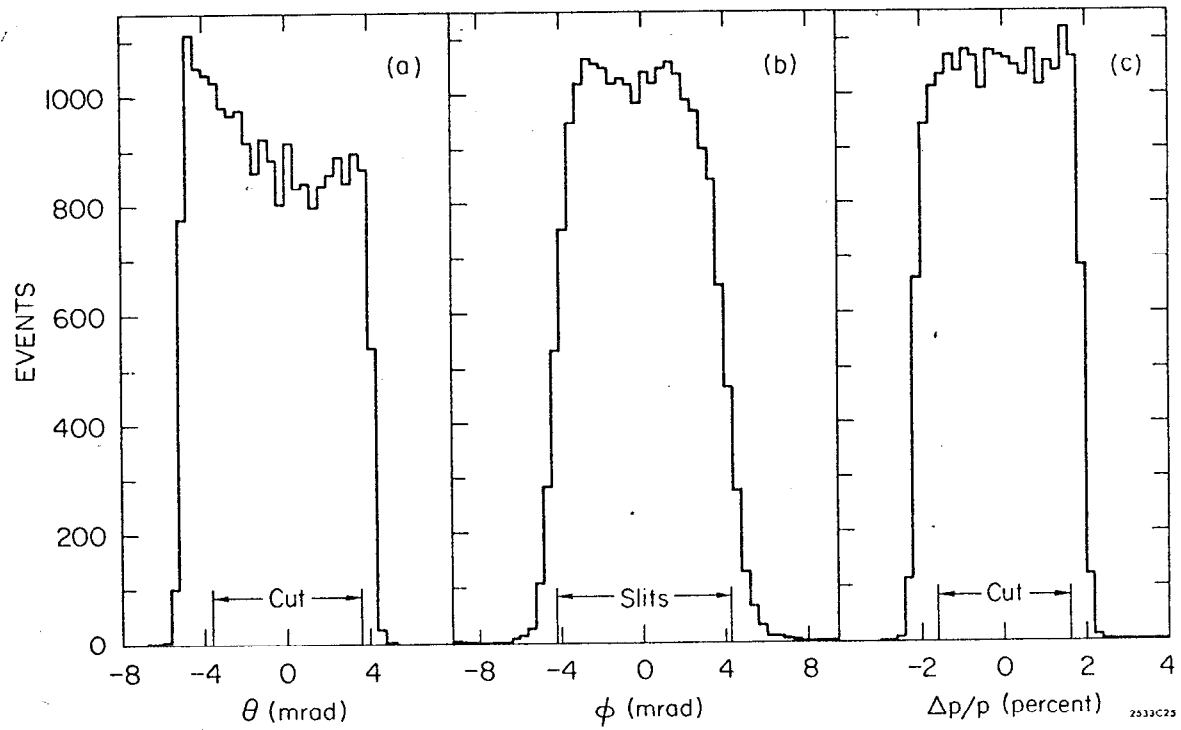


Fig. 3

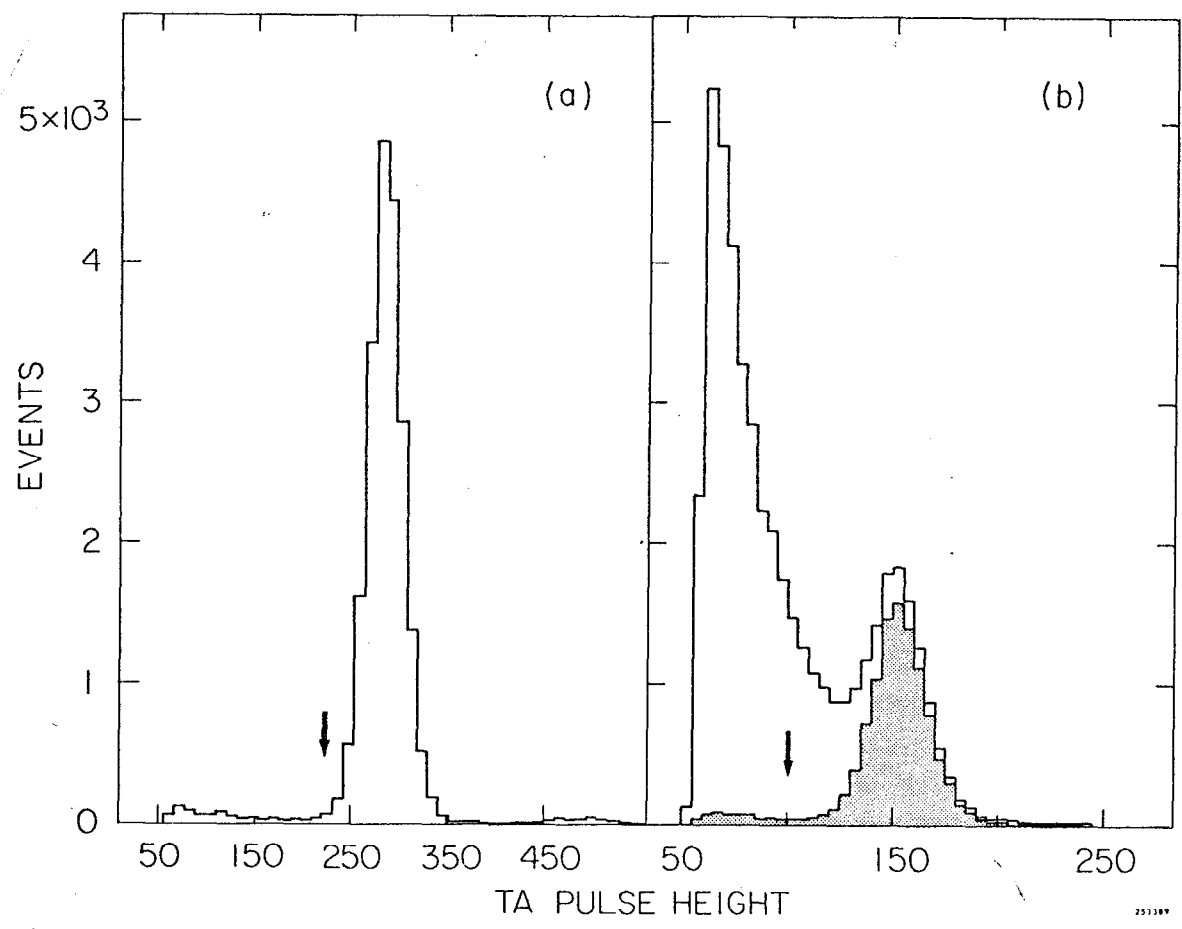


Fig. 4

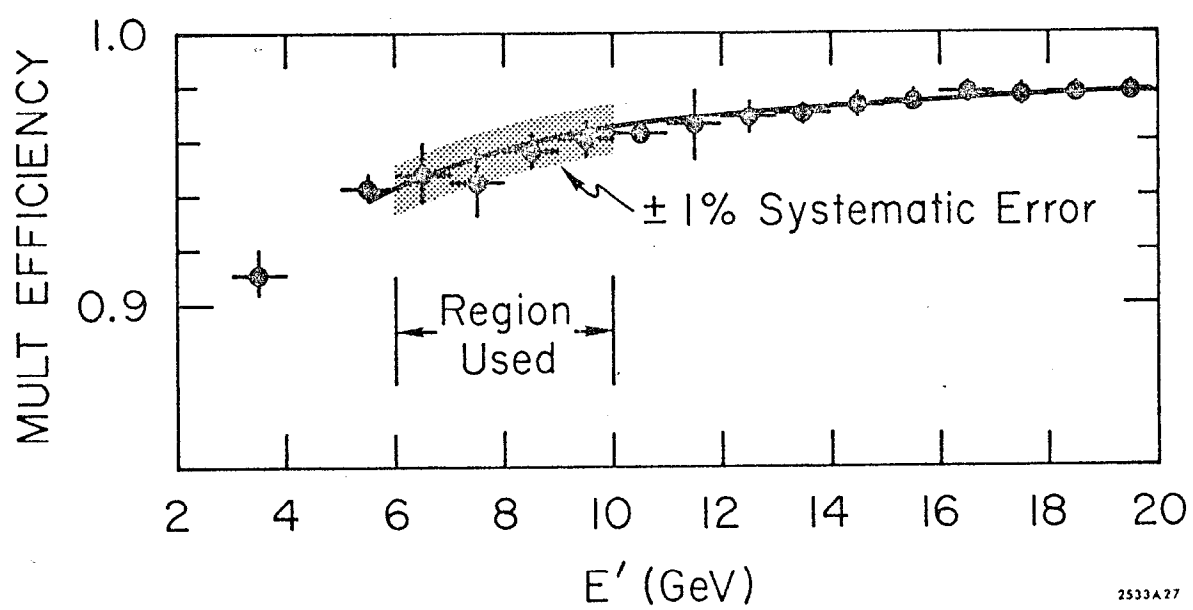


Fig. 5

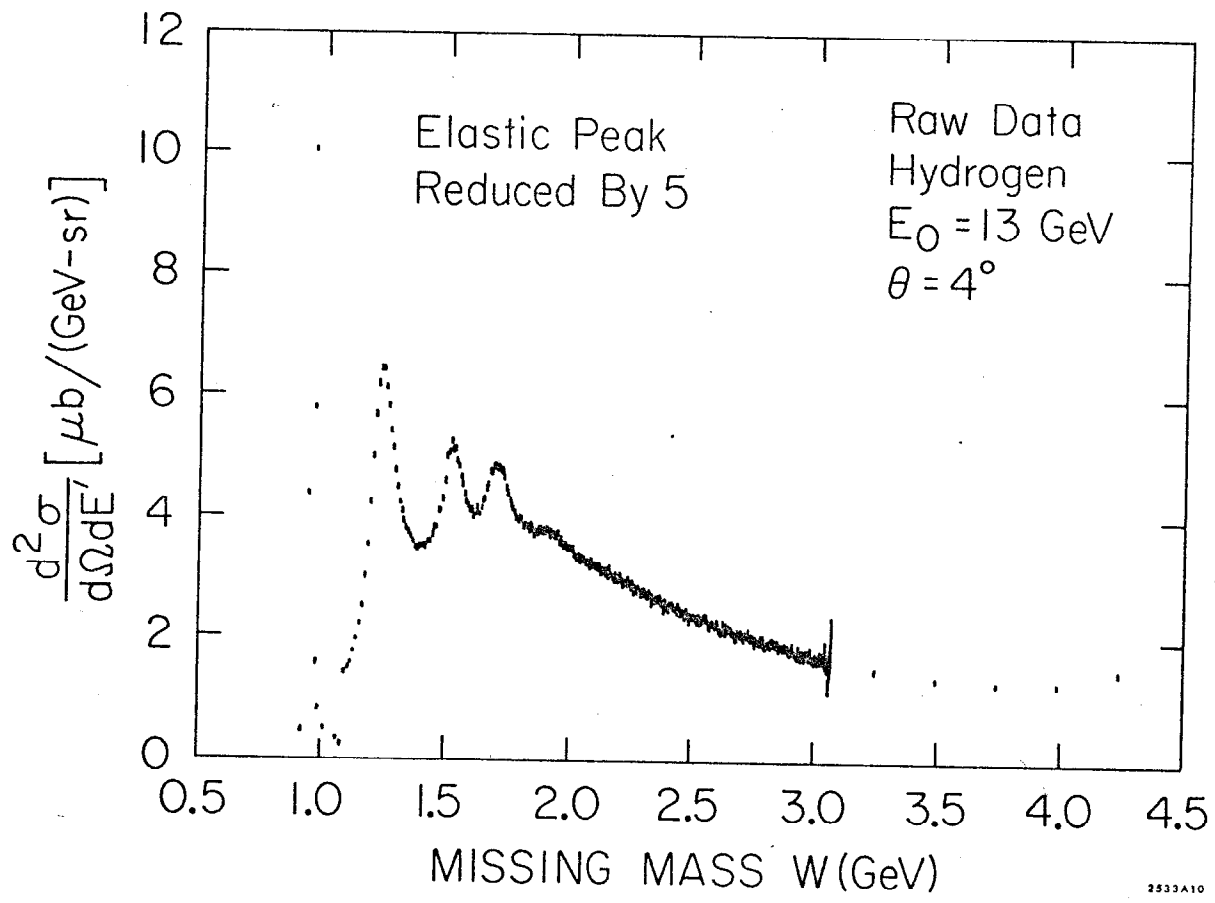
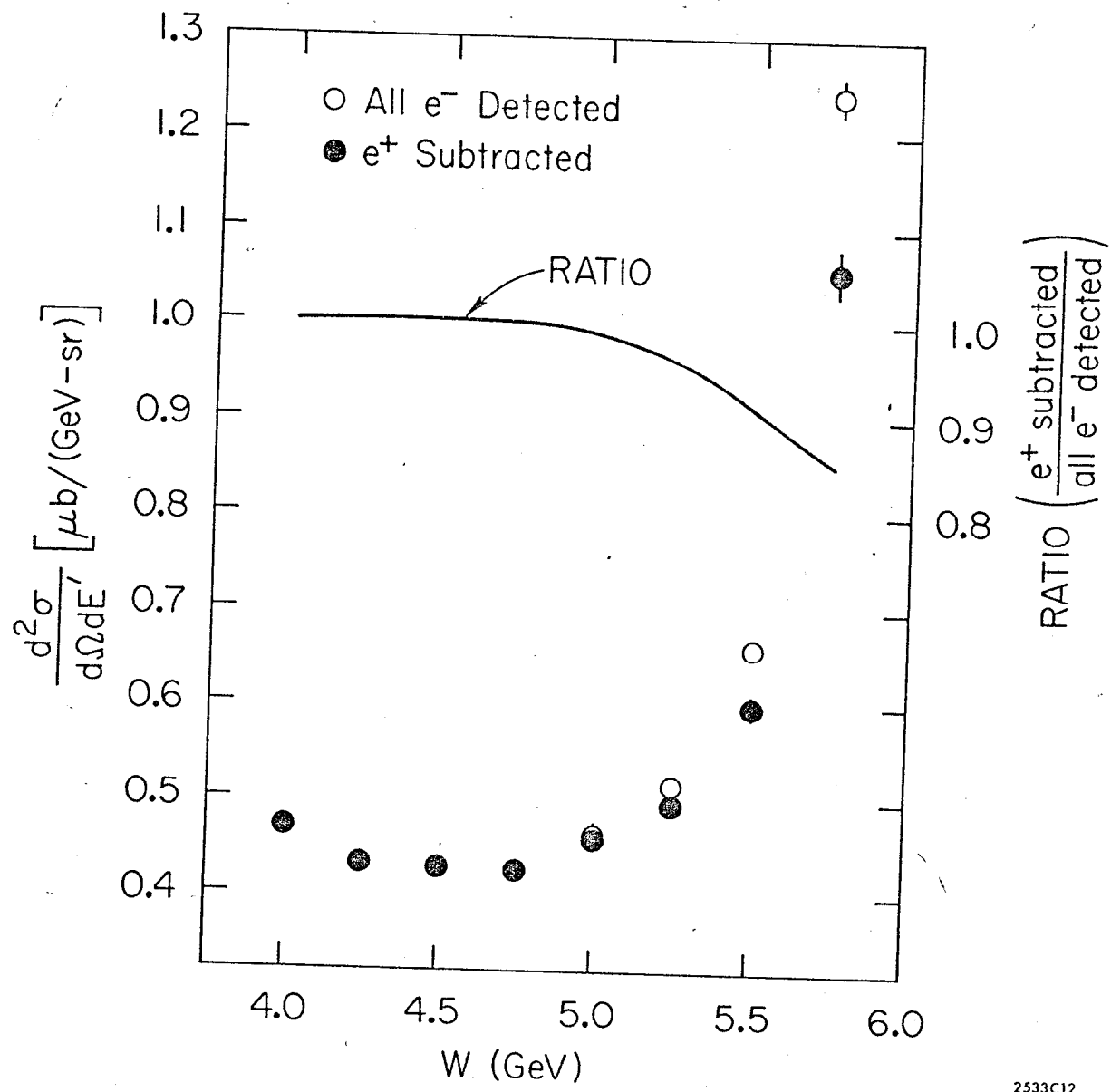


Fig. 6



2533C12

Fig. 7

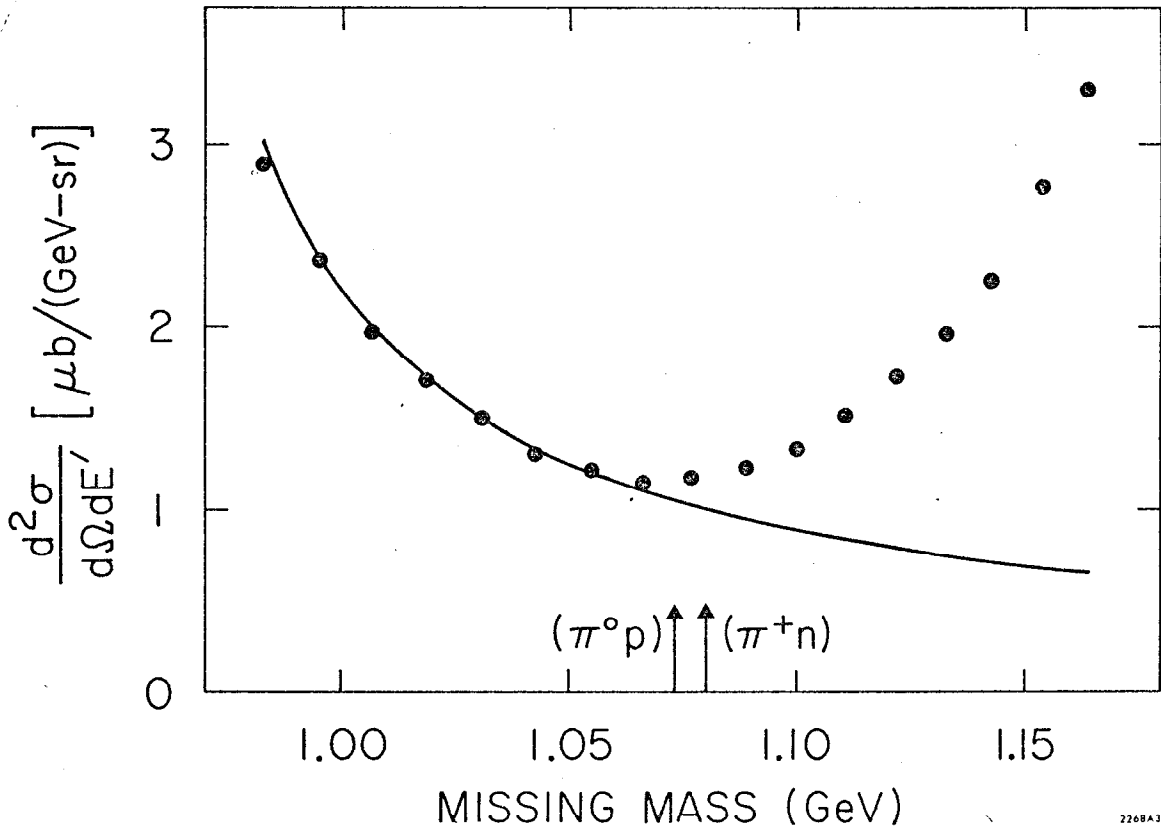


Fig. 8

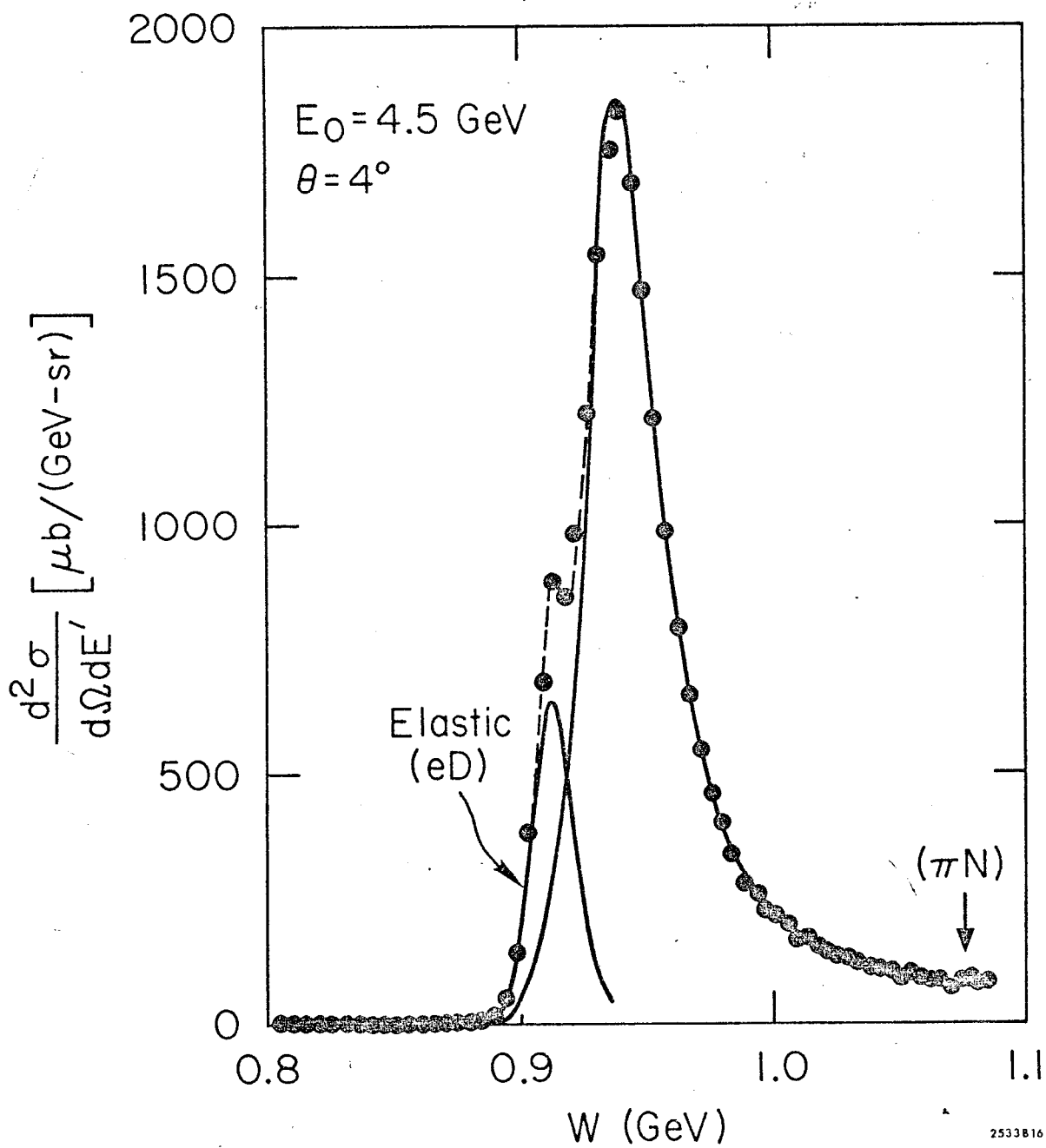


Fig. 9

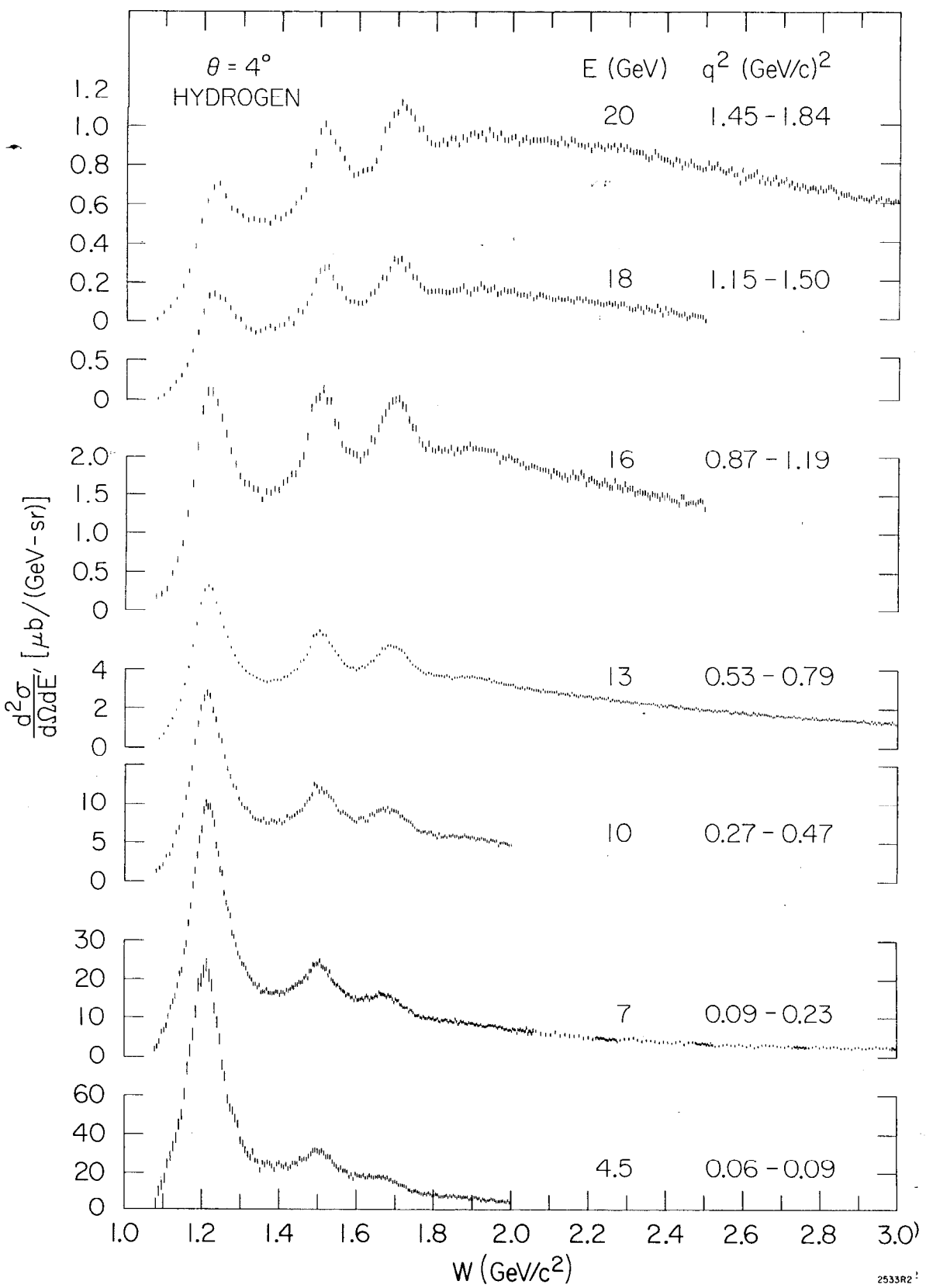


Fig. 10 a

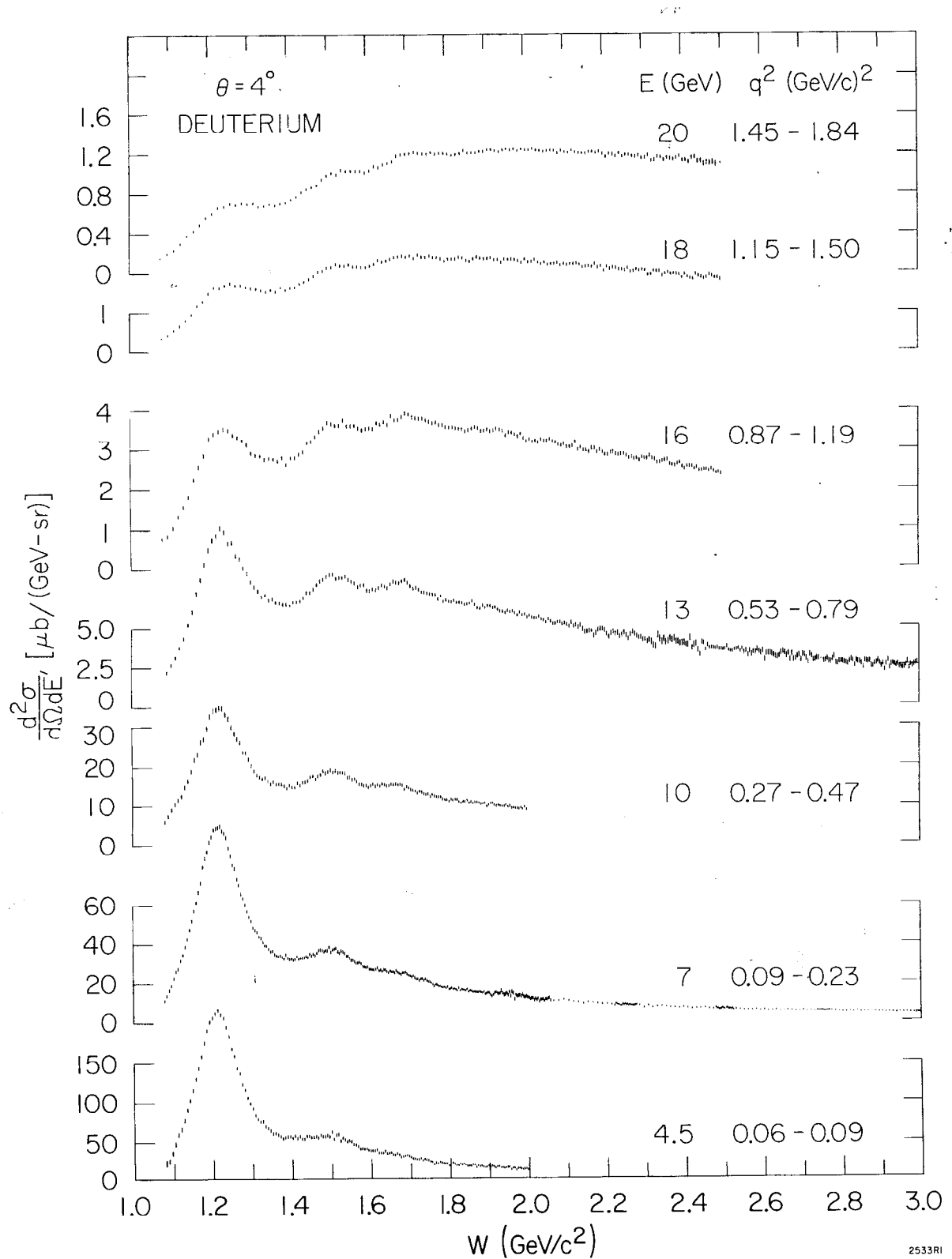


Fig. 10b

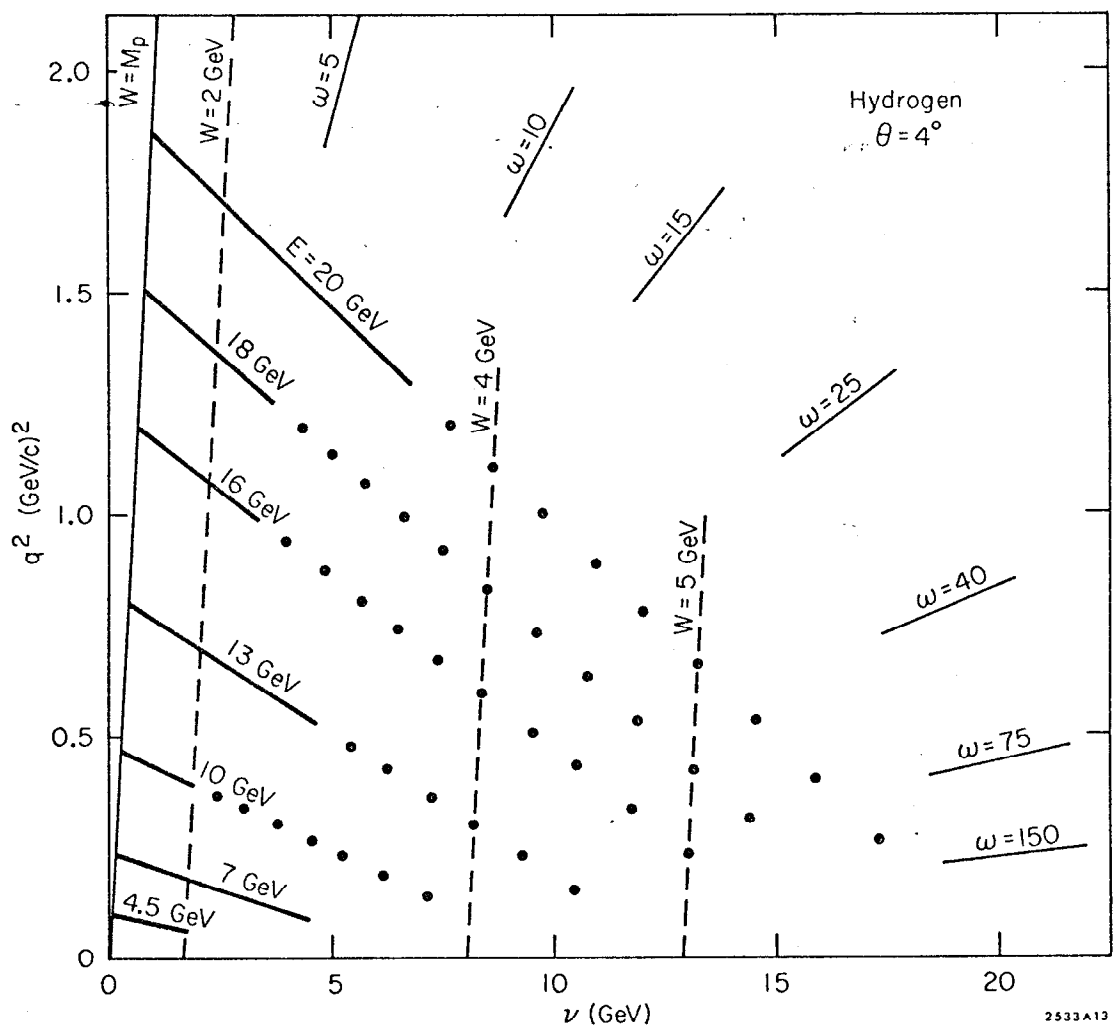


Fig. 11

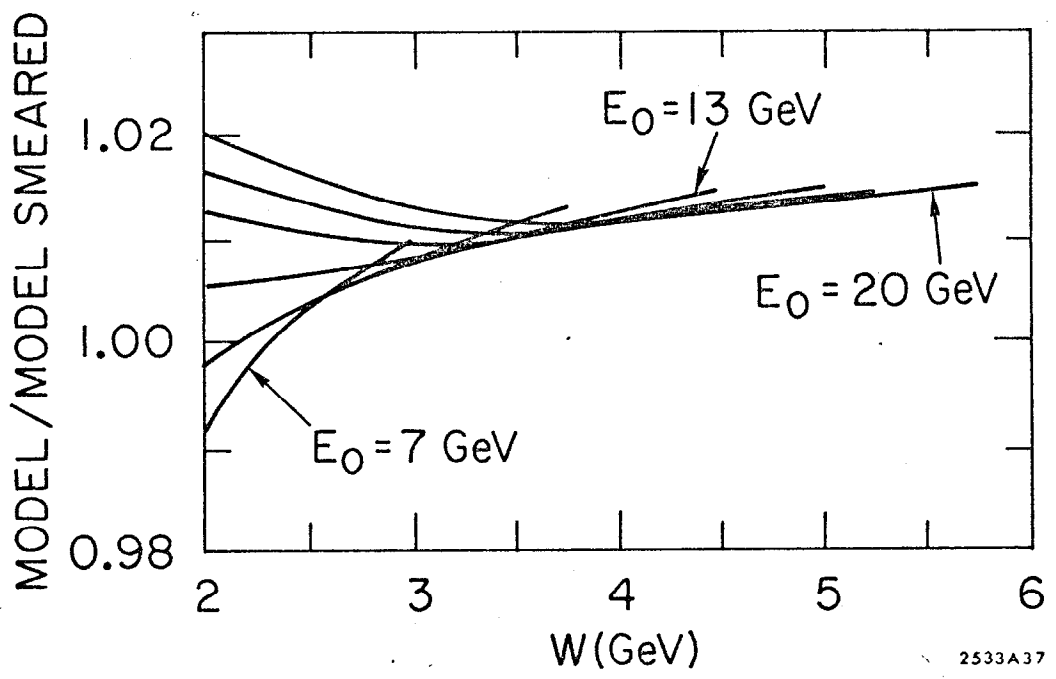


Fig. 12

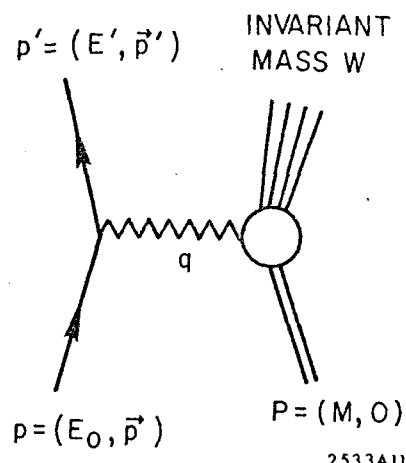


Fig. 13

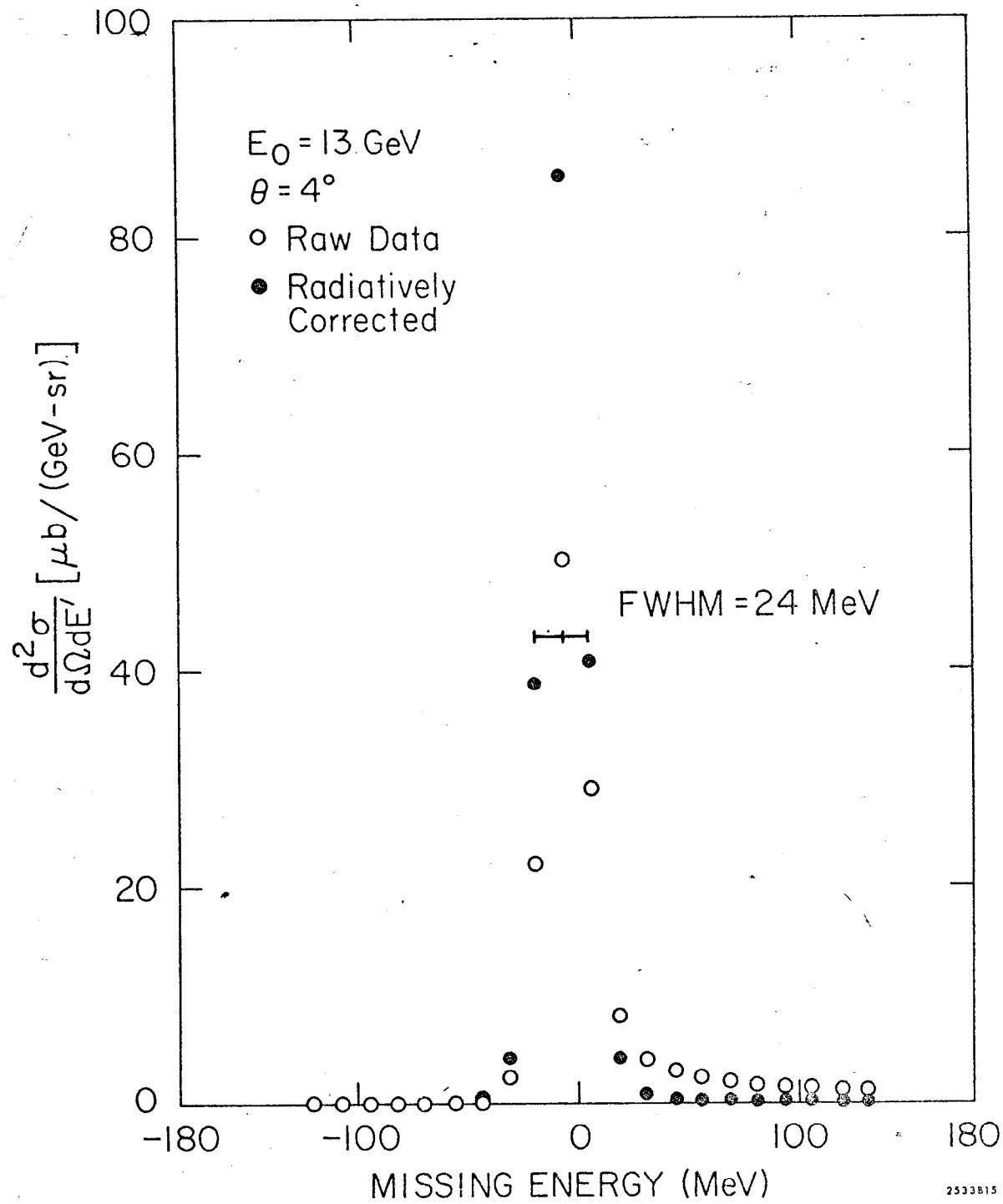


Fig. 14

2533B15

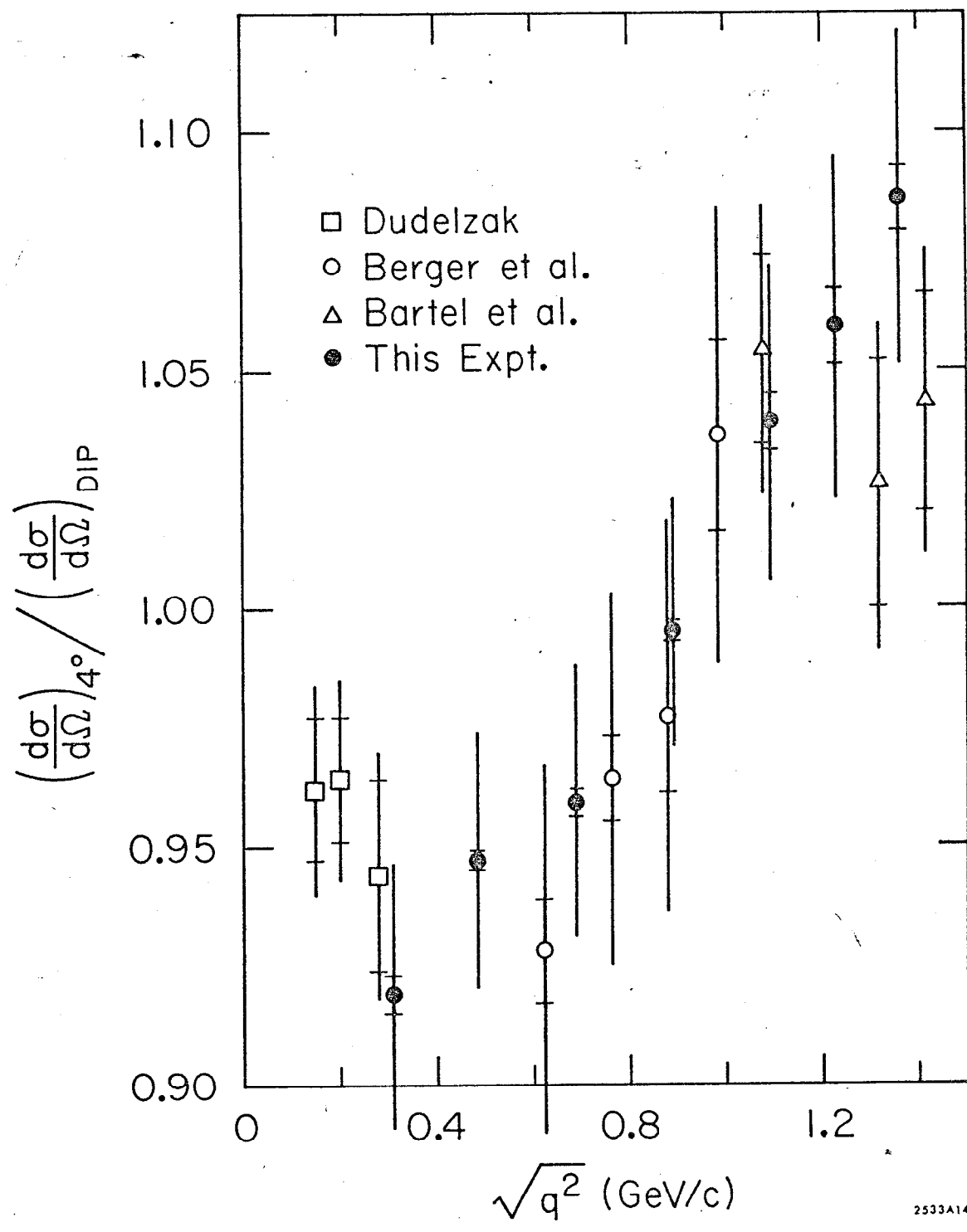


Fig. 15

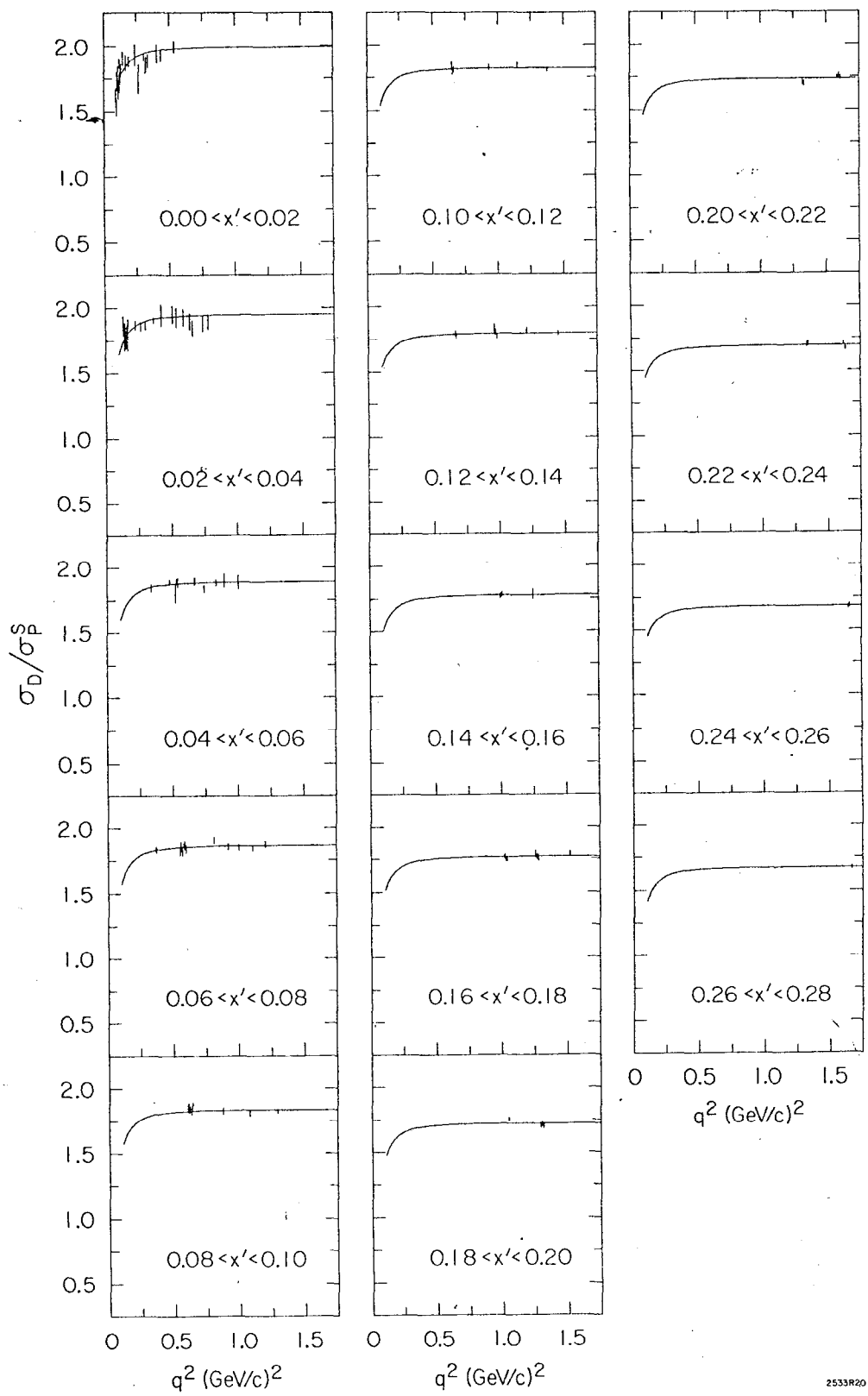


Fig. 16

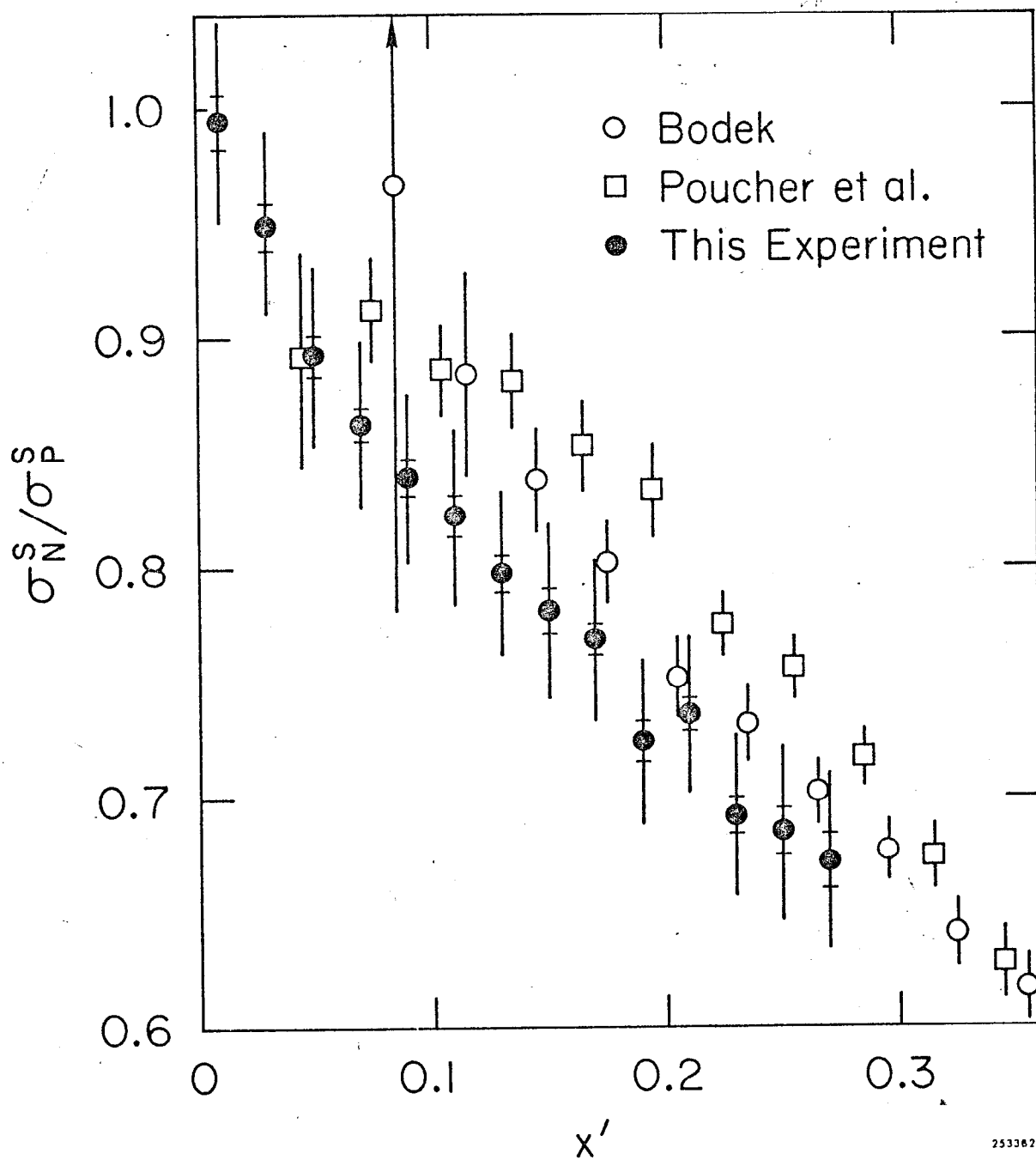


Fig. 17

2533626

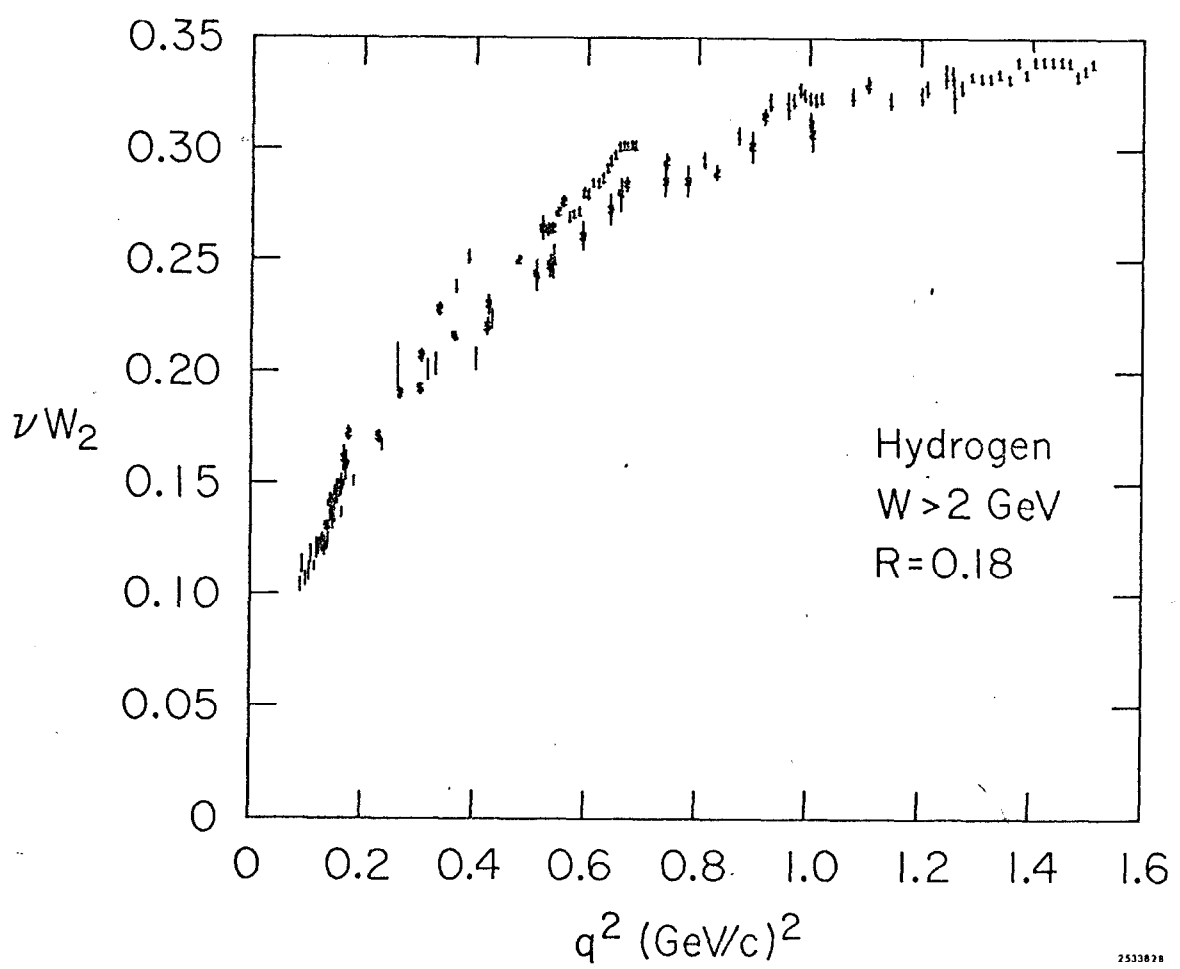


Fig. 18

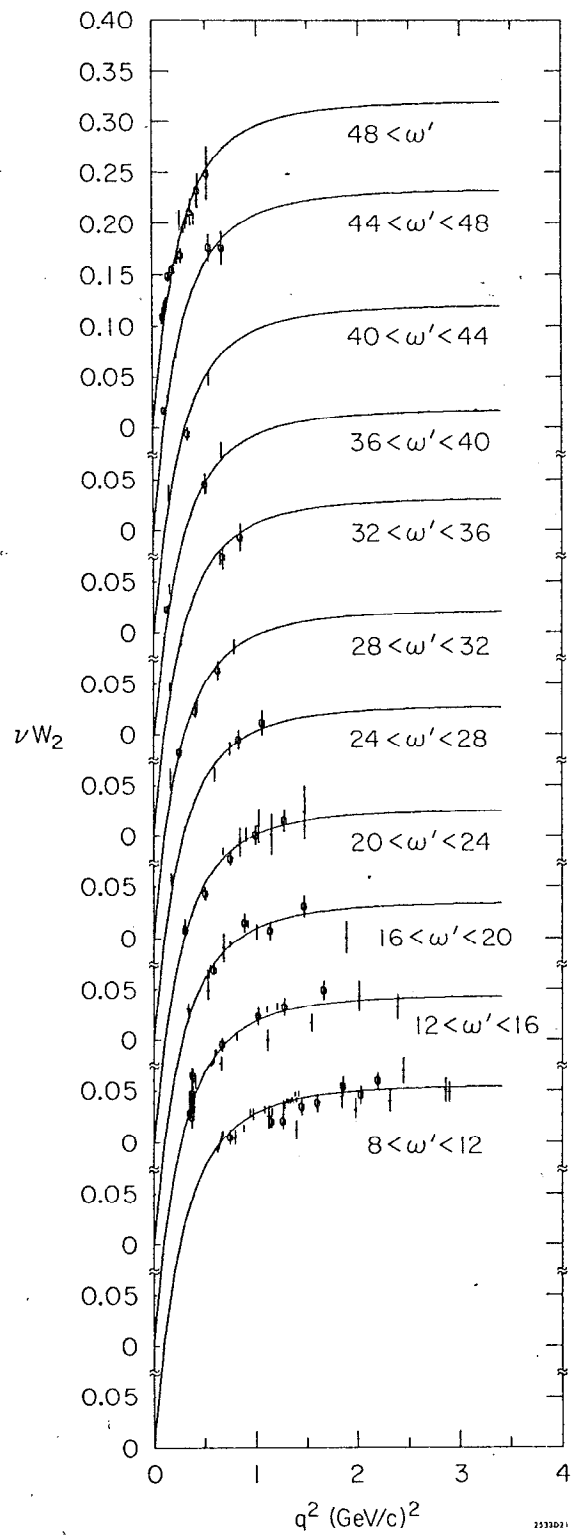


Fig. 19

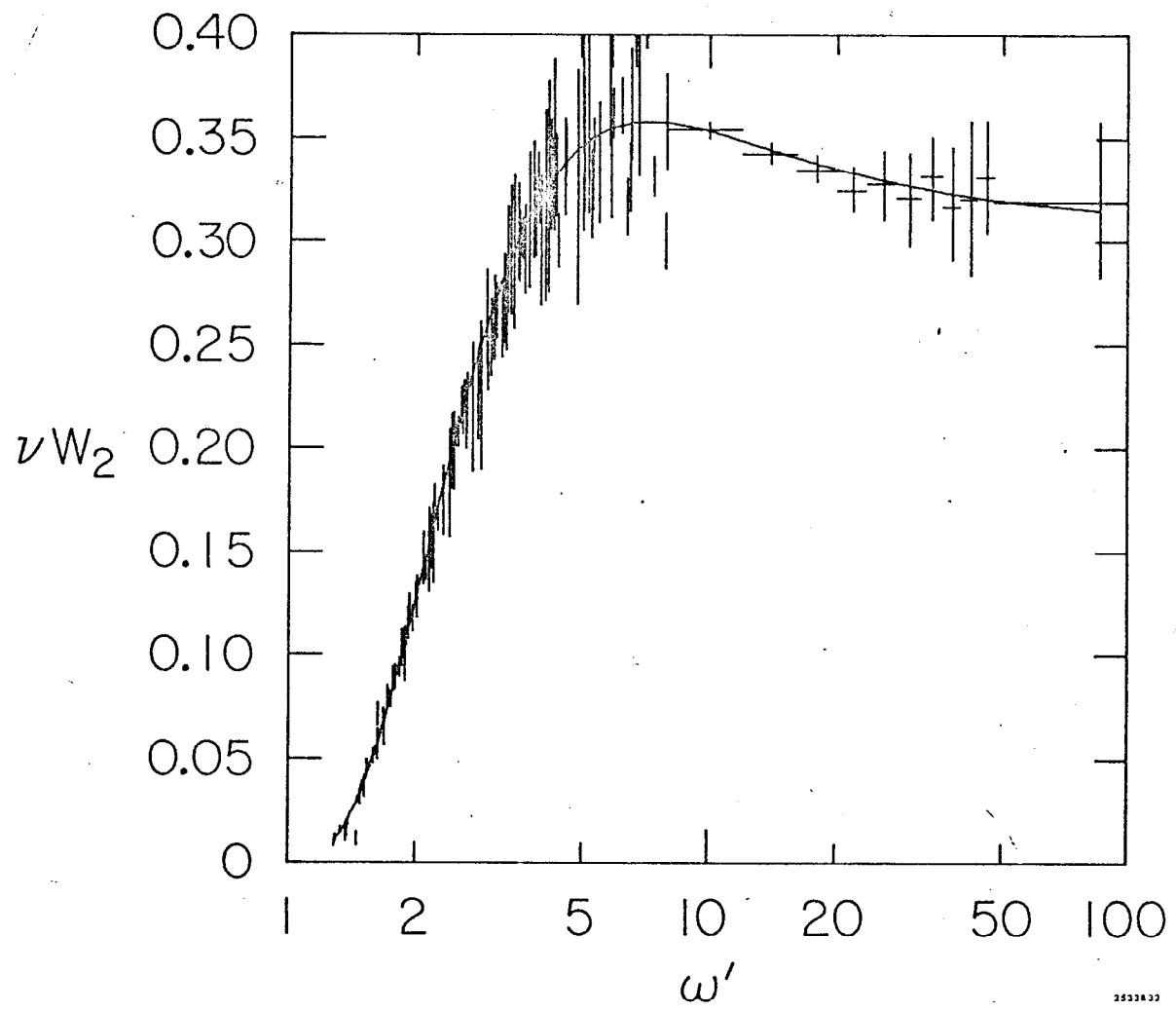


Fig. 20

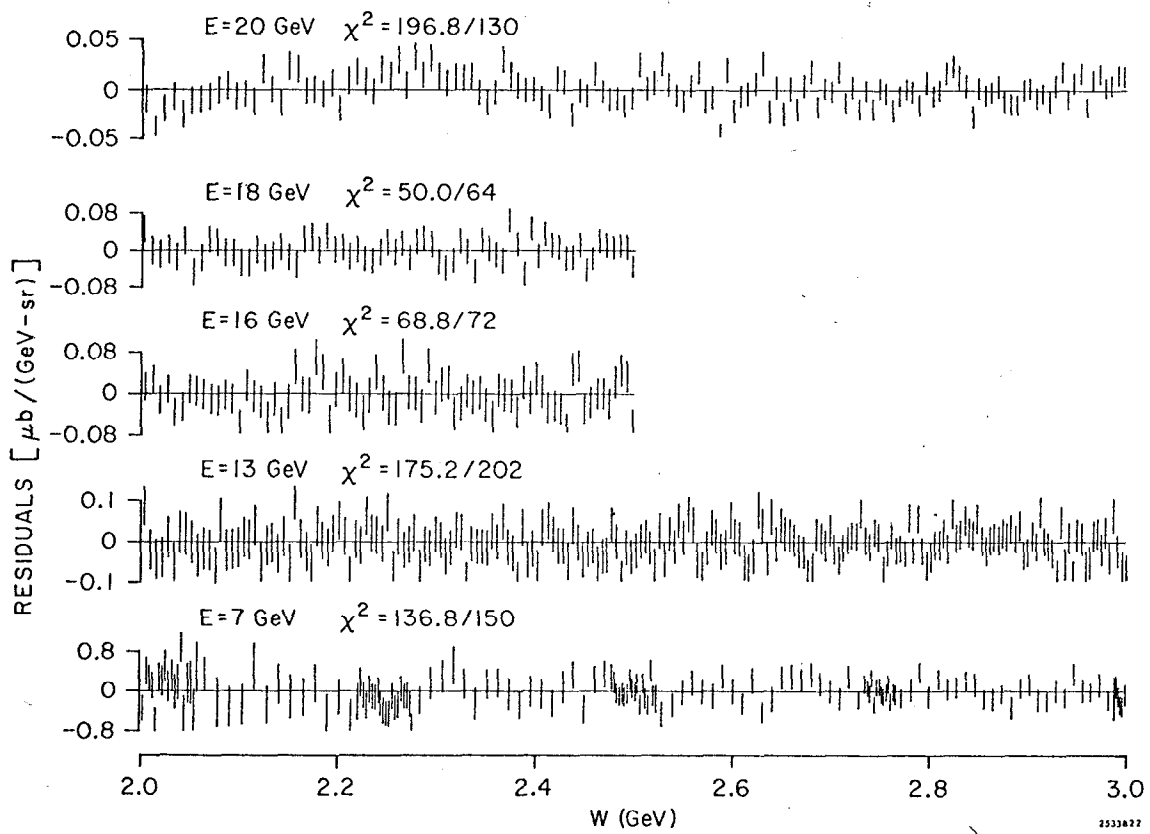


Fig. 21

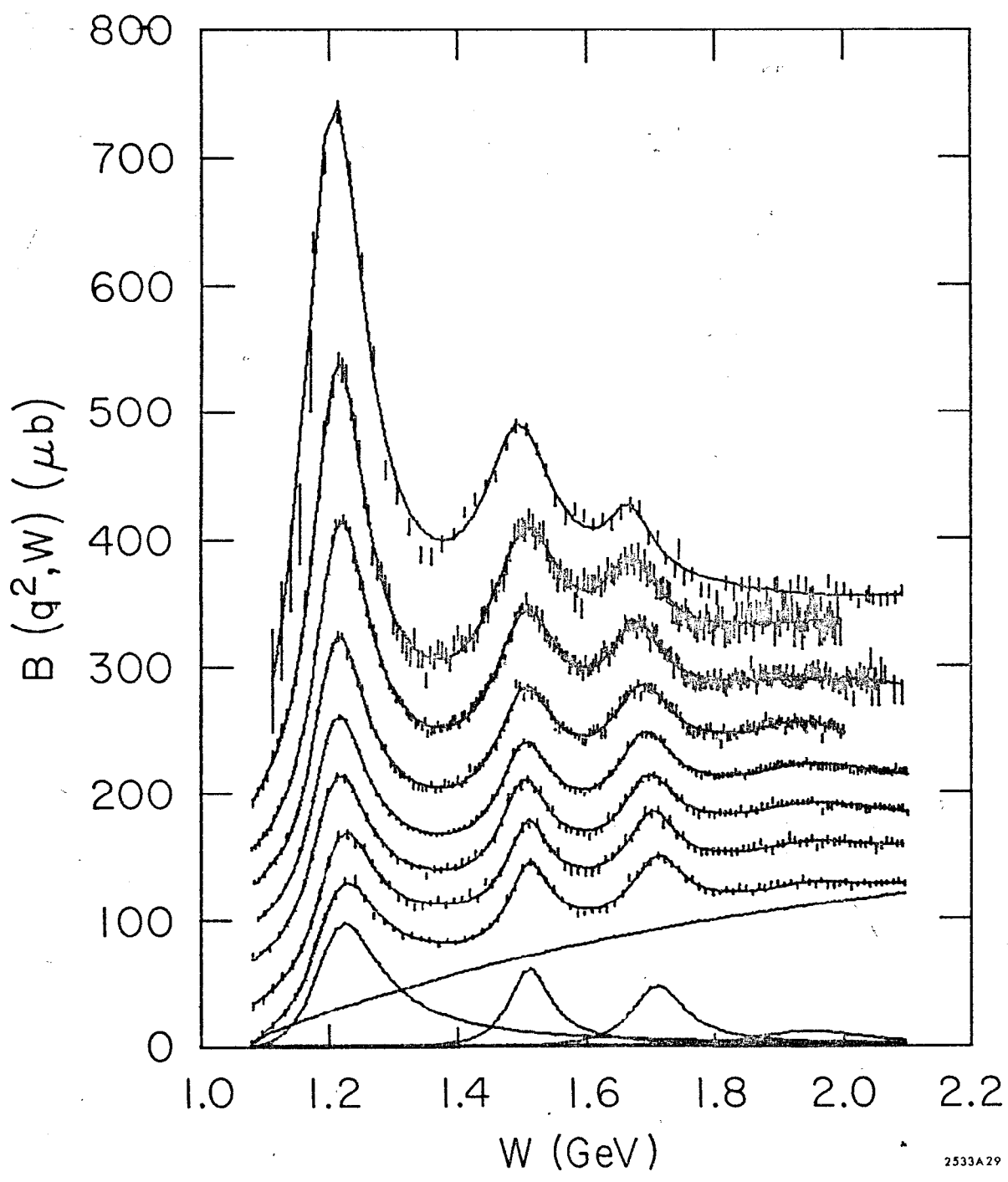


Fig. 22

2533A29

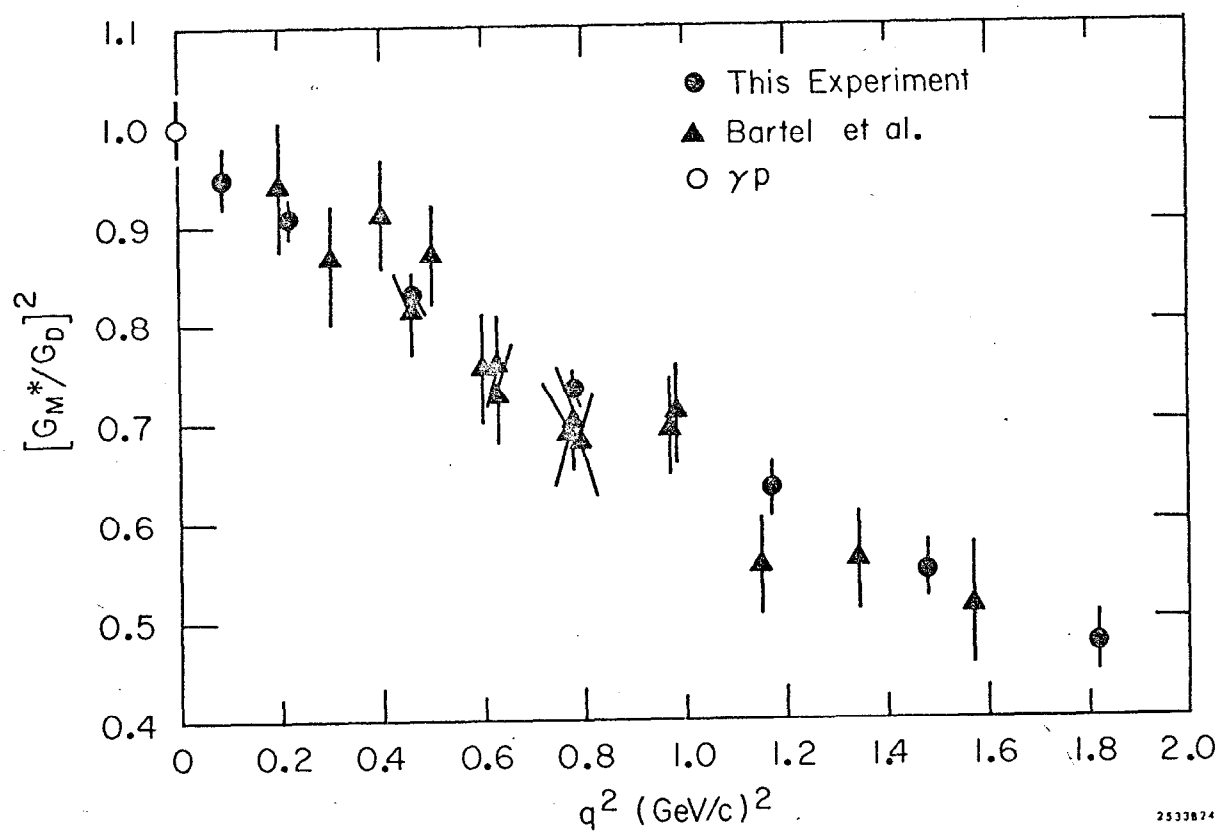


Fig. 23

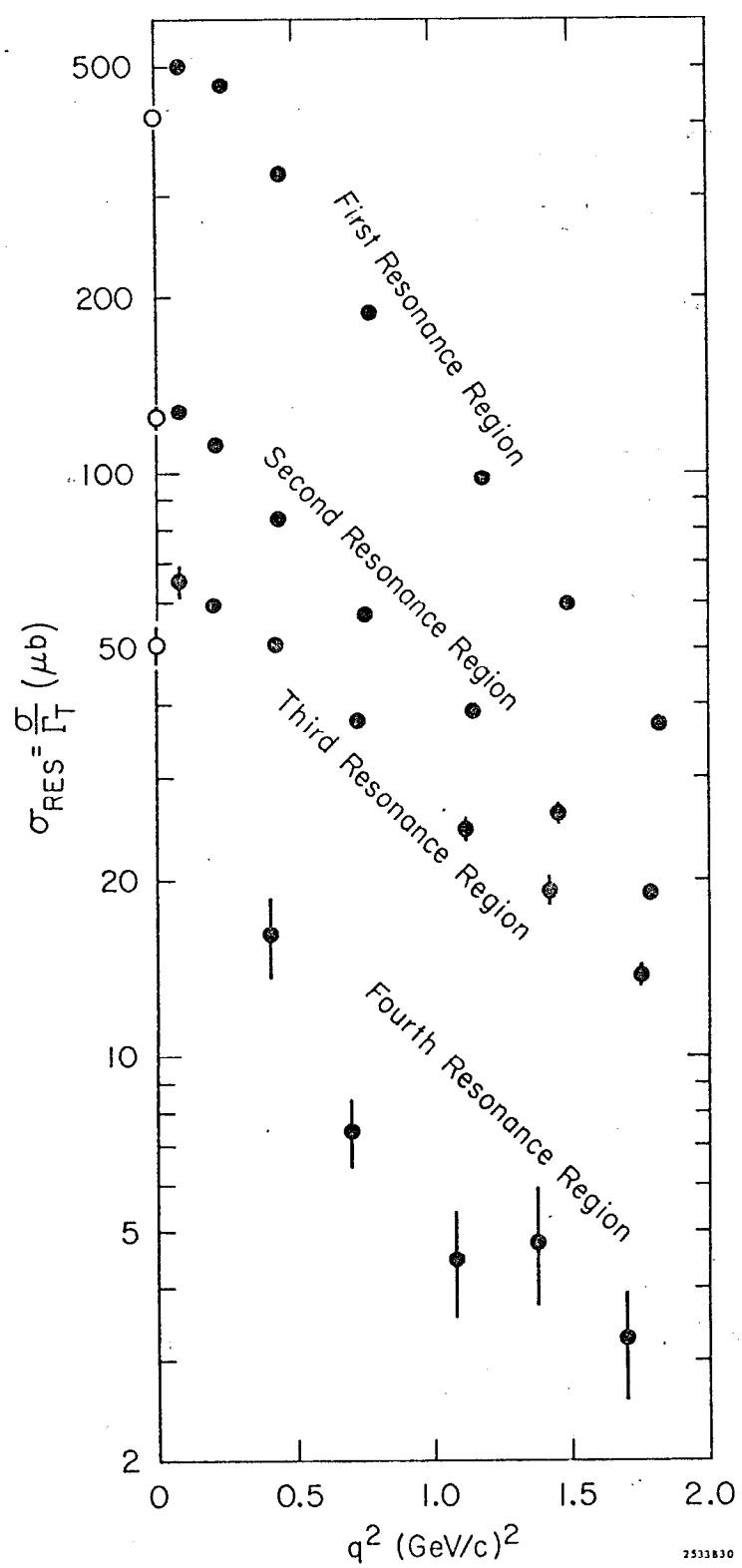


Fig. 24

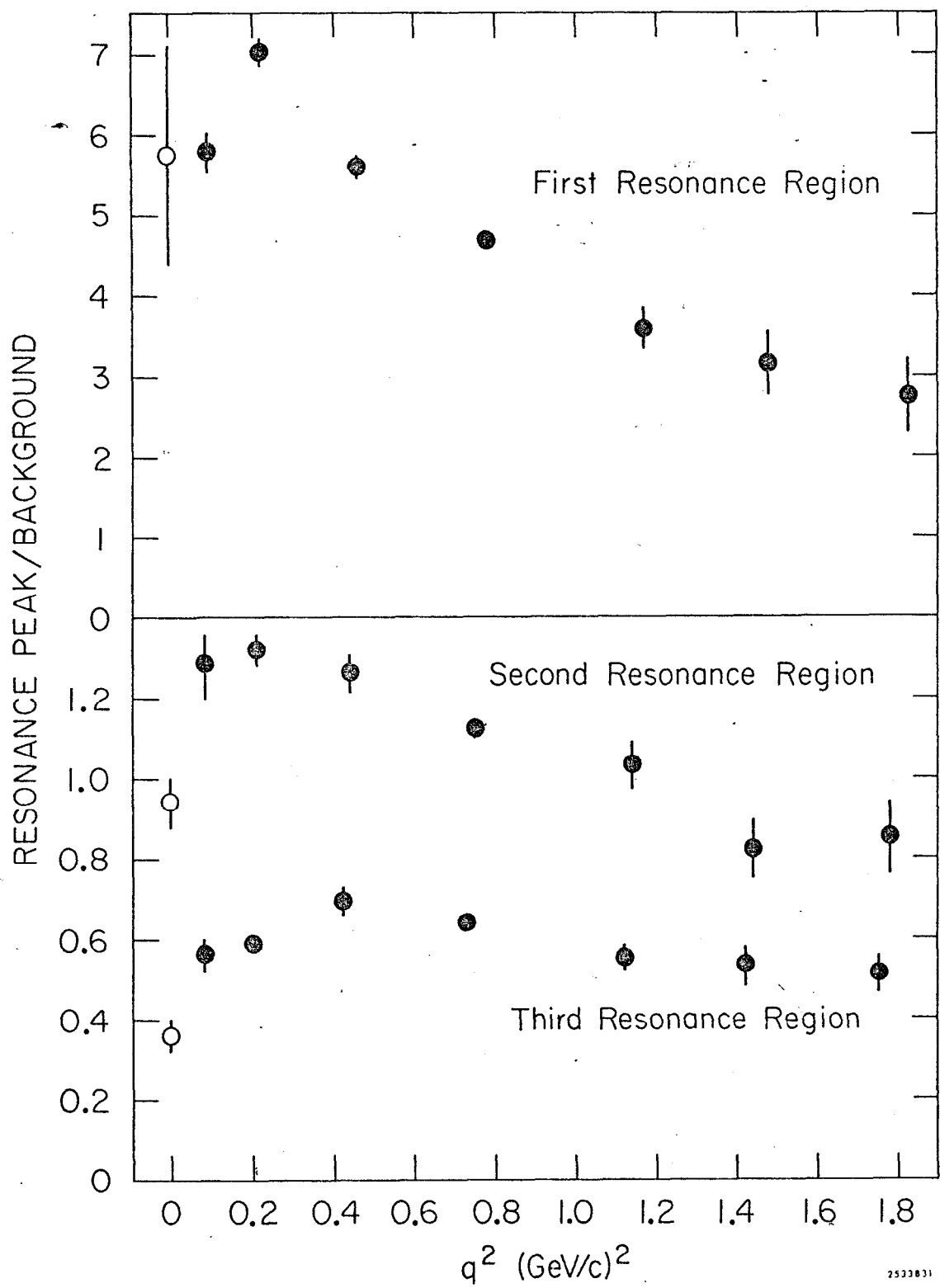


Fig. 25

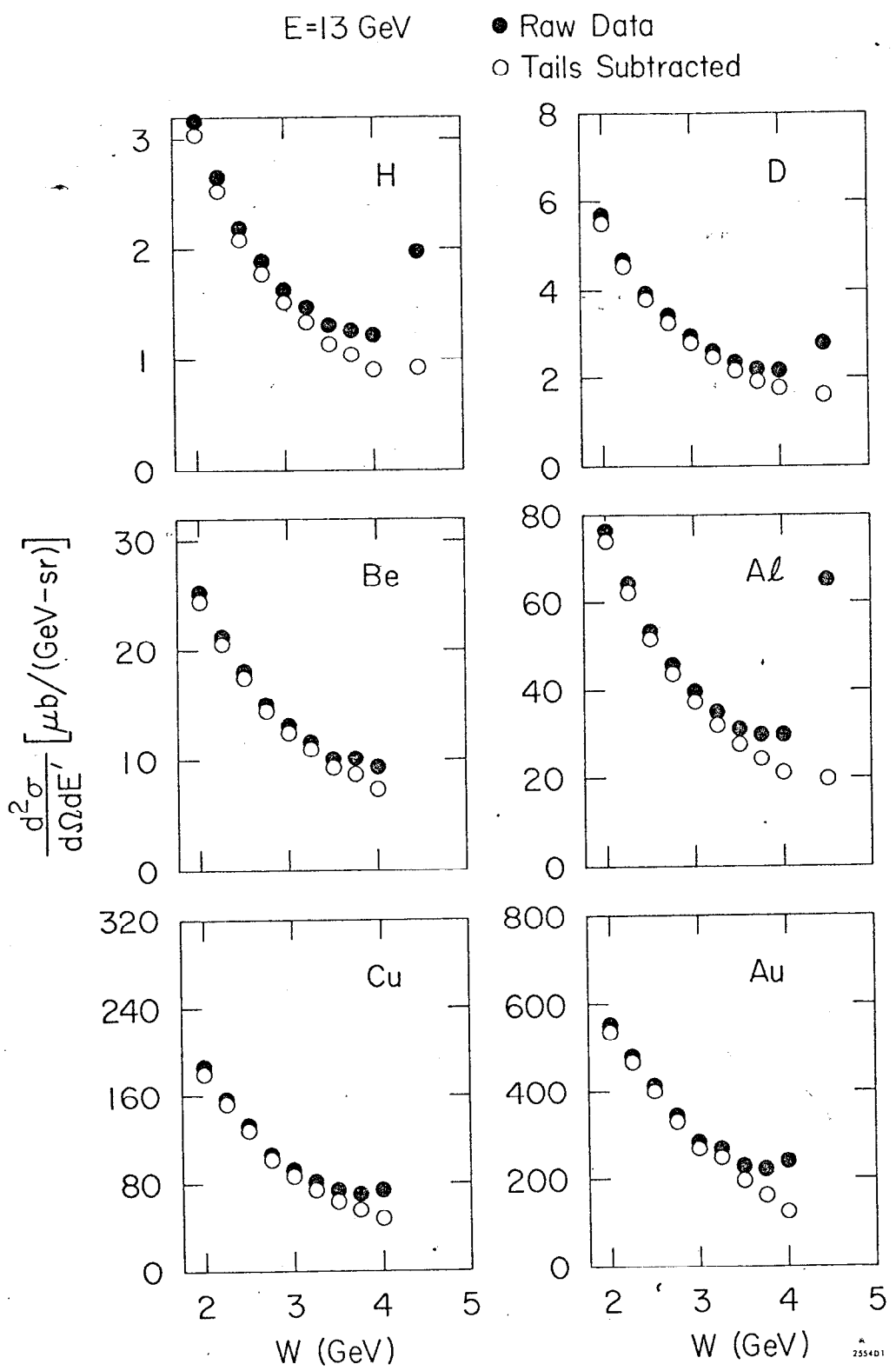


Fig. 26a

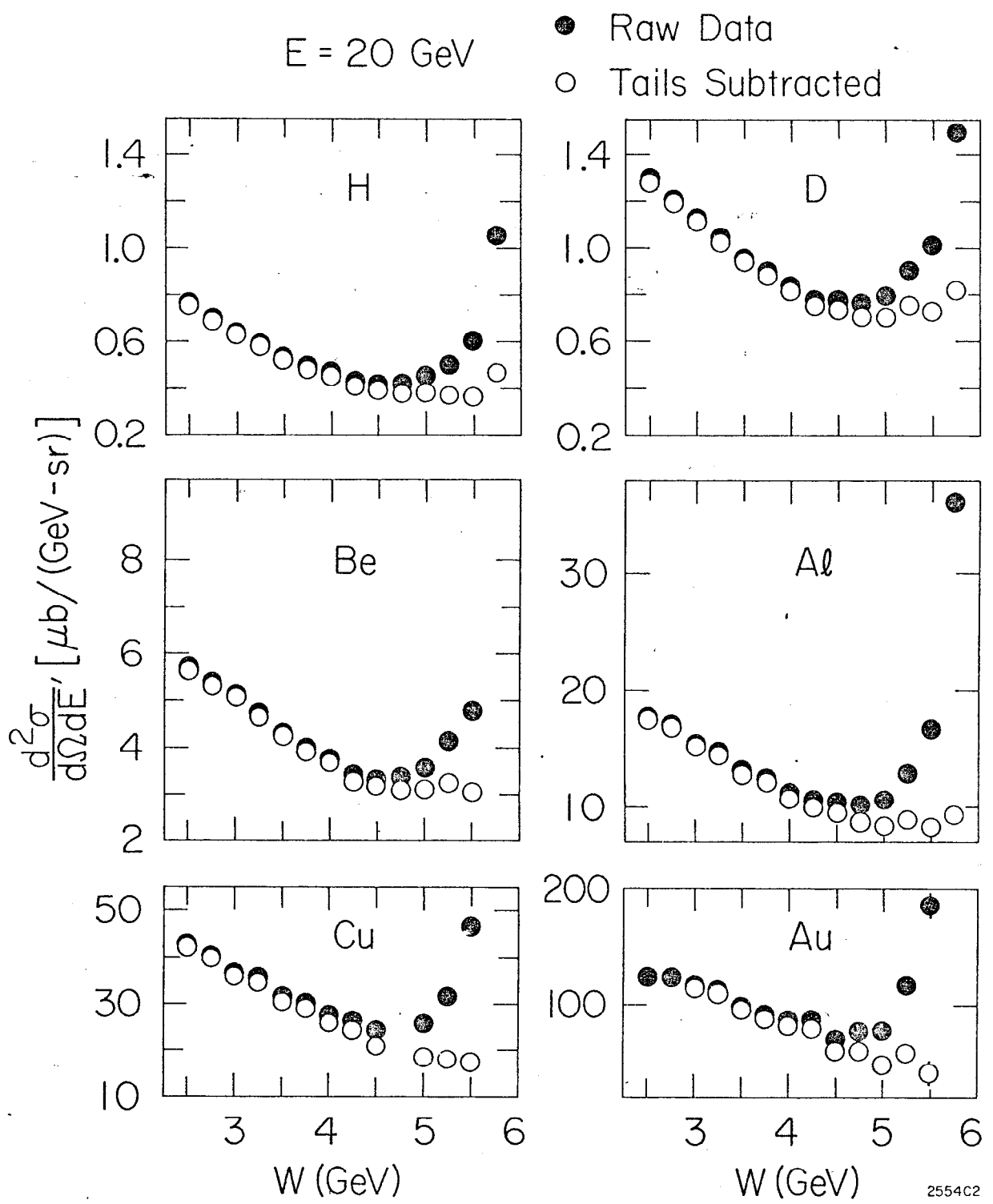


Fig. 26b

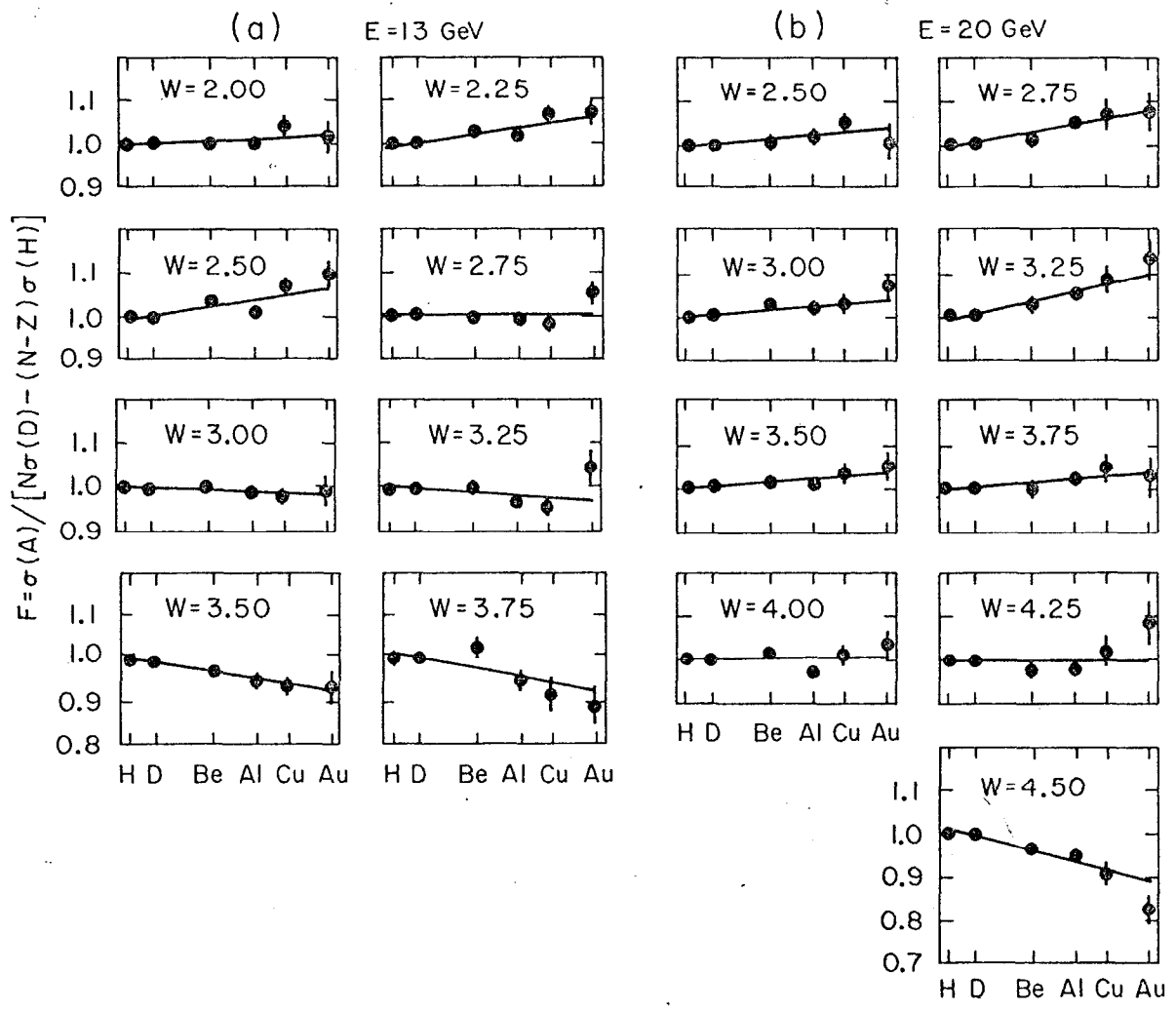


Fig. 27

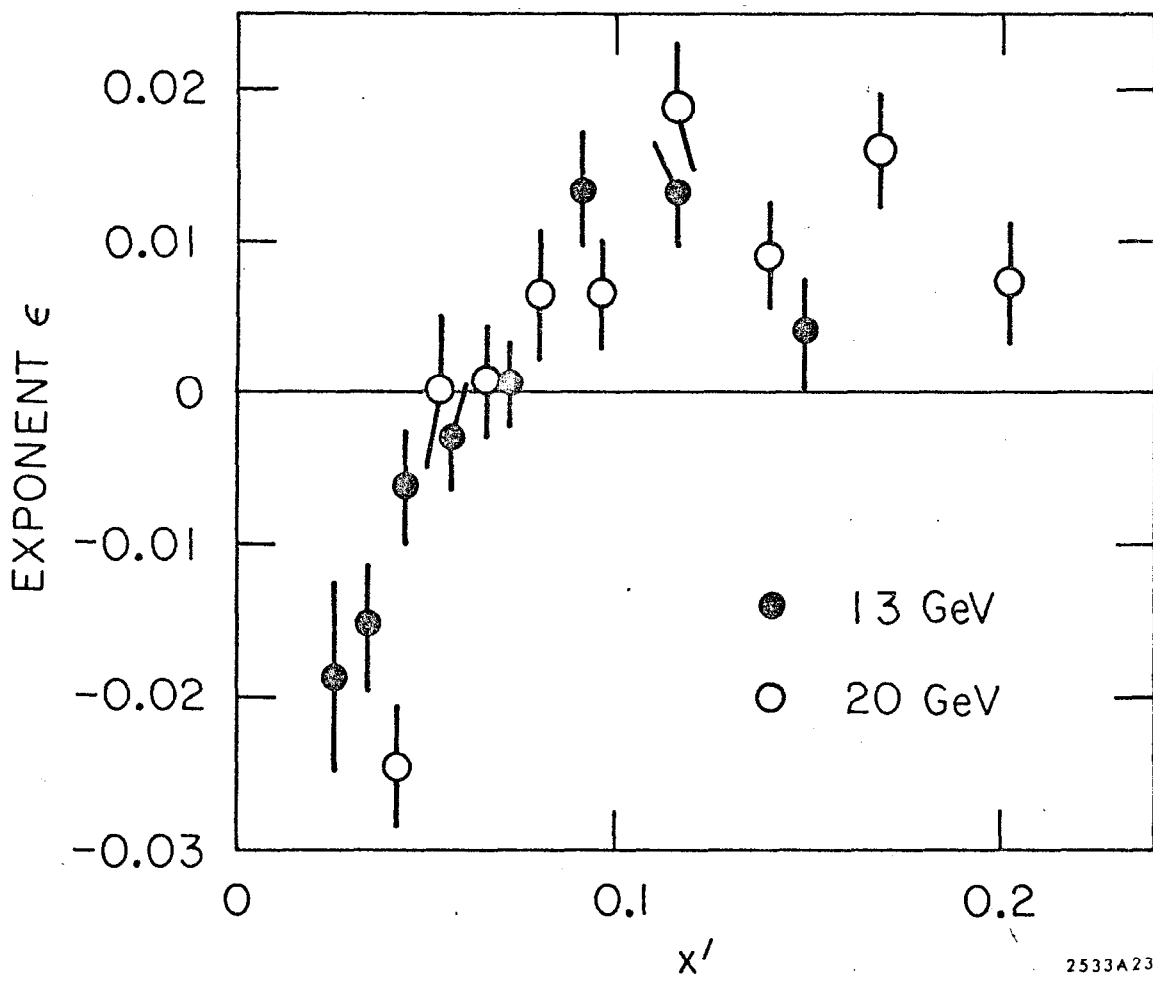


Fig. 28

APPENDIX C

TABLE OF CROSS SECTIONS FOR HYDROGEN AND DEUTERIUM

All of the cross sections are listed as a function of the missing mass W for each of the different energies. The errors are just statistical except for ten points on each target as explained in the text.

These are the tables referred to in S. Stein et al., Phys. Rev. D 12, 1884 (1975), on p. 1891, as reference 15a.

C.1

E = 4.499 GeV Hydrogen

W (GeV)	$\frac{d\sigma}{d\Omega dE}$ [$\mu b/(GeV \cdot sr)$]	W (GeV)	$\frac{d\sigma}{d\Omega dE}$ [$\mu b/(GeV \cdot sr)$]	W (GeV)	$\frac{d\sigma}{d\Omega dE}$ [$\mu b/(GeV \cdot sr)$]	W (GeV)	$\frac{d\sigma}{d\Omega dE}$ [$\mu b/(GeV \cdot sr)$]
1.080	7.694 ± 2.558	1.089	13.956 ± 2.487	1.096	17.070 ± 2.453	1.104	20.537 ± 2.434
1.111	28.145 ± 2.480	1.119	32.054 ± 2.514	1.126	37.143 ± 2.586	1.134	41.517 ± 2.618
1.141	48.283 ± 2.708	1.149	53.513 ± 2.797	1.156	64.099 ± 2.932	1.163	77.134 ± 3.109
1.170	86.537 ± 3.192	1.178	94.889 ± 3.114	1.185	106.444 ± 3.175	1.192	120.279 ± 3.281
1.199	122.640 ± 3.275	1.206	127.244 ± 3.291	1.213	130.475 ± 3.290	1.220	125.017 ± 3.181
1.227	120.021 ± 3.083	1.234	108.151 ± 2.917	1.240	100.938 ± 2.798	1.247	92.353 ± 2.661
1.254	78.817 ± 2.484	1.261	72.961 ± 2.393	1.267	61.720 ± 2.210	1.274	56.936 ± 2.124
1.281	55.395 ± 2.068	1.287	51.443 ± 1.990	1.294	48.534 ± 1.923	1.300	40.326 ± 1.800
1.307	38.631 ± 1.753	1.313	35.412 ± 1.693	1.320	33.025 ± 1.653	1.326	31.464 ± 1.592
1.332	34.543 ± 1.589	1.339	29.054 ± 1.464	1.345	29.359 ± 1.409	1.351	24.840 ± 1.297
1.357	28.901 ± 1.311	1.364	27.503 ± 1.248	1.370	29.152 ± 1.235	1.376	28.287 ± 1.186
1.382	26.837 ± 1.147	1.388	25.086 ± 1.100	1.394	27.802 ± 1.110	1.400	28.991 ± 1.094
1.406	26.836 ± 1.049	1.412	26.194 ± 1.039	1.418	27.743 ± 1.058	1.424	25.579 ± 1.022
1.430	26.445 ± 1.039	1.436	28.772 ± 1.056	1.442	28.457 ± 1.066	1.448	27.987 ± 1.064
1.454	31.156 ± 1.117	1.450	30.158 ± 1.110	1.465	30.822 ± 1.109	1.471	30.544 ± 1.117
1.477	32.374 ± 1.152	1.482	33.567 ± 1.178	1.488	35.211 ± 1.191	1.494	35.390 ± 1.218
1.499	35.058 ± 1.226	1.505	34.270 ± 1.254	1.511	35.052 ± 1.276	1.516	33.977 ± 1.245
1.522	32.020 ± 1.205	1.527	32.134 ± 1.199	1.533	31.906 ± 1.182	1.538	29.435 ± 1.151
1.544	27.743 ± 1.115	1.549	26.823 ± 1.096	1.555	25.100 ± 1.067	1.560	25.964 ± 1.068
1.565	24.552 ± 1.042	1.571	24.467 ± 1.009	1.576	24.021 ± 0.984	1.581	21.506 ± 0.939
1.587	22.719 ± 0.941	1.592	20.414 ± 0.900	1.597	23.068 ± 0.917	1.603	22.256 ± 0.893
1.608	21.950 ± 0.880	1.613	21.765 ± 0.867	1.618	22.346 ± 0.867	1.624	20.922 ± 0.845
1.629	21.218 ± 0.848	1.634	22.195 ± 0.856	1.639	21.558 ± 0.854	1.644	21.026 ± 0.849
1.640	21.435 ± 0.856	1.655	21.577 ± 0.855	1.660	21.867 ± 0.855	1.665	21.079 ± 0.850
1.670	21.602 ± 0.851	1.675	20.657 ± 0.841	1.680	21.293 ± 0.841	1.685	19.782 ± 0.828
1.690	20.322 ± 0.824	1.695	18.921 ± 0.805	1.700	19.063 ± 0.804	1.705	18.667 ± 0.792
1.710	17.330 ± 0.773	1.715	17.228 ± 0.768	1.720	17.161 ± 0.761	1.724	16.707 ± 0.752
1.729	16.373 ± 0.746	1.734	14.877 ± 0.724	1.739	14.634 ± 0.718	1.744	13.950 ± 0.709
1.749	14.224 ± 0.706	1.754	14.531 ± 0.705	1.758	13.772 ± 0.698	1.763	13.404 ± 0.691
1.768	12.886 ± 0.685	1.773	12.492 ± 0.682	1.778	13.125 ± 0.688	1.782	12.499 ± 0.693
1.787	13.288 ± 0.698	1.792	12.651 ± 0.691	1.796	11.818 ± 0.685	1.801	12.170 ± 0.687
1.806	12.731 ± 0.692	1.810	12.536 ± 0.692	1.815	11.295 ± 0.678	1.820	11.401 ± 0.679
1.824	11.325 ± 0.677	1.829	11.556 ± 0.676	1.834	12.214 ± 0.675	1.838	11.022 ± 0.665
1.843	12.069 ± 0.677	1.847	11.423 ± 0.670	1.852	12.352 ± 0.688	1.857	11.657 ± 0.678
1.861	10.783 ± 0.675	1.866	11.629 ± 0.678	1.870	11.406 ± 0.679	1.875	10.918 ± 0.674
1.879	11.218 ± 0.676	1.884	11.251 ± 0.676	1.889	11.252 ± 0.675	1.893	9.904 ± 0.661
1.897	10.390 ± 0.656	1.901	10.256 ± 0.656	1.906	11.045 ± 0.662	1.910	11.093 ± 0.664
1.915	10.358 ± 0.654	1.919	10.720 ± 0.659	1.923	9.369 ± 0.643	1.928	10.226 ± 0.653
1.932	9.895 ± 0.647	1.937	9.040 ± 0.639	1.941	9.567 ± 0.642	1.945	9.830 ± 0.646
1.950	10.570 ± 0.652	1.954	9.937 ± 0.642	1.958	9.707 ± 0.640	1.963	8.862 ± 0.629
1.967	8.795 ± 0.628	1.971	8.963 ± 0.629	1.975	9.177 ± 0.630	1.980	9.385 ± 0.631
1.984	8.906 ± 0.626	1.988	8.573 ± 0.623	1.992	9.459 ± 0.630	1.997	8.401 ± 0.620

E = 7.000 GeV Hydrogen

1.078	2.123 ± 0.664	1.084	2.762 ± 0.645	1.090	4.049 ± 0.636	1.096	6.475 ± 0.644
1.102	6.910 ± 0.635	1.108	9.014 ± 0.635	1.114	10.373 ± 0.644	1.120	12.733 ± 0.655
1.125	14.319 ± 0.563	1.132	15.759 ± 0.666	1.138	18.423 ± 0.685	1.143	21.432 ± 0.707
1.149	22.332 ± 0.710	1.155	27.225 ± 0.747	1.160	29.282 ± 0.758	1.166	34.465 ± 0.795
1.172	38.957 ± 0.823	1.177	44.328 ± 0.858	1.183	48.057 ± 0.879	1.188	52.110 ± 0.901
1.194	56.122 ± 0.921	1.199	58.726 ± 0.931	1.205	63.630 ± 0.953	1.210	65.632 ± 0.950
1.216	64.738 ± 0.930	1.221	64.735 ± 0.920	1.226	62.584 ± 0.898	1.232	60.253 ± 0.875
1.237	54.684 ± 0.831	1.242	52.337 ± 0.807	1.248	48.277 ± 0.773	1.253	47.289 ± 0.756
1.258	42.293 ± 0.715	1.263	39.763 ± 0.691	1.269	38.098 ± 0.671	1.274	36.280 ± 0.652
1.279	31.970 ± 0.614	1.284	31.096 ± 0.604	1.289	29.033 ± 0.582	1.294	26.849 ± 0.561
1.299	25.695 ± 0.547	1.304	24.042 ± 0.530	1.309	23.734 ± 0.525	1.314	22.848 ± 0.514
1.310	21.327 ± 0.490	1.324	20.577 ± 0.491	1.329	19.930 ± 0.482	1.334	18.840 ± 0.471
1.330	18.845 ± 0.468	1.344	17.878 ± 0.459	1.349	18.531 ± 0.462	1.354	16.633 ± 0.444
1.359	16.787 ± 0.444	1.363	16.827 ± 0.443	1.368	17.494 ± 0.448	1.373	16.548 ± 0.439
1.378	16.440 ± 0.437	1.383	16.425 ± 0.436	1.387	16.455 ± 0.438	1.392	16.863 ± 0.439
1.397	16.815 ± 0.439	1.401	16.001 ± 0.430	1.406	16.773 ± 0.438	1.411	16.772 ± 0.438
1.415	16.292 ± 0.433	1.420	17.348 ± 0.445	1.425	17.104 ± 0.443	1.429	17.561 ± 0.450
1.434	18.086 ± 0.455	1.438	17.869 ± 0.457	1.443	18.534 ± 0.462	1.448	18.671 ± 0.464
1.452	19.373 ± 0.471	1.457	19.214 ± 0.472	1.461	19.425 ± 0.474	1.466	20.398 ± 0.483
1.470	20.984 ± 0.491	1.475	20.296 ± 0.487	1.479	22.121 ± 0.507	1.483	22.177 ± 0.506
1.488	23.899 ± 0.521	1.492	23.710 ± 0.519	1.497	23.986 ± 0.521	1.501	24.039 ± 0.521
1.505	24.827 ± 0.526	1.510	23.445 ± 0.512	1.514	23.121 ± 0.508	1.518	22.603 ± 0.503
1.523	22.762 ± 0.499	1.527	21.064 ± 0.480	1.531	21.991 ± 0.485	1.536	20.052 ± 0.465

W (GeV)	$\frac{d\sigma}{d\Omega dE^t}$ [$\mu b/(GeV \cdot sr)$]	W (GeV)	$\frac{d\sigma}{d\Omega dE^t}$ [$\mu b/(GeV \cdot sr)$]	W (GeV)	$\frac{d\sigma}{d\Omega dE^t}$ [$\mu b/(GeV \cdot sr)$]	W (GeV)	$\frac{d\sigma}{d\Omega dE^t}$ [$\mu b/(GeV \cdot sr)$]
1.540	19.622 ± 0.458	1.544	18.970 ± 0.448	1.548	18.473 ± 0.441	1.553	18.673 ± 0.443
1.557	17.974 ± 0.432	1.561	17.423 ± 0.425	1.565	17.075 ± 0.420	1.569	16.863 ± 0.417
1.574	15.876 ± 0.406	1.578	16.303 ± 0.409	1.582	16.157 ± 0.410	1.586	15.369 ± 0.400
1.590	15.450 ± 0.400	1.594	14.656 ± 0.393	1.598	15.607 ± 0.402	1.603	14.741 ± 0.394
1.607	14.801 ± 0.395	1.611	14.944 ± 0.398	1.615	15.233 ± 0.400	1.619	14.695 ± 0.395
1.623	15.405 ± 0.403	1.627	15.931 ± 0.409	1.631	15.427 ± 0.406	1.635	14.674 ± 0.399
1.639	15.446 ± 0.409	1.643	15.197 ± 0.405	1.647	15.601 ± 0.411	1.651	16.034 ± 0.414
1.655	15.664 ± 0.411	1.659	16.774 ± 0.422	1.663	16.330 ± 0.419	1.667	16.222 ± 0.416
1.671	16.175 ± 0.415	1.675	15.950 ± 0.412	1.679	15.449 ± 0.406	1.683	16.138 ± 0.412
1.686	15.643 ± 0.407	1.690	15.814 ± 0.405	1.694	15.025 ± 0.396	1.698	14.117 ± 0.384
1.702	15.023 ± 0.394	1.706	14.569 ± 0.388	1.710	14.679 ± 0.386	1.713	13.614 ± 0.372
1.717	13.482 ± 0.368	1.721	12.937 ± 0.361	1.725	12.780 ± 0.360	1.729	12.748 ± 0.356
1.733	12.763 ± 0.354	1.736	11.526 ± 0.339	1.740	12.209 ± 0.344	1.744	11.965 ± 0.341
1.748	11.362 ± 0.335	1.751	10.689 ± 0.324	1.755	10.598 ± 0.322	1.759	10.633 ± 0.321
1.763	10.752 ± 0.323	1.766	10.228 ± 0.317	1.770	9.980 ± 0.313	1.774	10.419 ± 0.317
1.777	9.988 ± 0.312	1.781	9.884 ± 0.313	1.785	9.895 ± 0.310	1.789	10.253 ± 0.313
1.792	9.923 ± 0.310	1.796	9.773 ± 0.308	1.799	10.148 ± 0.313	1.803	9.566 ± 0.305
1.807	9.587 ± 0.305	1.810	9.940 ± 0.310	1.814	9.239 ± 0.301	1.818	9.030 ± 0.300
1.821	9.499 ± 0.304	1.825	9.370 ± 0.303	1.828	9.499 ± 0.304	1.832	9.684 ± 0.308
1.836	9.423 ± 0.303	1.839	9.013 ± 0.297	1.843	9.377 ± 0.302	1.846	9.266 ± 0.302
1.850	8.972 ± 0.297	1.853	8.928 ± 0.296	1.857	9.865 ± 0.308	1.861	9.194 ± 0.300
1.864	8.508 ± 0.290	1.868	8.825 ± 0.294	1.871	9.282 ± 0.299	1.875	9.019 ± 0.298
1.878	9.107 ± 0.297	1.882	8.705 ± 0.291	1.885	8.671 ± 0.291	1.889	8.482 ± 0.289
1.892	8.955 ± 0.295	1.895	8.791 ± 0.291	1.899	8.772 ± 0.291	1.902	8.765 ± 0.292
1.906	8.459 ± 0.287	1.909	8.298 ± 0.285	1.913	8.681 ± 0.289	1.916	8.168 ± 0.284
1.920	8.180 ± 0.281	1.923	8.517 ± 0.286	1.926	7.965 ± 0.279	1.930	8.016 ± 0.279
1.933	7.833 ± 0.276	1.937	7.902 ± 0.277	1.940	8.092 ± 0.279	1.943	8.305 ± 0.282
1.947	8.229 ± 0.281	1.950	8.210 ± 0.281	1.953	8.260 ± 0.282	1.957	7.993 ± 0.276
1.960	8.260 ± 0.279	1.964	7.833 ± 0.275	1.967	7.512 ± 0.269	1.970	7.867 ± 0.273
1.974	7.984 ± 0.275	1.977	7.557 ± 0.269	1.980	7.670 ± 0.270	1.984	7.177 ± 0.263
1.987	7.255 ± 0.264	1.990	7.383 ± 0.265	1.993	6.967 ± 0.259	1.997	7.032 ± 0.260
2.000	7.161 ± 0.262	2.003	6.686 ± 0.260	2.007	7.414 ± 0.277	2.010	7.235 ± 0.276
2.013	7.069 ± 0.278	2.016	6.296 ± 0.275	2.020	7.165 ± 0.295	2.023	7.040 ± 0.302
2.026	7.327 ± 0.318	2.029	6.887 ± 0.321	2.033	7.072 ± 0.335	2.036	6.718 ± 0.343
2.039	6.882 ± 0.360	2.042	7.665 ± 0.393	2.045	6.172 ± 0.383	2.049	6.782 ± 0.404
2.052	6.753 ± 0.421	2.055	6.150 ± 0.441	2.058	7.002 ± 0.497	2.066	6.800 ± 0.325
2.079	6.128 ± 0.496	2.091	5.917 ± 0.420	2.104	5.854 ± 0.413	2.116	6.514 ± 0.488
2.129	5.654 ± 0.398	2.141	5.972 ± 0.404	2.153	5.619 ± 0.450	2.166	5.509 ± 0.374
2.178	5.699 ± 0.376	2.190	4.986 ± 0.403	2.202	5.228 ± 0.356	2.214	4.751 ± 0.353
2.221	4.994 ± 0.369	2.224	5.378 ± 0.288	2.227	5.102 ± 0.274	2.230	4.863 ± 0.268
2.233	5.163 ± 0.277	2.236	5.013 ± 0.273	2.239	4.982 ± 0.270	2.242	5.093 ± 0.272
2.244	4.804 ± 0.270	2.247	4.631 ± 0.266	2.250	4.563 ± 0.265	2.253	4.539 ± 0.273
2.256	4.867 ± 0.273	2.259	4.626 ± 0.261	2.262	4.640 ± 0.263	2.265	4.949 ± 0.269
2.268	4.781 ± 0.265	2.271	4.772 ± 0.265	2.274	4.572 ± 0.257	2.276	4.078 ± 0.264
2.284	4.598 ± 0.287	2.295	4.865 ± 0.330	2.307	4.936 ± 0.334	2.318	5.086 ± 0.372
2.329	4.628 ± 0.312	2.340	4.171 ± 0.334	2.352	4.489 ± 0.310	2.363	4.453 ± 0.297
2.374	4.161 ± 0.331	2.385	3.868 ± 0.275	2.396	4.090 ± 0.305	2.407	3.978 ± 0.292
2.418	3.721 ± 0.268	2.429	4.006 ± 0.320	2.439	4.212 ± 0.278	2.450	3.431 ± 0.283
2.461	3.994 ± 0.281	2.471	4.056 ± 0.270	2.478	3.982 ± 0.263	2.481	3.840 ± 0.220
2.483	3.614 ± 0.209	2.486	3.541 ± 0.203	2.489	3.599 ± 0.207	2.491	3.523 ± 0.202
2.494	3.565 ± 0.208	2.497	3.838 ± 0.209	2.499	3.658 ± 0.206	2.502	3.569 ± 0.208
2.504	3.724 ± 0.214	2.507	3.287 ± 0.204	2.510	3.696 ± 0.205	2.512	3.376 ± 0.203
2.515	3.232 ± 0.197	2.518	3.940 ± 0.209	2.520	3.397 ± 0.209	2.523	3.324 ± 0.278
2.529	2.996 ± 0.265	2.540	3.118 ± 0.231	2.550	3.356 ± 0.262	2.560	3.504 ± 0.250
2.570	3.275 ± 0.246	2.581	3.151 ± 0.254	2.591	3.515 ± 0.237	2.601	3.180 ± 0.254
2.611	2.899 ± 0.215	2.621	3.341 ± 0.262	2.631	2.662 ± 0.211	2.641	2.879 ± 0.247
2.651	3.288 ± 0.225	2.661	3.293 ± 0.250	2.671	3.209 ± 0.227	2.681	3.280 ± 0.245
2.690	3.069 ± 0.226	2.700	2.881 ± 0.231	2.710	2.711 ± 0.218	2.719	3.129 ± 0.233
2.729	2.634 ± 0.175	2.735	2.948 ± 0.177	2.738	2.868 ± 0.166	2.740	2.741 ± 0.168
2.742	3.069 ± 0.177	2.745	2.507 ± 0.163	2.747	2.875 ± 0.165	2.750	2.880 ± 0.167
2.752	2.709 ± 0.163	2.754	2.665 ± 0.165	2.757	2.741 ± 0.165	2.759	2.906 ± 0.171
2.761	2.534 ± 0.168	2.764	2.727 ± 0.170	2.765	2.680 ± 0.206	2.772	2.593 ± 0.196
2.782	2.762 ± 0.228	2.791	3.097 ± 0.210	2.800	2.577 ± 0.227	2.810	2.934 ± 0.211
2.819	2.717 ± 0.221	2.828	2.738 ± 0.217	2.838	2.862 ± 0.216	2.847	2.768 ± 0.229
2.856	2.470 ± 0.195	2.865	2.460 ± 0.220	2.874	2.573 ± 0.194	2.884	2.278 ± 0.215
2.893	2.675 ± 0.207	2.902	2.747 ± 0.215	2.911	2.422 ± 0.218	2.920	2.397 ± 0.189
2.929	2.610 ± 0.222	2.938	2.475 ± 0.201	2.947	2.944 ± 0.221	2.956	2.610 ± 0.222
2.964	2.593 ± 0.195	2.973	2.732 ± 0.224	2.982	2.431 ± 0.214	2.988	2.455 ± 0.423
2.990	2.703 ± 0.218	2.992	2.504 ± 0.200	2.994	2.343 ± 0.196	2.996	2.319 ± 0.199
2.999	2.543 ± 0.212	3.001	2.618 ± 0.214	3.003	2.133 ± 0.206	3.005	2.435 ± 0.213
3.007	2.476 ± 0.216	3.010	2.621 ± 0.237	3.012	2.205 ± 0.353		

E = 9.993 GeV Hydrogen

W (GeV)	$\frac{d\sigma}{d\Omega dE^i}$ [$\mu b/(GeV \cdot sr)$]	W (GeV)	$\frac{d\sigma}{d\Omega dE^i}$ [$\mu b/(GeV \cdot sr)$]	W (GeV)	$\frac{d\sigma}{d\Omega dE^i}$ [$\mu b/(GeV \cdot sr)$]	W (GeV)	$\frac{d\sigma}{d\Omega dE^i}$ [$\mu b/(GeV \cdot sr)$]
1.082	1.429 ± 0.234	1.091	1.824 ± 0.229	1.099	2.278 ± 0.227	1.108	3.405 ± 0.235
1.116	3.684 ± 0.235	1.125	4.782 ± 0.245	1.133	6.473 ± 0.259	1.141	7.076 ± 0.264
1.149	8.673 ± 0.276	1.157	11.027 ± 0.296	1.165	12.733 ± 0.309	1.174	14.872 ± 0.326
1.181	18.261 ± 0.351	1.189	20.546 ± 0.368	1.197	22.560 ± 0.378	1.205	23.854 ± 0.394
1.213	24.551 ± 0.385	1.220	24.160 ± 0.377	1.229	22.274 ± 0.359	1.236	21.100 ± 0.347
1.243	19.120 ± 0.327	1.251	18.418 ± 0.317	1.258	16.354 ± 0.298	1.266	14.836 ± 0.282
1.273	13.809 ± 0.271	1.280	12.587 ± 0.259	1.289	12.288 ± 0.254	1.295	10.895 ± 0.239
1.302	10.191 ± 0.232	1.309	9.627 ± 0.225	1.317	9.560 ± 0.225	1.324	9.091 ± 0.219
1.331	8.436 ± 0.211	1.338	8.184 ± 0.207	1.345	8.070 ± 0.205	1.352	7.939 ± 0.203
1.359	8.252 ± 0.206	1.365	7.655 ± 0.201	1.372	7.680 ± 0.199	1.379	8.061 ± 0.203
1.386	7.950 ± 0.203	1.393	7.689 ± 0.199	1.399	8.079 ± 0.204	1.406	7.624 ± 0.199
1.413	7.857 ± 0.200	1.419	8.612 ± 0.209	1.426	8.299 ± 0.207	1.432	8.515 ± 0.209
1.430	8.698 ± 0.212	1.446	9.032 ± 0.216	1.452	9.261 ± 0.218	1.459	9.418 ± 0.221
1.465	10.161 ± 0.239	1.471	10.571 ± 0.233	1.478	10.990 ± 0.238	1.484	11.580 ± 0.244
1.490	12.861 ± 0.255	1.496	12.581 ± 0.251	1.503	11.870 ± 0.243	1.509	12.269 ± 0.244
1.515	11.757 ± 0.238	1.521	11.855 ± 0.237	1.527	11.357 ± 0.231	1.534	11.092 ± 0.227
1.540	10.774 ± 0.223	1.546	10.038 ± 0.215	1.552	9.399 ± 0.207	1.558	9.050 ± 0.202
1.564	9.215 ± 0.203	1.570	8.943 ± 0.199	1.576	8.741 ± 0.197	1.582	8.506 ± 0.195
1.589	8.255 ± 0.192	1.594	7.964 ± 0.189	1.599	7.833 ± 0.188	1.605	8.330 ± 0.193
1.611	8.445 ± 0.195	1.617	8.427 ± 0.194	1.623	7.996 ± 0.190	1.628	7.981 ± 0.191
1.634	8.793 ± 0.199	1.640	8.942 ± 0.201	1.646	8.740 ± 0.199	1.651	9.286 ± 0.206
1.657	9.362 ± 0.206	1.663	9.460 ± 0.208	1.668	9.640 ± 0.209	1.674	9.362 ± 0.207
1.679	9.845 ± 0.213	1.685	9.104 ± 0.207	1.691	9.443 ± 0.210	1.696	9.376 ± 0.208
1.702	9.250 ± 0.206	1.707	9.162 ± 0.204	1.713	9.614 ± 0.199	1.718	8.706 ± 0.198
1.724	8.268 ± 0.192	1.729	8.102 ± 0.189	1.734	8.013 ± 0.188	1.740	7.868 ± 0.186
1.745	7.537 ± 0.181	1.751	7.127 ± 0.176	1.756	5.820 ± 0.172	1.761	6.792 ± 0.171
1.767	6.567 ± 0.168	1.772	6.640 ± 0.169	1.777	6.662 ± 0.168	1.782	6.389 ± 0.166
1.789	6.609 ± 0.168	1.793	6.620 ± 0.168	1.799	6.247 ± 0.164	1.803	6.213 ± 0.163
1.808	5.808 ± 0.158	1.814	6.399 ± 0.164	1.819	5.957 ± 0.158	1.824	6.007 ± 0.157
1.829	6.135 ± 0.150	1.834	5.953 ± 0.157	1.839	6.151 ± 0.150	1.844	6.116 ± 0.158
1.849	6.226 ± 0.160	1.855	6.061 ± 0.158	1.860	5.122 ± 0.159	1.865	5.909 ± 0.156
1.870	6.008 ± 0.156	1.875	6.030 ± 0.156	1.880	6.287 ± 0.159	1.885	6.052 ± 0.157
1.890	5.968 ± 0.156	1.895	5.872 ± 0.155	1.899	6.037 ± 0.156	1.904	5.877 ± 0.155
1.900	5.574 ± 0.151	1.914	5.524 ± 0.153	1.919	5.719 ± 0.152	1.924	5.896 ± 0.154
1.920	5.717 ± 0.151	1.934	5.677 ± 0.150	1.939	5.508 ± 0.149	1.943	5.401 ± 0.147
1.948	5.680 ± 0.151	1.953	5.567 ± 0.149	1.958	5.421 ± 0.147	1.963	5.530 ± 0.148
1.967	4.904 ± 0.141	1.972	5.240 ± 0.145	1.977	5.292 ± 0.145	1.982	5.316 ± 0.145
1.986	5.233 ± 0.143	1.991	5.096 ± 0.141	1.996	4.899 ± 0.140	2.000	5.007 ± 0.140
2.250	3.669 ± 0.040	2.500	2.771 ± 0.032	2.750	2.131 ± 0.026	3.000	1.719 ± 0.022
3.250	1.418 ± 0.020	3.500	1.212 ± 0.020	3.750	1.069 ± 0.025		

E = 13.000 GeV Hydrogen

1.080	0.472 ± 0.041	1.100	0.725 ± 0.040	1.111	1.109 ± 0.041	1.122	1.496 ± 0.042
1.133	1.015 ± 0.044	1.143	2.432 ± 0.046	1.154	3.263 ± 0.049	1.164	4.122 ± 0.053
1.175	5.234 ± 0.057	1.195	6.354 ± 0.061	1.195	7.417 ± 0.064	1.206	8.124 ± 0.066
1.214	8.338 ± 0.044	1.226	8.160 ± 0.064	1.236	7.492 ± 0.061	1.245	6.896 ± 0.058
1.255	6.220 ± 0.055	1.255	5.691 ± 0.052	1.275	5.157 ± 0.050	1.284	4.716 ± 0.048
1.293	4.338 ± 0.046	1.303	4.135 ± 0.045	1.312	3.922 ± 0.044	1.321	3.778 ± 0.043
1.331	3.607 ± 0.043	1.340	3.580 ± 0.043	1.349	3.499 ± 0.042	1.358	3.417 ± 0.042
1.347	3.366 ± 0.042	1.376	3.415 ± 0.042	1.395	3.469 ± 0.042	1.393	3.481 ± 0.043
1.402	3.496 ± 0.043	1.411	3.634 ± 0.044	1.419	3.695 ± 0.044	1.428	3.813 ± 0.045
1.436	3.996 ± 0.047	1.445	4.032 ± 0.048	1.453	4.412 ± 0.050	1.462	4.446 ± 0.050
1.470	4.787 ± 0.052	1.478	5.189 ± 0.055	1.497	5.762 ± 0.057	1.495	5.831 ± 0.058
1.503	6.026 ± 0.050	1.511	5.814 ± 0.057	1.519	5.769 ± 0.057	1.527	5.429 ± 0.055
1.535	5.237 ± 0.053	1.543	4.990 ± 0.052	1.551	4.744 ± 0.050	1.559	4.504 ± 0.049
1.564	4.308 ± 0.048	1.574	4.180 ± 0.047	1.582	4.108 ± 0.047	1.590	4.111 ± 0.046
1.597	3.978 ± 0.046	1.605	4.079 ± 0.046	1.612	4.192 ± 0.047	1.620	4.111 ± 0.047
1.628	4.259 ± 0.048	1.635	4.442 ± 0.049	1.642	4.459 ± 0.050	1.650	4.721 ± 0.051
1.657	4.806 ± 0.052	1.655	5.124 ± 0.053	1.672	5.102 ± 0.054	1.679	5.264 ± 0.054
1.684	5.262 ± 0.054	1.694	5.196 ± 0.054	1.701	5.197 ± 0.054	1.708	5.085 ± 0.054
1.715	5.034 ± 0.053	1.722	4.893 ± 0.053	1.729	4.624 ± 0.051	1.736	4.458 ± 0.051
1.743	4.271 ± 0.050	1.750	4.171 ± 0.049	1.757	4.078 ± 0.048	1.764	3.971 ± 0.048
1.771	3.851 ± 0.047	1.778	3.787 ± 0.047	1.785	3.853 ± 0.047	1.792	3.808 ± 0.048
1.799	3.605 ± 0.047	1.805	3.720 ± 0.047	1.812	3.704 ± 0.047	1.819	3.705 ± 0.047
1.825	3.661 ± 0.047	1.832	3.727 ± 0.047	1.839	3.653 ± 0.047	1.845	3.529 ± 0.046
1.852	3.625 ± 0.047	1.859	3.605 ± 0.047	1.865	3.648 ± 0.047	1.872	3.681 ± 0.047
1.878	3.626 ± 0.047	1.895	3.657 ± 0.047	1.891	3.638 ± 0.046	1.897	3.679 ± 0.047

W (GeV)	$\frac{d\sigma}{d\Omega dE^i}$ [$\mu b/(GeV \cdot sr)$]	W (GeV)	$\frac{d\sigma}{d\Omega dE^i}$ [$\mu b/(GeV \cdot sr)$]	W (GeV)	$\frac{d\sigma}{d\Omega dE^i}$ [$\mu b/(GeV \cdot sr)$]	W (GeV)	$\frac{d\sigma}{d\Omega dE^i}$ [$\mu b/(GeV \cdot sr)$]
1.004	3.646 ± 0.047	1.910	3.572 ± 0.046	1.917	3.602 ± 0.047	1.923	3.582 ± 0.047
1.029	3.519 ± 0.047	1.936	3.517 ± 0.048	1.942	3.563 ± 0.049	1.948	3.394 ± 0.048
1.054	3.440 ± 0.049	1.951	3.377 ± 0.049	1.967	3.337 ± 0.049	1.973	3.357 ± 0.049
1.070	3.278 ± 0.040	1.985	3.267 ± 0.050	1.992	3.271 ± 0.050	1.998	3.258 ± 0.051
2.004	3.270 ± 0.051	2.010	3.137 ± 0.051	2.016	3.097 ± 0.051	2.022	3.080 ± 0.052
2.028	3.116 ± 0.052	2.034	3.030 ± 0.052	2.040	3.095 ± 0.054	2.046	3.072 ± 0.054
2.052	3.035 ± 0.054	2.050	2.945 ± 0.054	2.064	2.984 ± 0.054	2.070	2.965 ± 0.054
2.076	2.912 ± 0.053	2.091	3.011 ± 0.054	2.087	2.915 ± 0.053	2.093	2.903 ± 0.052
2.099	2.890 ± 0.052	2.105	2.901 ± 0.052	2.110	2.879 ± 0.052	2.116	2.900 ± 0.052
2.122	2.793 ± 0.051	2.120	2.817 ± 0.051	2.133	2.809 ± 0.051	2.139	2.766 ± 0.050
2.145	2.795 ± 0.051	2.151	2.711 ± 0.050	2.156	2.859 ± 0.051	2.162	2.743 ± 0.050
2.168	2.697 ± 0.050	2.173	2.652 ± 0.049	2.179	2.733 ± 0.050	2.184	2.682 ± 0.049
2.190	2.652 ± 0.049	2.195	2.672 ± 0.049	2.201	2.690 ± 0.050	2.207	2.636 ± 0.049
2.212	2.523 ± 0.048	2.218	2.601 ± 0.048	2.223	2.573 ± 0.048	2.229	2.634 ± 0.049
2.234	2.577 ± 0.048	2.239	2.557 ± 0.048	2.245	2.523 ± 0.048	2.250	2.591 ± 0.048
2.256	2.433 ± 0.047	2.261	2.503 ± 0.047	2.267	2.455 ± 0.047	2.272	2.456 ± 0.047
2.277	2.474 ± 0.047	2.283	2.373 ± 0.046	2.288	2.421 ± 0.046	2.293	2.397 ± 0.046
2.299	2.421 ± 0.046	2.304	2.393 ± 0.046	2.309	2.340 ± 0.046	2.314	2.351 ± 0.046
2.320	2.394 ± 0.046	2.325	2.364 ± 0.046	2.330	2.233 ± 0.045	2.335	2.313 ± 0.046
2.341	2.294 ± 0.046	2.346	2.282 ± 0.046	2.351	2.268 ± 0.046	2.356	2.298 ± 0.046
2.361	2.261 ± 0.046	2.367	2.301 ± 0.046	2.372	2.225 ± 0.046	2.377	2.198 ± 0.046
2.382	2.119 ± 0.046	2.387	2.242 ± 0.046	2.392	2.147 ± 0.046	2.397	2.164 ± 0.046
2.402	2.105 ± 0.046	2.407	2.199 ± 0.046	2.413	2.205 ± 0.047	2.418	2.151 ± 0.046
2.423	2.121 ± 0.046	2.428	2.110 ± 0.046	2.433	2.059 ± 0.046	2.438	2.142 ± 0.046
2.443	2.087 ± 0.046	2.448	2.034 ± 0.045	2.453	2.050 ± 0.045	2.458	2.048 ± 0.045
2.463	1.994 ± 0.045	2.468	2.004 ± 0.045	2.472	1.997 ± 0.045	2.477	2.065 ± 0.045
2.482	2.013 ± 0.045	2.487	1.909 ± 0.044	2.492	1.980 ± 0.044	2.497	1.945 ± 0.044
2.502	1.953 ± 0.044	2.507	1.966 ± 0.044	2.512	1.969 ± 0.044	2.516	1.931 ± 0.044
2.521	1.878 ± 0.043	2.526	1.958 ± 0.044	2.531	1.875 ± 0.043	2.536	1.933 ± 0.044
2.541	1.891 ± 0.043	2.545	1.948 ± 0.044	2.550	1.896 ± 0.044	2.555	1.950 ± 0.045
2.560	1.913 ± 0.044	2.564	1.814 ± 0.044	2.559	1.782 ± 0.044	2.574	1.829 ± 0.045
2.579	1.873 ± 0.045	2.583	1.842 ± 0.045	2.588	1.795 ± 0.045	2.593	1.799 ± 0.045
2.598	1.859 ± 0.046	2.602	1.808 ± 0.046	2.607	1.795 ± 0.045	2.612	1.729 ± 0.045
2.616	1.698 ± 0.044	2.621	1.729 ± 0.044	2.626	1.840 ± 0.046	2.630	1.788 ± 0.045
2.635	1.701 ± 0.044	2.639	1.799 ± 0.045	2.644	1.722 ± 0.044	2.649	1.763 ± 0.044
2.653	1.733 ± 0.044	2.655	1.723 ± 0.043	2.662	1.703 ± 0.042	2.667	1.669 ± 0.042
2.672	1.658 ± 0.041	2.676	1.592 ± 0.040	2.681	1.602 ± 0.040	2.685	1.684 ± 0.041
2.690	1.657 ± 0.040	2.594	1.640 ± 0.040	2.699	1.673 ± 0.040	2.703	1.618 ± 0.038
2.709	1.594 ± 0.037	2.712	1.609 ± 0.036	2.717	1.622 ± 0.036	2.721	1.628 ± 0.036
2.726	1.619 ± 0.035	2.730	1.672 ± 0.036	2.735	1.595 ± 0.035	2.739	1.574 ± 0.035
2.744	1.605 ± 0.035	2.748	1.644 ± 0.035	2.753	1.497 ± 0.034	2.757	1.533 ± 0.034
2.761	1.572 ± 0.035	2.756	1.527 ± 0.034	2.770	1.526 ± 0.034	2.775	1.509 ± 0.034
2.779	1.595 ± 0.035	2.783	1.505 ± 0.034	2.788	1.581 ± 0.035	2.792	1.492 ± 0.035
2.797	1.450 ± 0.035	2.801	1.467 ± 0.038	2.805	1.492 ± 0.038	2.810	1.487 ± 0.038
2.814	1.510 ± 0.038	2.818	1.466 ± 0.037	2.823	1.549 ± 0.038	2.827	1.483 ± 0.038
2.831	1.487 ± 0.038	2.836	1.517 ± 0.038	2.840	1.482 ± 0.038	2.844	1.470 ± 0.037
2.848	1.507 ± 0.038	2.853	1.444 ± 0.037	2.857	1.414 ± 0.037	2.861	1.437 ± 0.037
2.865	1.440 ± 0.037	2.870	1.428 ± 0.037	2.874	1.440 ± 0.037	2.878	1.427 ± 0.037
2.882	1.442 ± 0.037	2.887	1.413 ± 0.037	2.891	1.442 ± 0.037	2.895	1.362 ± 0.036
2.899	1.365 ± 0.036	2.904	1.401 ± 0.037	2.908	1.372 ± 0.036	2.912	1.455 ± 0.037
2.916	1.375 ± 0.036	2.920	1.357 ± 0.037	2.924	1.338 ± 0.037	2.929	1.278 ± 0.037
2.933	1.409 ± 0.039	2.937	1.297 ± 0.039	2.941	1.358 ± 0.040	2.945	1.258 ± 0.040
2.949	1.359 ± 0.042	2.954	1.344 ± 0.043	2.958	1.268 ± 0.043	2.962	1.279 ± 0.041
2.966	1.340 ± 0.040	2.970	1.343 ± 0.039	2.974	1.298 ± 0.039	2.978	1.340 ± 0.041
2.982	1.271 ± 0.041	2.986	1.376 ± 0.043	2.990	1.282 ± 0.043	2.995	1.235 ± 0.043
2.999	1.221 ± 0.043	3.249	1.076 ± 0.006	3.499	0.903 ± 0.015	3.749	0.800 ± 0.006
3.999	0.707 ± 0.008	4.249	0.653 ± 0.010	4.499	0.637 ± 0.015		

E = 16.000 GeV Hydrogen

1.080	0.195 ± 0.033	1.093	0.231 ± 0.032	1.107	0.295 ± 0.032	1.121	0.495 ± 0.034
1.134	0.668 ± 0.036	1.147	0.875 ± 0.038	1.160	1.253 ± 0.042	1.173	1.645 ± 0.046
1.186	2.140 ± 0.051	1.198	2.605 ± 0.055	1.211	2.855 ± 0.056	1.223	2.848 ± 0.055
1.235	2.705 ± 0.053	1.247	2.503 ± 0.050	1.259	2.299 ± 0.047	1.271	2.073 ± 0.045
1.283	1.899 ± 0.043	1.295	1.745 ± 0.041	1.306	1.654 ± 0.040	1.318	1.644 ± 0.039
1.329	1.584 ± 0.038	1.340	1.569 ± 0.038	1.351	1.442 ± 0.037	1.362	1.546 ± 0.038
1.373	1.531 ± 0.038	1.384	1.580 ± 0.038	1.395	1.564 ± 0.038	1.406	1.662 ± 0.039
1.416	1.694 ± 0.040	1.427	1.773 ± 0.040	1.437	1.774 ± 0.041	1.448	1.907 ± 0.042
1.458	2.006 ± 0.043	1.468	2.265 ± 0.046	1.479	2.637 ± 0.049	1.489	2.750 ± 0.051
1.499	2.790 ± 0.051	1.509	2.886 ± 0.051	1.519	2.731 ± 0.050	1.529	2.729 ± 0.049
1.538	2.449 ± 0.046	1.548	2.409 ± 0.046	1.558	2.167 ± 0.043	1.567	2.086 ± 0.042

W (GeV)	$\frac{d\sigma}{d\Omega dE^I}$ [$\mu\text{b}/(\text{GeV-sr})$]	W (GeV)	$\frac{d\sigma}{d\Omega dE^I}$ [$\mu\text{b}/(\text{GeV-sr})$]	W (GeV)	$\frac{d\sigma}{d\Omega dE^T}$ [$\mu\text{b}/(\text{GeV-sr})$]	W (GeV)	$\frac{d\sigma}{d\Omega dE^I}$ [$\mu\text{b}/(\text{GeV-sr})$]
1.577	2.070 ± 0.042	1.596	2.040 ± 0.042	1.596	2.018 ± 0.041	1.605	1.954 ± 0.041
1.615	2.026 ± 0.042	1.624	2.060 ± 0.042	1.633	2.237 ± 0.044	1.642	2.212 ± 0.044
1.651	2.371 ± 0.045	1.650	2.483 ± 0.046	1.669	2.573 ± 0.047	1.678	2.661 ± 0.048
1.687	2.729 ± 0.049	1.696	2.745 ± 0.049	1.705	2.750 ± 0.049	1.714	2.670 ± 0.048
1.722	2.635 ± 0.047	1.731	2.484 ± 0.045	1.740	2.387 ± 0.044	1.748	2.372 ± 0.043
1.757	2.223 ± 0.041	1.756	2.167 ± 0.039	1.774	2.102 ± 0.038	1.782	2.178 ± 0.038
1.781	2.092 ± 0.037	1.799	2.077 ± 0.036	1.808	2.117 ± 0.036	1.816	2.076 ± 0.035
1.824	2.130 ± 0.035	1.832	2.072 ± 0.034	1.840	2.124 ± 0.034	1.849	2.036 ± 0.033
1.857	2.102 ± 0.033	1.855	2.060 ± 0.032	1.873	2.115 ± 0.032	1.881	2.118 ± 0.032
1.899	2.171 ± 0.032	1.897	2.108 ± 0.031	1.905	2.119 ± 0.031	1.912	2.098 ± 0.031
1.920	2.133 ± 0.030	1.928	2.092 ± 0.030	1.936	2.083 ± 0.029	1.944	2.082 ± 0.029
1.951	2.083 ± 0.029	1.959	2.039 ± 0.029	1.967	1.928 ± 0.028	1.974	1.988 ± 0.028
1.982	1.973 ± 0.028	1.989	2.008 ± 0.028	1.997	1.986 ± 0.028	2.004	1.948 ± 0.028
2.012	1.953 ± 0.028	2.019	1.902 ± 0.028	2.027	1.913 ± 0.028	2.034	1.857 ± 0.029
2.042	1.861 ± 0.029	2.049	1.888 ± 0.029	2.056	1.874 ± 0.030	2.063	1.859 ± 0.030
2.071	1.940 ± 0.030	2.078	1.827 ± 0.030	2.085	1.831 ± 0.030	2.092	1.814 ± 0.030
2.100	1.752 ± 0.030	2.107	1.823 ± 0.031	2.114	1.794 ± 0.031	2.121	1.773 ± 0.032
2.120	1.734 ± 0.032	2.135	1.763 ± 0.033	2.142	1.705 ± 0.033	2.149	1.740 ± 0.034
2.156	1.893 ± 0.035	2.163	1.739 ± 0.035	2.170	1.728 ± 0.035	2.177	1.798 ± 0.036
2.184	1.759 ± 0.036	2.191	1.650 ± 0.035	2.197	1.708 ± 0.036	2.204	1.727 ± 0.036
2.211	1.684 ± 0.035	2.218	1.664 ± 0.035	2.225	1.630 ± 0.035	2.231	1.658 ± 0.035
2.238	1.699 ± 0.035	2.245	1.648 ± 0.035	2.251	1.611 ± 0.035	2.258	1.601 ± 0.034
2.265	1.609 ± 0.035	2.271	1.619 ± 0.035	2.278	1.610 ± 0.034	2.284	1.577 ± 0.034
2.291	1.652 ± 0.035	2.298	1.580 ± 0.034	2.304	1.650 ± 0.034	2.311	1.597 ± 0.034
2.317	1.527 ± 0.033	2.324	1.540 ± 0.034	2.330	1.558 ± 0.034	2.336	1.538 ± 0.034
2.343	1.540 ± 0.034	2.349	1.511 ± 0.033	2.356	1.479 ± 0.033	2.362	1.526 ± 0.033
2.368	1.539 ± 0.033	2.375	1.501 ± 0.033	2.381	1.461 ± 0.032	2.387	1.514 ± 0.033
2.394	1.478 ± 0.033	2.400	1.509 ± 0.033	2.406	1.477 ± 0.032	2.412	1.438 ± 0.032
2.410	1.436 ± 0.032	2.425	1.422 ± 0.032	2.431	1.378 ± 0.031	2.437	1.491 ± 0.032
2.443	1.449 ± 0.033	2.449	1.397 ± 0.031	2.455	1.404 ± 0.032	2.462	1.417 ± 0.032
2.469	1.410 ± 0.031	2.474	1.385 ± 0.031	2.480	1.421 ± 0.032	2.486	1.440 ± 0.032
2.492	1.420 ± 0.031	2.498	1.320 ± 0.031	2.750	1.148 ± 0.012	3.000	0.942 ± 0.010
3.250	0.798 ± 0.009	3.500	0.695 ± 0.008	3.750	0.614 ± 0.007	4.000	0.529 ± 0.013
4.250	0.478 ± 0.013	4.500	0.430 ± 0.007	4.750	0.439 ± 0.009	5.000	0.433 ± 0.015

 $E = 18.010 \text{ GeV Hydrogen}$

1.081	0.008 ± 0.020	1.096	0.056 ± 0.020	1.111	0.133 ± 0.020	1.126	0.223 ± 0.021
1.141	0.309 ± 0.022	1.156	0.436 ± 0.024	1.171	0.615 ± 0.027	1.185	0.857 ± 0.031
1.199	1.119 ± 0.034	1.213	1.337 ± 0.035	1.227	1.361 ± 0.035	1.241	1.310 ± 0.034
1.254	1.294 ± 0.033	1.268	1.174 ± 0.031	1.291	1.060 ± 0.029	1.294	1.023 ± 0.029
1.307	0.925 ± 0.027	1.320	0.895 ± 0.027	1.333	0.857 ± 0.026	1.345	0.878 ± 0.027
1.358	0.939 ± 0.027	1.370	0.939 ± 0.027	1.382	0.902 ± 0.027	1.395	0.944 ± 0.027
1.407	0.960 ± 0.028	1.419	1.035 ± 0.029	1.430	0.971 ± 0.028	1.442	1.140 ± 0.030
1.454	1.123 ± 0.030	1.465	1.230 ± 0.032	1.477	1.367 ± 0.033	1.488	1.527 ± 0.035
1.503	1.652 ± 0.036	1.511	1.690 ± 0.036	1.522	1.699 ± 0.036	1.533	1.563 ± 0.034
1.544	1.459 ± 0.033	1.555	1.432 ± 0.032	1.566	1.303 ± 0.031	1.577	1.257 ± 0.030
1.587	1.261 ± 0.030	1.598	1.236 ± 0.030	1.609	1.236 ± 0.030	1.619	1.264 ± 0.031
1.620	1.363 ± 0.032	1.640	1.390 ± 0.032	1.650	1.470 ± 0.033	1.660	1.569 ± 0.034
1.670	1.559 ± 0.034	1.680	1.571 ± 0.035	1.690	1.806 ± 0.037	1.700	1.775 ± 0.036
1.710	1.805 ± 0.037	1.720	1.674 ± 0.035	1.730	1.724 ± 0.035	1.740	1.577 ± 0.034
1.749	1.563 ± 0.033	1.754	1.473 ± 0.032	1.769	1.431 ± 0.032	1.778	1.391 ± 0.031
1.788	1.400 ± 0.031	1.797	1.402 ± 0.031	1.806	1.401 ± 0.031	1.816	1.396 ± 0.031
1.825	1.383 ± 0.031	1.834	1.382 ± 0.031	1.843	1.410 ± 0.031	1.853	1.409 ± 0.032
1.862	1.426 ± 0.032	1.871	1.462 ± 0.032	1.880	1.392 ± 0.031	1.889	1.369 ± 0.031
1.898	1.427 ± 0.032	1.906	1.429 ± 0.032	1.915	1.493 ± 0.032	1.924	1.446 ± 0.032
1.933	1.408 ± 0.031	1.942	1.423 ± 0.031	1.950	1.452 ± 0.032	1.959	1.364 ± 0.031
1.968	1.383 ± 0.031	1.976	1.522 ± 0.031	1.985	1.398 ± 0.031	1.993	1.401 ± 0.031
2.002	1.416 ± 0.031	2.010	1.365 ± 0.030	2.018	1.351 ± 0.030	2.027	1.359 ± 0.030
2.035	1.339 ± 0.033	2.043	1.371 ± 0.030	2.052	1.297 ± 0.030	2.060	1.324 ± 0.030
2.068	1.361 ± 0.030	2.076	1.350 ± 0.030	2.084	1.323 ± 0.030	2.092	1.319 ± 0.030
2.103	1.292 ± 0.029	2.108	1.288 ± 0.029	2.116	1.313 ± 0.029	2.124	1.290 ± 0.029
2.132	1.291 ± 0.029	2.140	1.305 ± 0.029	2.148	1.278 ± 0.029	2.156	1.257 ± 0.029
2.164	1.310 ± 0.029	2.172	1.313 ± 0.029	2.179	1.276 ± 0.029	2.187	1.304 ± 0.029
2.195	1.266 ± 0.029	2.203	1.269 ± 0.029	2.210	1.244 ± 0.028	2.218	1.256 ± 0.028
2.225	1.229 ± 0.028	2.233	1.220 ± 0.028	2.241	1.235 ± 0.028	2.248	1.252 ± 0.028
2.256	1.225 ± 0.028	2.263	1.239 ± 0.028	2.271	1.203 ± 0.028	2.278	1.234 ± 0.028
2.285	1.237 ± 0.028	2.293	1.218 ± 0.028	2.300	1.175 ± 0.027	2.307	1.156 ± 0.027
2.315	1.168 ± 0.027	2.322	1.204 ± 0.028	2.329	1.177 ± 0.027	2.337	1.128 ± 0.027
2.344	1.192 ± 0.028	2.351	1.168 ± 0.027	2.359	1.149 ± 0.027	2.365	1.131 ± 0.027
2.372	1.216 ± 0.028	2.390	1.157 ± 0.027	2.387	1.088 ± 0.026	2.394	1.181 ± 0.027

| $\frac{d\sigma}{dWdE^i}$
[$\mu b/(GeV \cdot sr)$] |
|--|--|--|--|
| 2.431 | 1.114 ± 0.026 | 2.434 | 1.159 ± 0.027 |
| 2.429 | 1.090 ± 0.026 | 2.431 | 1.086 ± 0.026 |
| 2.456 | 1.065 ± 0.026 | 2.453 | 1.099 ± 0.026 |
| 2.484 | 1.072 ± 0.026 | 2.491 | 1.064 ± 0.025 |
| 3.000 | 0.751 ± 0.009 | 3.250 | 0.663 ± 0.007 |
| 4.000 | 0.433 ± 0.005 | 4.250 | 0.404 ± 0.009 |
| 5.000 | 0.335 ± 0.007 | 5.250 | 0.351 ± 0.010 |

 $E = 20.005 \text{ GeV Hydrogen}$

1.078	0.010 ± 0.000	1.095	0.046 ± 0.008	1.112	0.075 ± 0.008	1.129	0.120 ± 0.009
1.145	0.183 ± 0.009	1.162	0.258 ± 0.010	1.178	0.388 ± 0.012	1.194	0.515 ± 0.013
1.200	0.619 ± 0.014	1.225	0.689 ± 0.014	1.240	0.710 ± 0.014	1.255	0.646 ± 0.013
1.270	0.590 ± 0.012	1.284	0.567 ± 0.012	1.299	0.543 ± 0.012	1.313	0.520 ± 0.011
1.328	0.527 ± 0.011	1.342	0.519 ± 0.011	1.356	0.519 ± 0.011	1.369	0.504 ± 0.011
1.383	0.535 ± 0.011	1.396	0.527 ± 0.011	1.410	0.551 ± 0.012	1.423	0.567 ± 0.012
1.436	0.636 ± 0.012	1.449	0.639 ± 0.013	1.462	0.579 ± 0.013	1.475	0.801 ± 0.014
1.488	0.867 ± 0.015	1.500	0.974 ± 0.016	1.513	1.014 ± 0.016	1.525	0.972 ± 0.015
1.537	0.922 ± 0.015	1.549	0.883 ± 0.014	1.561	0.836 ± 0.014	1.573	0.788 ± 0.013
1.585	0.751 ± 0.013	1.597	0.758 ± 0.013	1.609	0.775 ± 0.013	1.620	0.781 ± 0.013
1.632	0.786 ± 0.013	1.643	0.825 ± 0.014	1.655	0.890 ± 0.014	1.666	0.984 ± 0.015
1.677	1.009 ± 0.015	1.689	1.060 ± 0.016	1.700	1.072 ± 0.016	1.711	1.123 ± 0.016
1.722	1.097 ± 0.016	1.732	1.075 ± 0.016	1.743	1.044 ± 0.015	1.754	0.987 ± 0.015
1.765	0.990 ± 0.015	1.775	0.943 ± 0.014	1.786	0.917 ± 0.014	1.796	0.906 ± 0.014
1.807	0.909 ± 0.014	1.817	0.931 ± 0.014	1.827	0.913 ± 0.014	1.838	0.944 ± 0.014
1.848	0.941 ± 0.014	1.858	0.906 ± 0.014	1.868	0.949 ± 0.014	1.878	0.934 ± 0.014
1.888	0.963 ± 0.014	1.898	0.969 ± 0.014	1.908	0.953 ± 0.014	1.918	0.968 ± 0.014
1.927	0.937 ± 0.014	1.937	0.986 ± 0.014	1.947	0.958 ± 0.014	1.956	0.944 ± 0.014
1.966	0.969 ± 0.014	1.975	0.934 ± 0.014	1.985	0.933 ± 0.014	1.994	0.946 ± 0.014
2.004	0.951 ± 0.014	2.013	0.916 ± 0.014	2.022	0.935 ± 0.014	2.032	0.945 ± 0.014
2.041	0.924 ± 0.014	2.050	0.935 ± 0.014	2.059	0.933 ± 0.014	2.068	0.933 ± 0.014
2.077	0.936 ± 0.014	2.086	0.938 ± 0.014	2.095	0.924 ± 0.014	2.104	0.924 ± 0.014
2.113	0.914 ± 0.014	2.122	0.944 ± 0.014	2.131	0.920 ± 0.014	2.140	0.904 ± 0.014
2.148	0.938 ± 0.014	2.157	0.932 ± 0.014	2.165	0.908 ± 0.014	2.174	0.906 ± 0.014
2.183	0.899 ± 0.013	2.192	0.907 ± 0.014	2.200	0.879 ± 0.013	2.209	0.905 ± 0.014
2.217	0.911 ± 0.014	2.226	0.898 ± 0.013	2.234	0.885 ± 0.013	2.242	0.905 ± 0.013
2.251	0.895 ± 0.013	2.259	0.908 ± 0.013	2.267	0.880 ± 0.013	2.276	0.906 ± 0.013
2.284	0.895 ± 0.013	2.292	0.899 ± 0.013	2.300	0.879 ± 0.013	2.308	0.869 ± 0.013
2.317	0.872 ± 0.013	2.325	0.869 ± 0.013	2.333	0.868 ± 0.013	2.341	0.848 ± 0.013
2.349	0.835 ± 0.013	2.357	0.843 ± 0.013	2.365	0.874 ± 0.013	2.373	0.855 ± 0.013
2.380	0.842 ± 0.013	2.388	0.834 ± 0.013	2.396	0.833 ± 0.013	2.404	0.820 ± 0.013
2.412	0.810 ± 0.012	2.420	0.835 ± 0.012	2.427	0.829 ± 0.012	2.435	0.793 ± 0.012
2.443	0.815 ± 0.012	2.450	0.807 ± 0.012	2.459	0.826 ± 0.012	2.466	0.806 ± 0.012
2.473	0.795 ± 0.012	2.481	0.794 ± 0.012	2.488	0.783 ± 0.012	2.496	0.789 ± 0.012
2.503	0.819 ± 0.012	2.511	0.793 ± 0.012	2.519	0.796 ± 0.012	2.526	0.813 ± 0.012
2.533	0.789 ± 0.012	2.541	0.776 ± 0.012	2.548	0.767 ± 0.012	2.555	0.780 ± 0.012
2.563	0.791 ± 0.012	2.570	0.759 ± 0.011	2.577	0.760 ± 0.012	2.585	0.719 ± 0.011
2.592	0.783 ± 0.012	2.594	0.739 ± 0.012	2.606	0.751 ± 0.012	2.613	0.751 ± 0.012
2.621	0.759 ± 0.012	2.628	0.775 ± 0.012	2.635	0.725 ± 0.012	2.642	0.747 ± 0.012
2.649	0.717 ± 0.012	2.656	0.740 ± 0.012	2.663	0.717 ± 0.012	2.670	0.739 ± 0.012
2.677	0.750 ± 0.011	2.684	0.712 ± 0.011	2.691	0.727 ± 0.011	2.698	0.722 ± 0.011
2.705	0.739 ± 0.011	2.712	0.706 ± 0.011	2.719	0.719 ± 0.011	2.726	0.694 ± 0.011
2.733	0.709 ± 0.011	2.740	0.689 ± 0.011	2.747	0.707 ± 0.011	2.753	0.699 ± 0.011
2.760	0.670 ± 0.011	2.757	0.692 ± 0.011	2.774	0.696 ± 0.011	2.780	0.691 ± 0.011
2.787	0.675 ± 0.011	2.794	0.696 ± 0.011	2.801	0.679 ± 0.011	2.807	0.681 ± 0.011
2.814	0.697 ± 0.011	2.821	0.701 ± 0.011	2.827	0.688 ± 0.011	2.834	0.677 ± 0.011
2.841	0.642 ± 0.011	2.847	0.669 ± 0.011	2.854	0.659 ± 0.011	2.860	0.660 ± 0.011
2.867	0.663 ± 0.011	2.873	0.645 ± 0.011	2.880	0.640 ± 0.011	2.886	0.637 ± 0.011
2.893	0.649 ± 0.011	2.899	0.648 ± 0.011	2.906	0.636 ± 0.011	2.912	0.638 ± 0.011
2.910	0.627 ± 0.011	2.925	0.642 ± 0.011	2.932	0.652 ± 0.011	2.938	0.622 ± 0.010
2.944	0.636 ± 0.010	2.951	0.644 ± 0.010	2.957	0.607 ± 0.010	2.963	0.632 ± 0.010
2.970	0.636 ± 0.010	2.976	0.619 ± 0.010	2.982	0.619 ± 0.010	2.989	0.627 ± 0.010
2.995	0.623 ± 0.010	3.001	0.610 ± 0.010	3.007	0.624 ± 0.010	3.014	0.614 ± 0.010
3.020	0.600 ± 0.010	3.026	0.607 ± 0.010	3.032	0.618 ± 0.010	3.039	0.596 ± 0.010
3.045	0.605 ± 0.010	3.051	0.614 ± 0.010	3.057	0.581 ± 0.010	3.063	0.602 ± 0.010
3.069	0.596 ± 0.010	3.075	0.561 ± 0.010	3.091	0.596 ± 0.010	3.088	0.595 ± 0.010
3.094	0.595 ± 0.010	3.100	0.599 ± 0.010	3.106	0.589 ± 0.010	3.112	0.562 ± 0.010
3.118	0.584 ± 0.010	3.124	0.582 ± 0.010	3.130	0.585 ± 0.010	3.136	0.575 ± 0.010
3.142	0.559 ± 0.010	3.148	0.567 ± 0.010	3.154	0.554 ± 0.010	3.160	0.567 ± 0.010
3.166	0.572 ± 0.010	3.172	0.575 ± 0.010	3.177	0.553 ± 0.010	3.183	0.543 ± 0.010
3.189	0.564 ± 0.010	3.195	0.542 ± 0.010	3.201	0.547 ± 0.009	3.207	0.552 ± 0.009

W (GeV)	$\frac{d\sigma}{d\Omega dE^i}$ [$\mu\text{b}/(\text{GeV-sr})$]						
3.213	0.541 ± 0.009	3.219	0.524 ± 0.009	3.226	0.545 ± 0.009	3.230	0.560 ± 0.009
3.236	0.539 ± 0.009	3.242	0.543 ± 0.009	3.248	0.543 ± 0.009	3.253	0.547 ± 0.009
3.250	0.552 ± 0.009	3.265	0.535 ± 0.009	3.271	0.509 ± 0.009	3.276	0.508 ± 0.009
3.282	0.524 ± 0.009	3.288	0.520 ± 0.009	3.293	0.514 ± 0.009	3.299	0.522 ± 0.009
3.305	0.513 ± 0.009	3.311	0.521 ± 0.009	3.316	0.513 ± 0.009	3.322	0.515 ± 0.009
3.327	0.503 ± 0.009	3.333	0.515 ± 0.009	3.339	0.512 ± 0.009	3.344	0.501 ± 0.009
3.350	0.521 ± 0.009	3.356	0.512 ± 0.009	3.361	0.505 ± 0.009	3.367	0.496 ± 0.009
3.372	0.505 ± 0.009	3.378	0.484 ± 0.009	3.383	0.494 ± 0.009	3.389	0.501 ± 0.009
3.394	0.505 ± 0.009	3.400	0.499 ± 0.009	3.406	0.479 ± 0.009	3.411	0.492 ± 0.009
3.417	0.485 ± 0.009	3.422	0.502 ± 0.009	3.428	0.488 ± 0.009	3.433	0.483 ± 0.009
3.430	0.483 ± 0.009	3.444	0.472 ± 0.009	3.449	0.486 ± 0.009	3.455	0.483 ± 0.009
3.460	0.488 ± 0.009	3.456	0.474 ± 0.008	3.471	0.486 ± 0.009	3.476	0.475 ± 0.008
3.492	0.464 ± 0.008	3.497	0.487 ± 0.009	3.493	0.481 ± 0.008	3.498	0.465 ± 0.008
3.750	0.417 ± 0.005	4.000	0.379 ± 0.004	4.250	0.330 ± 0.008	4.500	0.309 ± 0.007
4.750	0.287 ± 0.007	5.000	0.285 ± 0.008	5.250	0.270 ± 0.005	5.500	0.257 ± 0.008

 $E = 4.499 \text{ GeV Deuterium}$

1.080	24.063 ± 4.479	1.088	26.965 ± 3.553	1.096	37.034 ± 3.117	1.104	48.614 ± 2.850
1.111	60.368 ± 2.666	1.119	67.329 ± 2.497	1.126	78.468 ± 2.399	1.134	92.295 ± 2.321
1.141	104.059 ± 2.254	1.149	116.682 ± 2.211	1.156	130.916 ± 2.153	1.163	144.243 ± 2.118
1.170	159.323 ± 2.104	1.178	176.673 ± 2.097	1.185	191.233 ± 2.083	1.192	202.162 ± 2.091
1.199	207.431 ± 2.008	1.206	212.499 ± 2.099	1.213	216.365 ± 2.090	1.220	211.090 ± 2.035
1.227	206.769 ± 1.903	1.234	195.875 ± 1.929	1.240	184.882 ± 1.865	1.247	168.911 ± 1.787
1.254	150.637 ± 1.743	1.261	143.649 ± 1.693	1.267	137.462 ± 1.683	1.274	123.893 ± 1.644
1.281	117.219 ± 1.639	1.287	107.114 ± 1.625	1.294	99.819 ± 1.613	1.300	93.924 ± 1.625
1.307	84.352 ± 1.610	1.313	79.684 ± 1.654	1.320	76.150 ± 1.684	1.326	76.691 ± 1.758
1.332	70.452 ± 1.801	1.339	68.101 ± 1.902	1.345	65.012 ± 1.887	1.351	61.476 ± 1.833
1.357	61.933 ± 1.931	1.374	60.064 ± 1.810	1.370	57.950 ± 1.762	1.376	55.168 ± 1.727
1.392	56.444 ± 1.741	1.398	57.848 ± 1.753	1.394	57.692 ± 1.740	1.400	56.062 ± 1.718
1.426	58.558 ± 1.755	1.412	55.434 ± 1.709	1.418	57.906 ± 1.737	1.424	54.861 ± 1.699
1.430	54.546 ± 1.699	1.436	58.325 ± 1.739	1.442	58.229 ± 1.749	1.448	56.832 ± 1.747
1.454	57.014 ± 1.741	1.459	57.771 ± 1.760	1.465	56.081 ± 1.735	1.471	59.301 ± 1.774
1.477	57.457 ± 1.773	1.482	57.733 ± 1.766	1.488	59.079 ± 1.778	1.494	57.651 ± 1.778
1.499	63.428 ± 1.837	1.505	54.421 ± 1.753	1.511	59.491 ± 1.815	1.516	60.481 ± 1.802
1.522	52.216 ± 1.698	1.527	55.886 ± 1.730	1.533	53.574 ± 1.706	1.538	51.378 ± 1.661
1.544	52.493 ± 1.647	1.549	51.393 ± 1.645	1.555	47.763 ± 1.588	1.560	46.945 ± 1.582
1.565	45.319 ± 1.543	1.571	42.280 ± 1.500	1.576	42.484 ± 1.492	1.581	41.875 ± 1.488
1.587	42.187 ± 1.478	1.542	40.451 ± 1.456	1.597	39.842 ± 1.442	1.603	39.923 ± 1.447
1.608	39.915 ± 1.437	1.513	41.122 ± 1.453	1.619	37.160 ± 1.400	1.624	37.141 ± 1.407
1.629	37.188 ± 1.396	1.634	39.265 ± 1.424	1.639	36.479 ± 1.380	1.644	36.813 ± 1.392
1.640	37.718 ± 1.303	1.655	34.957 ± 1.356	1.660	34.211 ± 1.342	1.665	36.363 ± 1.378
1.670	34.566 ± 1.341	1.675	31.896 ± 1.299	1.680	32.449 ± 1.312	1.685	33.242 ± 1.314
1.690	34.021 ± 1.321	1.695	32.823 ± 1.307	1.700	31.417 ± 1.277	1.705	29.740 ± 1.251
1.710	29.588 ± 1.250	1.715	28.817 ± 1.226	1.720	28.789 ± 1.225	1.724	29.858 ± 1.232
1.729	27.424 ± 1.200	1.734	29.176 ± 1.218	1.739	28.025 ± 1.200	1.744	27.726 ± 1.185
1.749	26.249 ± 1.164	1.754	25.713 ± 1.154	1.758	22.277 ± 1.092	1.763	24.771 ± 1.128
1.768	23.826 ± 1.115	1.773	25.407 ± 1.133	1.778	24.535 ± 1.118	1.782	23.883 ± 1.111
1.787	23.460 ± 1.099	1.792	23.251 ± 1.099	1.796	20.425 ± 1.049	1.801	22.435 ± 1.076
1.806	24.597 ± 1.111	1.810	22.691 ± 1.076	1.815	21.098 ± 1.047	1.820	21.061 ± 1.050
1.824	22.355 ± 1.064	1.829	21.750 ± 1.055	1.834	22.697 ± 1.065	1.838	21.451 ± 1.051
1.843	19.750 ± 1.017	1.847	20.164 ± 1.023	1.852	20.088 ± 1.024	1.857	21.772 ± 1.049
1.861	21.647 ± 1.048	1.856	18.176 ± 0.988	1.870	20.835 ± 1.034	1.875	19.000 ± 0.999
1.879	20.094 ± 1.017	1.884	18.486 ± 0.995	1.888	18.093 ± 0.983	1.893	18.499 ± 0.993
1.897	20.057 ± 1.013	1.901	18.740 ± 0.994	1.906	19.577 ± 1.006	1.910	18.827 ± 0.996
1.915	17.158 ± 0.965	1.919	18.641 ± 0.990	1.923	18.952 ± 0.994	1.928	17.574 ± 0.970
1.932	17.634 ± 0.968	1.937	16.892 ± 0.956	1.941	17.378 ± 0.962	1.945	17.950 ± 0.972
1.950	18.195 ± 0.971	1.954	14.594 ± 0.910	1.958	17.128 ± 0.950	1.963	16.928 ± 0.951
1.967	14.413 ± 0.906	1.971	16.555 ± 0.940	1.975	17.014 ± 0.949	1.980	16.053 ± 0.931
1.984	15.191 ± 0.916	1.988	15.724 ± 0.922	1.992	16.110 ± 0.931	1.997	14.755 ± 0.907

 $E = 7.000 \text{ GeV Deuterium}$

1.078	11.664 ± 0.675	1.084	14.121 ± 0.670	1.090	17.078 ± 0.666	1.096	19.360 ± 0.664
1.102	22.954 ± 0.672	1.108	26.349 ± 0.681	1.114	27.681 ± 0.678	1.120	31.847 ± 0.696
1.126	35.122 ± 0.704	1.132	39.077 ± 0.718	1.138	43.101 ± 0.733	1.143	47.758 ± 0.753
1.149	52.087 ± 0.770	1.155	57.154 ± 0.793	1.160	61.688 ± 0.812	1.166	66.823 ± 0.835
1.172	71.375 ± 0.847	1.177	79.133 ± 0.877	1.183	83.705 ± 0.893	1.188	87.060 ± 0.902

W (GeV)	$\frac{d\sigma}{d\Omega dE}$ [$\mu b/(GeV \cdot sr)$]	W (GeV)	$\frac{d\sigma}{d\Omega dE}$ [$\mu b/(GeV \cdot sr)$]	W (GeV)	$\frac{d\sigma}{d\Omega dE}$ [$\mu b/(GeV \cdot sr)$]	W (GeV)	$\frac{d\sigma}{d\Omega dE}$ [$\mu b/(GeV \cdot sr)$]
1.194	91.863 ± 0.918	1.199	94.595 ± 0.924	1.205	98.207 ± 0.938	1.210	98.808 ± 0.930
1.216	99.132 ± 0.926	1.221	99.861 ± 0.920	1.226	97.467 ± 0.904	1.232	95.448 ± 0.892
1.237	94.115 ± 0.876	1.242	88.952 ± 0.847	1.248	84.686 ± 0.827	1.253	80.260 ± 0.797
1.258	78.423 ± 0.778	1.263	73.068 ± 0.749	1.269	70.368 ± 0.737	1.274	65.935 ± 0.715
1.279	63.758 ± 0.706	1.284	60.612 ± 0.694	1.289	56.870 ± 0.678	1.294	54.036 ± 0.667
1.299	51.944 ± 0.655	1.304	48.564 ± 0.639	1.309	47.350 ± 0.635	1.314	46.319 ± 0.632
1.319	44.153 ± 0.623	1.324	43.460 ± 0.622	1.329	41.459 ± 0.615	1.334	39.678 ± 0.610
1.339	39.620 ± 0.614	1.344	37.893 ± 0.608	1.349	36.488 ± 0.604	1.354	36.761 ± 0.610
1.359	35.058 ± 0.605	1.363	34.466 ± 0.606	1.368	34.116 ± 0.612	1.373	34.404 ± 0.620
1.378	33.725 ± 0.624	1.383	32.813 ± 0.625	1.387	34.945 ± 0.651	1.392	33.275 ± 0.651
1.397	32.398 ± 0.656	1.401	32.830 ± 0.664	1.406	32.054 ± 0.661	1.411	32.439 ± 0.667
1.415	33.945 ± 0.679	1.420	32.735 ± 0.668	1.425	33.060 ± 0.668	1.429	33.196 ± 0.674
1.434	33.246 ± 0.674	1.438	33.985 ± 0.682	1.443	33.566 ± 0.680	1.447	35.312 ± 0.696
1.452	34.299 ± 0.689	1.457	35.170 ± 0.694	1.461	34.404 ± 0.688	1.466	35.795 ± 0.698
1.470	37.219 ± 0.711	1.474	37.345 ± 0.712	1.479	37.202 ± 0.712	1.483	36.588 ± 0.707
1.488	37.129 ± 0.712	1.492	36.949 ± 0.711	1.497	38.787 ± 0.725	1.501	36.234 ± 0.707
1.505	37.511 ± 0.716	1.510	37.876 ± 0.718	1.514	38.137 ± 0.720	1.518	36.355 ± 0.702
1.523	35.736 ± 0.694	1.527	36.835 ± 0.701	1.531	36.341 ± 0.695	1.536	35.566 ± 0.686
1.540	34.144 ± 0.672	1.544	34.170 ± 0.667	1.548	33.061 ± 0.655	1.553	31.848 ± 0.643
1.557	31.795 ± 0.642	1.561	31.058 ± 0.634	1.565	30.184 ± 0.624	1.569	30.459 ± 0.628
1.574	30.737 ± 0.629	1.578	29.988 ± 0.621	1.582	28.487 ± 0.607	1.586	28.537 ± 0.607
1.590	28.059 ± 0.599	1.594	28.401 ± 0.604	1.598	27.306 ± 0.592	1.603	27.296 ± 0.592
1.607	27.049 ± 0.589	1.611	27.023 ± 0.588	1.615	27.242 ± 0.591	1.619	27.978 ± 0.598
1.623	26.483 ± 0.583	1.627	26.785 ± 0.586	1.631	26.157 ± 0.580	1.635	27.037 ± 0.588
1.639	27.002 ± 0.587	1.643	26.005 ± 0.578	1.647	25.444 ± 0.573	1.651	26.310 ± 0.579
1.655	25.867 ± 0.576	1.659	25.888 ± 0.574	1.663	25.306 ± 0.569	1.667	26.620 ± 0.581
1.671	25.727 ± 0.575	1.675	25.122 ± 0.568	1.679	24.590 ± 0.561	1.682	25.439 ± 0.569
1.686	25.426 ± 0.567	1.690	25.772 ± 0.570	1.694	24.714 ± 0.559	1.698	24.138 ± 0.551
1.702	23.855 ± 0.548	1.706	23.244 ± 0.540	1.710	23.883 ± 0.546	1.713	22.981 ± 0.536
1.717	22.207 ± 0.526	1.721	22.406 ± 0.528	1.725	21.424 ± 0.516	1.729	22.270 ± 0.524
1.732	22.374 ± 0.524	1.736	21.584 ± 0.514	1.740	22.361 ± 0.521	1.744	21.496 ± 0.511
1.748	20.887 ± 0.505	1.751	20.922 ± 0.504	1.755	20.247 ± 0.495	1.759	19.610 ± 0.487
1.763	18.621 ± 0.476	1.766	19.624 ± 0.486	1.770	19.429 ± 0.483	1.774	18.734 ± 0.474
1.777	18.697 ± 0.473	1.781	18.150 ± 0.466	1.785	17.902 ± 0.463	1.788	18.302 ± 0.466
1.792	17.727 ± 0.459	1.796	18.398 ± 0.466	1.799	17.038 ± 0.450	1.803	17.200 ± 0.452
1.807	17.800 ± 0.458	1.810	17.087 ± 0.449	1.814	17.367 ± 0.452	1.818	17.052 ± 0.448
1.821	16.473 ± 0.442	1.825	17.733 ± 0.456	1.828	16.380 ± 0.439	1.832	17.026 ± 0.447
1.836	16.849 ± 0.444	1.839	16.622 ± 0.444	1.843	16.337 ± 0.442	1.846	17.131 ± 0.449
1.850	15.985 ± 0.436	1.853	16.433 ± 0.441	1.857	16.132 ± 0.436	1.860	15.700 ± 0.434
1.864	15.851 ± 0.442	1.867	15.773 ± 0.450	1.871	15.645 ± 0.456	1.874	15.624 ± 0.464
1.878	15.868 ± 0.477	1.881	15.520 ± 0.483	1.885	15.255 ± 0.489	1.888	15.793 ± 0.507
1.892	14.640 ± 0.504	1.895	14.972 ± 0.525	1.899	15.367 ± 0.544	1.902	15.172 ± 0.554
1.906	14.159 ± 0.556	1.909	13.340 ± 0.561	1.913	14.285 ± 0.595	1.916	15.197 ± 0.634
1.920	15.550 ± 0.656	1.923	14.978 ± 0.658	1.926	14.590 ± 0.684	1.930	14.808 ± 0.726
1.933	16.256 ± 0.808	1.937	14.960 ± 0.828	1.940	14.170 ± 0.855	1.943	16.630 ± 0.896
1.947	15.116 ± 0.906	1.950	14.073 ± 0.873	1.953	15.515 ± 0.914	1.957	13.412 ± 0.859
1.960	15.674 ± 0.909	1.964	14.888 ± 0.895	1.967	12.028 ± 0.820	1.970	14.035 ± 0.866
1.974	13.574 ± 0.856	1.977	13.801 ± 0.858	1.980	14.020 ± 0.871	1.984	13.409 ± 0.852
1.987	14.188 ± 0.867	1.990	13.261 ± 0.850	1.993	12.744 ± 0.833	1.997	13.491 ± 0.826
2.000	12.948 ± 0.769	2.003	12.735 ± 0.763	2.007	11.961 ± 0.753	2.010	12.383 ± 0.781
2.013	12.533 ± 0.748	2.016	11.269 ± 0.688	2.020	12.236 ± 0.721	2.023	11.552 ± 0.719
2.026	12.209 ± 0.746	2.029	10.672 ± 0.656	2.032	11.762 ± 0.679	2.036	11.594 ± 0.681
2.039	11.967 ± 0.703	2.042	11.060 ± 0.658	2.045	11.821 ± 0.650	2.049	11.794 ± 0.658
2.052	12.237 ± 0.680	2.055	12.558 ± 0.696	2.058	11.045 ± 0.619	2.066	13.954 ± 0.314
2.079	11.097 ± 0.316	2.091	11.576 ± 0.322	2.104	11.037 ± 0.315	2.116	10.557 ± 0.308
2.129	10.425 ± 0.308	2.141	9.737 ± 0.299	2.153	10.364 ± 0.304	2.165	10.194 ± 0.303
2.178	9.728 ± 0.295	2.190	9.402 ± 0.291	2.202	9.394 ± 0.288	2.213	9.081 ± 0.284
2.221	8.538 ± 0.398	2.224	9.573 ± 0.357	2.227	9.376 ± 0.357	2.230	8.897 ± 0.345
2.233	8.954 ± 0.345	2.236	8.344 ± 0.335	2.239	8.565 ± 0.342	2.242	9.339 ± 0.352
2.244	8.801 ± 0.342	2.247	9.269 ± 0.349	2.250	8.714 ± 0.344	2.253	9.074 ± 0.350
2.256	8.554 ± 0.336	2.259	8.846 ± 0.340	2.262	8.682 ± 0.343	2.265	8.619 ± 0.342
2.268	8.480 ± 0.335	2.271	8.528 ± 0.336	2.274	8.772 ± 0.341	2.276	8.895 ± 0.359
2.284	8.615 ± 0.255	2.295	7.490 ± 0.260	2.306	8.501 ± 0.273	2.318	7.598 ± 0.260
2.329	7.968 ± 0.265	2.340	8.031 ± 0.266	2.352	7.733 ± 0.261	2.363	7.364 ± 0.255
2.374	7.320 ± 0.254	2.385	7.118 ± 0.254	2.396	7.505 ± 0.259	2.407	7.272 ± 0.255
2.418	6.853 ± 0.247	2.428	6.936 ± 0.249	2.439	7.013 ± 0.249	2.450	7.246 ± 0.253
2.461	6.648 ± 0.244	2.471	6.522 ± 0.241	2.478	7.350 ± 0.327	2.481	6.691 ± 0.272
2.483	6.685 ± 0.274	2.486	6.308 ± 0.269	2.489	6.269 ± 0.266	2.491	6.341 ± 0.265
2.494	7.058 ± 0.284	2.497	6.763 ± 0.275	2.499	6.577 ± 0.269	2.502	6.297 ± 0.268
2.504	7.014 ± 0.281	2.507	6.977 ± 0.276	2.510	6.517 ± 0.268	2.512	6.501 ± 0.274
2.515	6.822 ± 0.276	2.518	6.215 ± 0.263	2.520	6.726 ± 0.284	2.523	6.073 ± 0.351
2.529	6.446 ± 0.241	2.539	6.222 ± 0.236	2.550	5.857 ± 0.231	2.560	5.875 ± 0.232
2.570	5.792 ± 0.232	2.581	6.194 ± 0.238	2.591	5.603 ± 0.229	2.601	5.963 ± 0.233

W (GeV)	$\frac{d\sigma}{d\Omega dE}$ [$\mu b/(GeV \cdot sr)$]	W (GeV)	$\frac{d\sigma}{d\Omega dE}$ [$\mu b/(GeV \cdot sr)$]	W (GeV)	$\frac{d\sigma}{d\Omega dE}$ [$\mu b/(GeV \cdot sr)$]	W (GeV)	$\frac{d\sigma}{d\Omega dE}$ [$\mu b/(GeV \cdot sr)$]
2.611	5.362 ± 0.226	2.621	5.469 ± 0.229	2.631	5.730 ± 0.231	2.641	5.108 ± 0.219
2.651	5.195 ± 0.220	2.661	5.635 ± 0.230	2.671	5.351 ± 0.226	2.680	4.970 ± 0.218
2.690	5.043 ± 0.221	2.700	5.433 ± 0.229	2.710	4.977 ± 0.218	2.719	5.081 ± 0.220
2.720	4.893 ± 0.197	2.735	5.331 ± 0.239	2.737	5.101 ± 0.225	2.740	5.208 ± 0.231
2.742	5.256 ± 0.229	2.745	5.019 ± 0.223	2.747	5.466 ± 0.233	2.749	5.177 ± 0.226
2.752	4.929 ± 0.223	2.754	4.877 ± 0.226	2.757	5.053 ± 0.225	2.759	4.978 ± 0.225
2.761	5.024 ± 0.226	2.764	5.264 ± 0.230	2.765	5.354 ± 0.281	2.772	5.129 ± 0.224
2.781	4.946 ± 0.218	2.791	4.642 ± 0.216	2.800	4.506 ± 0.214	2.810	4.445 ± 0.212
2.819	4.771 ± 0.218	2.828	4.491 ± 0.213	2.837	5.022 ± 0.223	2.847	4.455 ± 0.211
2.856	4.583 ± 0.218	2.865	4.478 ± 0.213	2.874	4.796 ± 0.224	2.883	4.366 ± 0.213
2.892	4.340 ± 0.215	2.902	4.308 ± 0.215	2.911	4.056 ± 0.210	2.920	4.196 ± 0.212
2.920	4.146 ± 0.210	2.938	3.919 ± 0.212	2.946	4.172 ± 0.216	2.955	4.014 ± 0.211
2.964	4.159 ± 0.216	2.973	4.034 ± 0.218	2.982	3.925 ± 0.215	2.987	3.989 ± 0.454
2.990	4.339 ± 0.266	2.992	3.812 ± 0.242	2.994	3.973 ± 0.243	2.996	3.976 ± 0.242
2.992	4.089 ± 0.249	3.001	3.594 ± 0.242	3.003	4.091 ± 0.260	3.005	3.739 ± 0.255
3.007	4.026 ± 0.267	3.009	3.563 ± 0.275	3.012	4.038 ± 0.402		

 $E = 9.993 \text{ GeV Deuterium}$

1.092	5.993 ± 0.455	1.091	7.520 ± 0.454	1.099	9.159 ± 0.463	1.108	10.554 ± 0.464
1.116	11.774 ± 0.471	1.125	12.690 ± 0.471	1.133	15.087 ± 0.493	1.141	16.671 ± 0.502
1.149	18.995 ± 0.523	1.157	21.898 ± 0.544	1.165	23.189 ± 0.556	1.174	26.498 ± 0.580
1.181	27.239 ± 0.587	1.189	29.864 ± 0.603	1.197	32.828 ± 0.628	1.205	34.279 ± 0.631
1.213	34.473 ± 0.631	1.220	34.832 ± 0.628	1.229	34.761 ± 0.617	1.236	33.305 ± 0.603
1.243	32.243 ± 0.594	1.251	30.182 ± 0.564	1.258	28.474 ± 0.541	1.266	27.214 ± 0.528
1.273	26.319 ± 0.512	1.290	23.810 ± 0.489	1.288	23.655 ± 0.480	1.295	21.919 ± 0.464
1.302	20.353 ± 0.443	1.309	19.018 ± 0.431	1.317	17.927 ± 0.416	1.324	17.416 ± 0.411
1.331	16.092 ± 0.402	1.338	17.320 ± 0.406	1.345	16.469 ± 0.393	1.352	15.700 ± 0.387
1.350	16.323 ± 0.390	1.355	15.718 ± 0.386	1.372	15.764 ± 0.383	1.379	15.722 ± 0.384
1.386	15.299 ± 0.380	1.393	14.635 ± 0.369	1.399	15.414 ± 0.380	1.406	14.992 ± 0.372
1.413	14.895 ± 0.373	1.419	15.947 ± 0.382	1.426	15.429 ± 0.380	1.432	16.126 ± 0.384
1.439	16.142 ± 0.388	1.446	16.516 ± 0.389	1.452	17.510 ± 0.402	1.458	17.700 ± 0.409
1.465	16.893 ± 0.410	1.471	17.693 ± 0.418	1.478	17.981 ± 0.424	1.484	18.962 ± 0.435
1.490	18.437 ± 0.425	1.496	18.719 ± 0.431	1.503	19.181 ± 0.431	1.509	18.664 ± 0.428
1.515	19.016 ± 0.427	1.521	18.574 ± 0.424	1.527	18.551 ± 0.420	1.534	18.498 ± 0.421
1.549	18.361 ± 0.415	1.546	17.287 ± 0.405	1.552	17.371 ± 0.405	1.558	16.756 ± 0.393
1.564	14.926 ± 0.307	1.570	16.345 ± 0.396	1.576	15.640 ± 0.391	1.582	15.599 ± 0.376
1.588	15.213 ± 0.374	1.594	15.327 ± 0.372	1.599	14.815 ± 0.369	1.605	15.210 ± 0.370
1.611	15.695 ± 0.378	1.617	15.079 ± 0.369	1.623	15.480 ± 0.366	1.628	15.138 ± 0.358
1.634	15.690 ± 0.361	1.640	15.491 ± 0.361	1.646	15.183 ± 0.355	1.651	15.275 ± 0.359
1.657	15.632 ± 0.360	1.663	15.536 ± 0.361	1.668	15.678 ± 0.362	1.674	15.429 ± 0.357
1.670	15.540 ± 0.340	1.685	15.328 ± 0.355	1.691	14.295 ± 0.346	1.696	14.920 ± 0.349
1.702	14.623 ± 0.348	1.707	14.210 ± 0.340	1.713	14.084 ± 0.341	1.718	13.819 ± 0.337
1.724	13.364 ± 0.329	1.729	13.739 ± 0.334	1.734	13.512 ± 0.329	1.740	13.197 ± 0.327
1.745	12.944 ± 0.321	1.751	13.121 ± 0.325	1.756	12.459 ± 0.317	1.761	12.999 ± 0.320
1.767	12.543 ± 0.314	1.772	12.362 ± 0.311	1.777	12.352 ± 0.313	1.782	12.356 ± 0.310
1.784	11.773 ± 0.304	1.793	11.624 ± 0.301	1.799	11.582 ± 0.302	1.803	11.197 ± 0.296
1.804	11.747 ± 0.301	1.814	11.522 ± 0.300	1.819	11.722 ± 0.299	1.824	11.636 ± 0.300
1.829	11.151 ± 0.294	1.834	10.714 ± 0.287	1.839	11.205 ± 0.295	1.844	11.129 ± 0.291
1.840	11.447 ± 0.297	1.855	10.688 ± 0.285	1.860	11.115 ± 0.292	1.865	10.647 ± 0.287
1.870	10.983 ± 0.288	1.875	10.942 ± 0.289	1.880	10.741 ± 0.284	1.885	10.452 ± 0.283
1.890	10.572 ± 0.293	1.895	10.712 ± 0.287	1.899	9.822 ± 0.275	1.904	10.277 ± 0.279
1.909	10.560 ± 0.284	1.914	10.708 ± 0.283	1.919	10.145 ± 0.278	1.924	9.882 ± 0.275
1.920	10.098 ± 0.275	1.934	9.866 ± 0.274	1.939	9.808 ± 0.271	1.943	9.829 ± 0.273
1.948	10.214 ± 0.278	1.953	9.705 ± 0.269	1.958	9.878 ± 0.273	1.963	9.378 ± 0.264
1.967	9.432 ± 0.266	1.972	9.293 ± 0.265	1.977	9.213 ± 0.262	1.982	9.137 ± 0.262
1.986	9.434 ± 0.263	1.991	9.112 ± 0.261	1.996	9.684 ± 0.271	2.000	8.980 ± 0.266
2.250	6.688 ± 0.044	2.500	5.086 ± 0.050	2.750	3.952 ± 0.040	3.000	3.172 ± 0.035
3.250	2.625 ± 0.031	3.500	2.253 ± 0.029	3.750	2.007 ± 0.036		

 $E = 13.000 \text{ GeV Deuterium}$

1.089	2.200 ± 0.108	1.100	2.677 ± 0.107	1.111	3.149 ± 0.107	1.122	3.766 ± 0.108
1.133	4.393 ± 0.111	1.143	5.253 ± 0.115	1.154	6.050 ± 0.120	1.164	7.244 ± 0.127
1.175	8.131 ± 0.132	1.185	9.092 ± 0.137	1.195	9.968 ± 0.142	1.206	10.640 ± 0.144
1.216	10.908 ± 0.145	1.226	11.372 ± 0.145	1.235	11.138 ± 0.142	1.245	10.422 ± 0.136
1.255	10.488 ± 0.135	1.265	9.638 ± 0.128	1.274	9.420 ± 0.126	1.284	8.859 ± 0.121
1.293	8.530 ± 0.118	1.303	7.981 ± 0.114	1.312	7.664 ± 0.111	1.321	7.398 ± 0.109
1.331	7.019 ± 0.104	1.340	7.124 ± 0.106	1.349	6.784 ± 0.104	1.358	6.861 ± 0.104

W (GeV)	$\frac{d\sigma}{d\Omega dE^i}$ [$\mu b/(GeV \cdot sr)$]	W (GeV)	$\frac{d\sigma}{d\Omega dE^i}$ [$\mu b/(GeV \cdot sr)$]	W (GeV)	$\frac{d\sigma}{d\Omega dE^i}$ [$\mu b/(GeV \cdot sr)$]	W (GeV)	$\frac{d\sigma}{d\Omega dE^i}$ [$\mu b/(GeV \cdot sr)$]
1.367	6.640 ± 0.102	1.376	6.609 ± 0.102	1.384	6.514 ± 0.101	1.393	6.519 ± 0.101
1.402	6.397 ± 0.100	1.411	6.649 ± 0.102	1.419	6.660 ± 0.101	1.428	6.712 ± 0.102
1.436	6.950 ± 0.104	1.445	7.282 ± 0.106	1.453	7.288 ± 0.106	1.462	7.494 ± 0.108
1.470	7.800 ± 0.110	1.478	8.029 ± 0.111	1.486	8.114 ± 0.112	1.495	8.301 ± 0.113
1.503	8.426 ± 0.114	1.511	8.463 ± 0.114	1.519	8.165 ± 0.112	1.527	8.241 ± 0.112
1.535	8.207 ± 0.111	1.543	8.296 ± 0.111	1.551	8.085 ± 0.110	1.558	7.959 ± 0.108
1.566	7.874 ± 0.108	1.574	7.648 ± 0.107	1.582	7.729 ± 0.108	1.589	7.753 ± 0.108
1.597	7.409 ± 0.105	1.605	7.375 ± 0.105	1.612	7.489 ± 0.106	1.620	7.440 ± 0.105
1.627	7.567 ± 0.106	1.635	7.746 ± 0.107	1.642	7.672 ± 0.107	1.650	7.563 ± 0.106
1.657	7.789 ± 0.107	1.664	7.973 ± 0.109	1.672	7.896 ± 0.108	1.679	7.863 ± 0.108
1.686	7.991 ± 0.108	1.693	8.079 ± 0.109	1.701	7.906 ± 0.107	1.708	7.692 ± 0.106
1.715	7.534 ± 0.105	1.722	7.575 ± 0.104	1.729	7.448 ± 0.104	1.736	7.283 ± 0.102
1.743	7.272 ± 0.102	1.750	7.224 ± 0.101	1.757	7.174 ± 0.100	1.764	7.133 ± 0.099
1.771	7.127 ± 0.098	1.778	6.805 ± 0.096	1.784	7.033 ± 0.097	1.791	6.672 ± 0.095
1.798	6.761 ± 0.095	1.805	6.660 ± 0.095	1.812	6.636 ± 0.094	1.818	6.733 ± 0.095
1.825	6.589 ± 0.094	1.832	6.599 ± 0.094	1.838	6.557 ± 0.093	1.845	6.446 ± 0.093
1.852	6.489 ± 0.093	1.858	6.536 ± 0.093	1.865	6.695 ± 0.094	1.871	6.442 ± 0.092
1.878	6.243 ± 0.091	1.884	6.194 ± 0.090	1.891	6.393 ± 0.091	1.897	6.239 ± 0.090
1.904	6.368 ± 0.091	1.910	6.352 ± 0.091	1.916	6.257 ± 0.090	1.923	6.290 ± 0.090
1.929	6.157 ± 0.088	1.935	6.027 ± 0.086	1.942	6.003 ± 0.086	1.948	5.926 ± 0.086
1.954	6.049 ± 0.086	1.960	5.988 ± 0.085	1.967	6.039 ± 0.086	1.973	5.902 ± 0.085
1.979	5.758 ± 0.084	1.985	5.935 ± 0.085	1.991	5.771 ± 0.084	1.997	5.802 ± 0.085
2.003	5.635 ± 0.084	2.009	5.737 ± 0.086	2.016	5.605 ± 0.086	2.022	5.577 ± 0.086
2.028	5.574 ± 0.087	2.034	5.673 ± 0.088	2.040	5.514 ± 0.088	2.046	5.447 ± 0.088
2.052	5.335 ± 0.089	2.057	5.506 ± 0.091	2.063	5.376 ± 0.091	2.069	5.232 ± 0.092
2.075	5.230 ± 0.094	2.081	5.332 ± 0.098	2.087	5.352 ± 0.101	2.093	5.209 ± 0.102
2.099	5.273 ± 0.106	2.105	5.173 ± 0.108	2.110	5.056 ± 0.112	2.116	5.301 ± 0.118
2.122	5.063 ± 0.120	2.128	5.138 ± 0.127	2.133	5.007 ± 0.130	2.139	5.124 ± 0.136
2.145	4.904 ± 0.136	2.151	4.703 ± 0.137	2.156	4.738 ± 0.141	2.162	4.773 ± 0.145
2.168	4.830 ± 0.150	2.173	4.462 ± 0.150	2.179	4.638 ± 0.158	2.184	4.833 ± 0.150
2.190	4.877 ± 0.144	2.195	4.897 ± 0.139	2.201	4.814 ± 0.139	2.206	4.585 ± 0.141
2.212	4.385 ± 0.140	2.217	4.619 ± 0.146	2.223	4.707 ± 0.147	2.228	4.575 ± 0.146
2.234	4.625 ± 0.146	2.239	4.421 ± 0.143	2.244	4.522 ± 0.144	2.250	4.664 ± 0.146
2.255	4.500 ± 0.143	2.261	4.285 ± 0.140	2.266	4.528 ± 0.144	2.271	4.692 ± 0.146
2.277	4.582 ± 0.144	2.282	4.430 ± 0.142	2.287	4.351 ± 0.140	2.293	4.346 ± 0.139
2.298	4.216 ± 0.138	2.303	4.221 ± 0.139	2.309	4.083 ± 0.147	2.314	4.192 ± 0.164
2.320	4.066 ± 0.192	2.325	3.838 ± 0.187	2.330	3.758 ± 0.186	2.335	4.505 ± 0.201
2.341	4.241 ± 0.195	2.346	4.067 ± 0.191	2.351	4.259 ± 0.197	2.356	4.039 ± 0.190
2.361	4.106 ± 0.192	2.367	4.267 ± 0.196	2.372	4.184 ± 0.193	2.377	4.279 ± 0.195
2.382	4.086 ± 0.191	2.387	4.074 ± 0.189	2.392	3.954 ± 0.186	2.397	3.995 ± 0.187
2.402	3.996 ± 0.186	2.407	3.883 ± 0.184	2.413	3.877 ± 0.184	2.418	4.319 ± 0.195
2.423	3.659 ± 0.179	2.428	3.873 ± 0.184	2.433	3.939 ± 0.186	2.438	3.519 ± 0.176
2.442	3.224 ± 0.153	2.447	4.040 ± 0.148	2.452	3.976 ± 0.132	2.457	3.557 ± 0.118
2.462	3.843 ± 0.122	2.467	3.652 ± 0.119	2.472	3.691 ± 0.120	2.477	3.657 ± 0.119
2.482	3.602 ± 0.118	2.487	3.659 ± 0.119	2.492	3.566 ± 0.118	2.496	3.578 ± 0.118
2.501	3.548 ± 0.118	2.506	3.583 ± 0.119	2.511	3.740 ± 0.121	2.516	3.493 ± 0.117
2.521	3.455 ± 0.116	2.526	3.433 ± 0.117	2.530	3.528 ± 0.117	2.535	3.569 ± 0.118
2.540	3.609 ± 0.119	2.545	3.430 ± 0.117	2.550	3.578 ± 0.130	2.555	3.326 ± 0.141
2.560	3.460 ± 0.174	2.564	3.173 ± 0.167	2.569	3.431 ± 0.174	2.574	3.208 ± 0.168
2.579	3.391 ± 0.172	2.583	3.342 ± 0.172	2.589	3.554 ± 0.176	2.593	3.391 ± 0.171
2.598	3.278 ± 0.170	2.602	3.452 ± 0.173	2.607	2.884 ± 0.159	2.612	3.267 ± 0.170
2.616	3.278 ± 0.169	2.621	3.277 ± 0.169	2.626	3.249 ± 0.169	2.630	3.149 ± 0.166
2.635	3.081 ± 0.163	2.639	3.040 ± 0.163	2.644	3.113 ± 0.165	2.649	3.308 ± 0.169
2.653	3.398 ± 0.173	2.658	3.285 ± 0.169	2.662	3.106 ± 0.165	2.667	3.251 ± 0.170
2.672	2.873 ± 0.159	2.676	3.236 ± 0.168	2.681	2.866 ± 0.160	2.685	2.904 ± 0.159
2.690	3.062 ± 0.163	2.694	3.155 ± 0.167	2.699	2.836 ± 0.158	2.703	3.188 ± 0.166
2.708	3.150 ± 0.167	2.712	2.941 ± 0.160	2.717	2.721 ± 0.154	2.721	3.186 ± 0.167
2.726	3.079 ± 0.163	2.730	2.832 ± 0.157	2.735	2.858 ± 0.159	2.739	2.949 ± 0.160
2.744	2.949 ± 0.160	2.750	2.903 ± 0.019	2.757	2.781 ± 0.156	2.761	2.804 ± 0.155
2.766	2.922 ± 0.158	2.770	2.760 ± 0.155	2.775	2.722 ± 0.153	2.779	2.887 ± 0.157
2.783	3.050 ± 0.162	2.788	2.640 ± 0.150	2.792	2.616 ± 0.149	2.797	2.745 ± 0.154
2.801	2.747 ± 0.153	2.805	2.737 ± 0.152	2.810	2.686 ± 0.153	2.814	2.656 ± 0.150
2.818	2.573 ± 0.148	2.823	2.761 ± 0.154	2.827	2.873 ± 0.156	2.831	2.776 ± 0.153
2.836	2.481 ± 0.147	2.840	2.787 ± 0.153	2.844	2.725 ± 0.154	2.848	2.718 ± 0.152
2.853	2.598 ± 0.149	2.857	2.386 ± 0.145	2.861	2.790 ± 0.154	2.865	2.745 ± 0.152
2.870	2.711 ± 0.153	2.874	2.743 ± 0.152	2.878	2.458 ± 0.145	2.882	2.434 ± 0.145
2.887	2.579 ± 0.148	2.891	2.637 ± 0.149	2.895	2.760 ± 0.154	2.899	2.627 ± 0.149
2.904	2.424 ± 0.145	2.908	2.575 ± 0.148	2.912	2.204 ± 0.138	2.916	2.570 ± 0.149
2.920	2.798 ± 0.153	2.924	2.320 ± 0.140	2.929	2.543 ± 0.148	2.933	2.593 ± 0.148
2.937	2.531 ± 0.146	2.941	2.468 ± 0.146	2.945	2.547 ± 0.147	2.949	2.395 ± 0.144
2.954	2.350 ± 0.141	2.958	2.330 ± 0.141	2.962	2.362 ± 0.143	2.966	2.509 ± 0.145
2.970	2.732 ± 0.151	2.974	2.298 ± 0.141	2.978	2.534 ± 0.146	2.982	2.446 ± 0.145
2.986	2.544 ± 0.146	2.990	2.616 ± 0.148	2.995	2.651 ± 0.151	3.000	2.393 ± 0.016

W (GeV)	$\frac{d\sigma}{d\Omega dE^T}$ [$\mu b/(GeV \cdot sr)$]	W (GeV)	$\frac{d\sigma}{d\Omega dE^T}$ [$\mu b/(GeV \cdot sr)$]	W (GeV)	$\frac{d\sigma}{d\Omega dE^T}$ [$\mu b/(GeV \cdot sr)$]	W (GeV)	$\frac{d\sigma}{d\Omega dE^T}$ [$\mu b/(GeV \cdot sr)$]
3.250	2.015 ± 0.014	3.500	1.700 ± 0.027	3.750	1.506 ± 0.014	4.000	1.338 ± 0.015
4.250	1.236 ± 0.021	4.500	1.173 ± 0.024				

E = 16.000 GeV Deuterium

1.080	0.771 ± 0.043	1.093	0.855 ± 0.041	1.107	1.052 ± 0.040	1.121	1.334 ± 0.041
1.134	1.573 ± 0.042	1.147	1.823 ± 0.043	1.160	2.277 ± 0.045	1.173	2.586 ± 0.047
1.186	2.871 ± 0.048	1.198	3.304 ± 0.051	1.211	3.426 ± 0.051	1.223	3.493 ± 0.051
1.235	3.557 ± 0.050	1.247	3.522 ± 0.049	1.259	3.403 ± 0.048	1.271	3.340 ± 0.047
1.283	3.251 ± 0.046	1.295	3.142 ± 0.045	1.306	2.926 ± 0.043	1.318	2.879 ± 0.043
1.329	2.864 ± 0.042	1.340	2.774 ± 0.042	1.351	2.801 ± 0.042	1.362	2.775 ± 0.041
1.373	2.732 ± 0.041	1.384	2.813 ± 0.042	1.395	2.641 ± 0.040	1.406	2.809 ± 0.042
1.416	2.811 ± 0.042	1.427	2.896 ± 0.042	1.437	2.957 ± 0.043	1.448	3.187 ± 0.044
1.458	3.226 ± 0.044	1.468	3.345 ± 0.045	1.479	3.482 ± 0.046	1.489	3.564 ± 0.047
1.490	3.704 ± 0.048	1.509	3.571 ± 0.047	1.519	3.630 ± 0.047	1.529	3.521 ± 0.047
1.538	3.757 ± 0.047	1.548	3.610 ± 0.046	1.558	3.613 ± 0.046	1.567	3.618 ± 0.046
1.577	3.557 ± 0.045	1.586	3.510 ± 0.045	1.596	3.547 ± 0.045	1.605	3.560 ± 0.045
1.615	3.538 ± 0.045	1.624	3.690 ± 0.046	1.633	3.656 ± 0.046	1.642	3.715 ± 0.046
1.651	3.646 ± 0.045	1.660	3.869 ± 0.047	1.669	3.757 ± 0.046	1.678	3.770 ± 0.046
1.687	3.849 ± 0.047	1.596	3.930 ± 0.047	1.705	3.900 ± 0.047	1.714	3.833 ± 0.046
1.723	3.804 ± 0.046	1.731	3.793 ± 0.046	1.740	3.793 ± 0.046	1.748	3.753 ± 0.045
1.757	3.715 ± 0.045	1.766	3.681 ± 0.045	1.774	3.702 ± 0.045	1.782	3.629 ± 0.044
1.791	3.629 ± 0.044	1.799	3.577 ± 0.044	1.808	3.569 ± 0.044	1.816	3.578 ± 0.044
1.824	3.554 ± 0.043	1.832	3.532 ± 0.043	1.840	3.517 ± 0.043	1.849	3.473 ± 0.043
1.857	3.501 ± 0.043	1.865	3.542 ± 0.043	1.873	3.577 ± 0.043	1.881	3.552 ± 0.043
1.889	3.476 ± 0.043	1.897	3.486 ± 0.043	1.905	3.512 ± 0.043	1.912	3.467 ± 0.043
1.920	3.493 ± 0.043	1.928	3.533 ± 0.043	1.936	3.508 ± 0.043	1.944	3.480 ± 0.042
1.951	3.364 ± 0.042	1.959	3.439 ± 0.042	1.967	3.432 ± 0.042	1.974	3.390 ± 0.042
1.982	3.333 ± 0.041	1.989	3.400 ± 0.042	1.997	3.293 ± 0.041	2.004	3.209 ± 0.040
2.012	3.265 ± 0.041	2.019	3.195 ± 0.040	2.027	3.221 ± 0.040	2.034	3.179 ± 0.040
2.042	3.250 ± 0.041	2.049	3.218 ± 0.041	2.056	3.219 ± 0.041	2.064	3.264 ± 0.041
2.071	3.203 ± 0.041	2.078	3.181 ± 0.041	2.085	3.124 ± 0.041	2.092	3.096 ± 0.041
2.100	3.148 ± 0.042	2.107	3.062 ± 0.042	2.114	3.056 ± 0.042	2.121	3.086 ± 0.043
2.128	3.194 ± 0.043	2.135	2.990 ± 0.042	2.142	3.047 ± 0.043	2.149	2.981 ± 0.043
2.156	2.977 ± 0.043	2.163	2.935 ± 0.043	2.170	3.033 ± 0.044	2.177	3.030 ± 0.045
2.184	2.934 ± 0.044	2.191	2.986 ± 0.045	2.197	2.933 ± 0.045	2.204	2.869 ± 0.045
2.211	2.852 ± 0.045	2.218	2.921 ± 0.045	2.225	2.927 ± 0.046	2.231	2.880 ± 0.045
2.239	2.852 ± 0.045	2.245	2.876 ± 0.045	2.251	2.885 ± 0.045	2.258	2.839 ± 0.045
2.265	2.778 ± 0.044	2.271	2.800 ± 0.045	2.278	2.750 ± 0.044	2.285	2.773 ± 0.044
2.291	2.722 ± 0.044	2.298	2.800 ± 0.044	2.304	2.769 ± 0.044	2.311	2.766 ± 0.044
2.317	2.829 ± 0.045	2.324	2.765 ± 0.044	2.330	2.748 ± 0.044	2.336	2.663 ± 0.043
2.343	2.672 ± 0.043	2.349	2.697 ± 0.043	2.356	2.720 ± 0.043	2.362	2.735 ± 0.043
2.368	2.624 ± 0.043	2.375	2.597 ± 0.042	2.381	2.588 ± 0.042	2.387	2.630 ± 0.042
2.394	2.662 ± 0.043	2.400	2.555 ± 0.042	2.405	2.505 ± 0.041	2.412	2.574 ± 0.042
2.419	2.558 ± 0.042	2.425	2.571 ± 0.041	2.431	2.500 ± 0.040	2.437	2.540 ± 0.039
2.443	2.462 ± 0.038	2.449	2.466 ± 0.037	2.456	2.485 ± 0.038	2.462	2.484 ± 0.038
2.468	2.450 ± 0.037	2.474	2.498 ± 0.038	2.480	2.441 ± 0.037	2.486	2.400 ± 0.037
2.492	2.410 ± 0.037	2.498	2.388 ± 0.037	2.750	2.077 ± 0.012	3.000	1.708 ± 0.016
3.250	1.505 ± 0.014	3.500	1.264 ± 0.012	3.750	1.151 ± 0.011	4.000	1.007 ± 0.022
4.250	0.921 ± 0.021	4.500	0.857 ± 0.011	4.750	0.815 ± 0.014	5.000	0.824 ± 0.022

E = 18.010 GeV Deuterium

1.080	0.348 ± 0.020	1.096	0.441 ± 0.021	1.111	0.559 ± 0.023	1.126	0.671 ± 0.025
1.141	0.807 ± 0.025	1.156	0.950 ± 0.026	1.171	1.175 ± 0.028	1.185	1.285 ± 0.029
1.190	1.483 ± 0.031	1.213	1.644 ± 0.031	1.227	1.630 ± 0.030	1.241	1.688 ± 0.030
1.254	1.755 ± 0.030	1.268	1.686 ± 0.030	1.281	1.697 ± 0.030	1.294	1.650 ± 0.030
1.307	1.611 ± 0.029	1.320	1.596 ± 0.029	1.333	1.557 ± 0.028	1.345	1.524 ± 0.028
1.358	1.565 ± 0.029	1.370	1.524 ± 0.029	1.382	1.630 ± 0.030	1.395	1.561 ± 0.030
1.407	1.626 ± 0.030	1.419	1.639 ± 0.030	1.430	1.734 ± 0.030	1.442	1.776 ± 0.031
1.454	1.841 ± 0.031	1.465	1.923 ± 0.032	1.477	2.033 ± 0.033	1.488	2.050 ± 0.034
1.500	2.125 ± 0.034	1.511	2.135 ± 0.033	1.522	2.215 ± 0.034	1.533	2.180 ± 0.034
1.544	2.170 ± 0.034	1.555	2.203 ± 0.034	1.566	2.153 ± 0.034	1.577	2.150 ± 0.035
1.587	2.137 ± 0.034	1.598	2.136 ± 0.034	1.608	2.169 ± 0.033	1.619	2.219 ± 0.033
1.629	2.305 ± 0.034	1.640	2.264 ± 0.034	1.650	2.249 ± 0.034	1.660	2.335 ± 0.035
1.670	2.378 ± 0.035	1.680	2.401 ± 0.035	1.690	2.410 ± 0.035	1.700	2.390 ± 0.035
1.710	2.422 ± 0.036	1.720	2.349 ± 0.036	1.730	2.441 ± 0.037	1.740	2.387 ± 0.036
1.749	2.378 ± 0.036	1.759	2.410 ± 0.036	1.768	2.371 ± 0.036	1.778	2.369 ± 0.036
1.787	2.342 ± 0.036	1.797	2.274 ± 0.035	1.806	2.338 ± 0.036	1.816	2.335 ± 0.036

W (GeV)	$\frac{d\sigma}{d\Omega dE^i}$ [$\mu b/(GeV \cdot sr)$]	W (GeV)	$\frac{d\sigma}{d\Omega dE^i}$ [$\mu b/(GeV \cdot sr)$]	W (GeV)	$\frac{d\sigma}{d\Omega dE^i}$ [$\mu b/(GeV \cdot sr)$]	W (GeV)	$\frac{d\sigma}{d\Omega dE^i}$ [$\mu b/(GeV \cdot sr)$]
1.825	2.332 ± 0.036	1.834	2.383 ± 0.036	1.843	2.357 ± 0.037	1.852	2.302 ± 0.037
1.862	2.273 ± 0.037	1.871	2.337 ± 0.038	1.880	2.385 ± 0.039	1.889	2.353 ± 0.037
1.898	2.335 ± 0.036	1.906	2.349 ± 0.035	1.915	2.363 ± 0.034	1.924	2.315 ± 0.033
1.933	2.313 ± 0.033	1.941	2.247 ± 0.033	1.950	2.330 ± 0.033	1.959	2.319 ± 0.033
1.967	2.326 ± 0.034	1.976	2.309 ± 0.034	1.985	2.286 ± 0.034	1.993	2.242 ± 0.034
2.001	2.328 ± 0.035	2.010	2.253 ± 0.034	2.018	2.262 ± 0.033	2.027	2.320 ± 0.033
2.035	2.244 ± 0.031	2.063	2.198 ± 0.030	2.051	2.245 ± 0.031	2.060	2.187 ± 0.030
2.069	2.292 ± 0.030	2.076	2.209 ± 0.030	2.084	2.232 ± 0.031	2.092	2.172 ± 0.031
2.100	2.202 ± 0.032	2.108	2.178 ± 0.033	2.116	2.197 ± 0.034	2.124	2.199 ± 0.035
2.132	2.214 ± 0.035	2.140	2.192 ± 0.034	2.148	2.123 ± 0.033	2.156	2.144 ± 0.032
2.164	2.153 ± 0.032	2.171	2.131 ± 0.032	2.179	2.208 ± 0.033	2.187	2.119 ± 0.032
2.195	2.146 ± 0.033	2.202	2.028 ± 0.032	2.210	2.135 ± 0.034	2.218	2.080 ± 0.035
2.225	2.111 ± 0.037	2.233	2.098 ± 0.039	2.240	2.065 ± 0.039	2.248	2.056 ± 0.037
2.255	2.040 ± 0.036	2.253	2.096 ± 0.035	2.270	2.000 ± 0.033	2.278	2.018 ± 0.033
2.285	2.055 ± 0.033	2.292	2.028 ± 0.033	2.300	2.048 ± 0.033	2.307	2.036 ± 0.033
2.314	1.926 ± 0.033	2.322	1.936 ± 0.034	2.329	2.022 ± 0.036	2.336	2.012 ± 0.038
2.344	2.015 ± 0.038	2.351	1.903 ± 0.036	2.358	1.957 ± 0.035	2.365	1.982 ± 0.034
2.372	1.937 ± 0.032	2.379	1.951 ± 0.032	2.386	1.941 ± 0.031	2.393	1.932 ± 0.031
2.400	1.856 ± 0.031	2.407	1.939 ± 0.032	2.415	1.867 ± 0.032	2.422	1.836 ± 0.033
2.429	1.819 ± 0.034	2.435	1.944 ± 0.037	2.442	1.898 ± 0.037	2.449	1.868 ± 0.036
2.456	1.831 ± 0.036	2.463	1.859 ± 0.036	2.470	1.926 ± 0.037	2.477	1.891 ± 0.036
2.484	1.850 ± 0.036	2.490	1.853 ± 0.036	2.497	1.804 ± 0.036	2.750	1.590 ± 0.010
3.000	1.371 ± 0.009	3.250	1.188 ± 0.008	3.500	1.043 ± 0.007	3.750	0.931 ± 0.007
4.000	0.806 ± 0.006	4.250	0.751 ± 0.016	4.500	0.703 ± 0.016	4.750	0.662 ± 0.017
5.000	0.634 ± 0.008	5.250	0.641 ± 0.013				

 $E = 20.005 \text{ GeV Deuterium}$

1.078	0.188 ± 0.011	1.095	0.248 ± 0.011	1.112	0.289 ± 0.010	1.129	0.371 ± 0.011
1.145	0.472 ± 0.011	1.162	0.540 ± 0.011	1.178	0.616 ± 0.012	1.194	0.708 ± 0.012
1.209	0.760 ± 0.012	1.225	0.836 ± 0.012	1.240	0.843 ± 0.012	1.255	0.879 ± 0.012
1.270	0.868 ± 0.012	1.284	0.889 ± 0.012	1.299	0.879 ± 0.012	1.313	0.888 ± 0.012
1.328	0.843 ± 0.012	1.342	0.854 ± 0.012	1.355	0.875 ± 0.012	1.369	0.860 ± 0.012
1.383	0.884 ± 0.012	1.396	0.892 ± 0.012	1.410	0.931 ± 0.012	1.423	0.964 ± 0.013
1.436	1.023 ± 0.013	1.449	1.060 ± 0.013	1.462	1.081 ± 0.014	1.475	1.109 ± 0.014
1.487	1.192 ± 0.015	1.500	1.235 ± 0.015	1.512	1.265 ± 0.016	1.525	1.247 ± 0.016
1.537	1.299 ± 0.016	1.549	1.286 ± 0.016	1.561	1.289 ± 0.016	1.573	1.285 ± 0.016
1.585	1.288 ± 0.016	1.597	1.266 ± 0.016	1.609	1.288 ± 0.016	1.620	1.346 ± 0.017
1.632	1.330 ± 0.016	1.643	1.364 ± 0.017	1.655	1.382 ± 0.017	1.666	1.401 ± 0.017
1.677	1.469 ± 0.017	1.698	1.482 ± 0.017	1.699	1.492 ± 0.017	1.710	1.499 ± 0.017
1.721	1.514 ± 0.016	1.732	1.507 ± 0.016	1.743	1.497 ± 0.016	1.754	1.491 ± 0.015
1.764	1.510 ± 0.015	1.775	1.492 ± 0.015	1.786	1.502 ± 0.015	1.796	1.501 ± 0.015
1.806	1.491 ± 0.014	1.817	1.480 ± 0.014	1.827	1.484 ± 0.014	1.837	1.499 ± 0.014
1.848	1.536 ± 0.014	1.858	1.505 ± 0.013	1.868	1.505 ± 0.013	1.878	1.509 ± 0.013
1.888	1.524 ± 0.013	1.898	1.521 ± 0.013	1.907	1.547 ± 0.013	1.917	1.543 ± 0.013
1.927	1.532 ± 0.013	1.937	1.518 ± 0.013	1.946	1.541 ± 0.013	1.956	1.551 ± 0.013
1.966	1.539 ± 0.013	1.975	1.549 ± 0.013	1.985	1.533 ± 0.012	1.994	1.552 ± 0.013
2.003	1.543 ± 0.012	2.013	1.540 ± 0.012	2.022	1.554 ± 0.013	2.031	1.537 ± 0.012
2.041	1.532 ± 0.012	2.050	1.518 ± 0.012	2.059	1.529 ± 0.013	2.068	1.534 ± 0.013
2.077	1.530 ± 0.013	2.086	1.501 ± 0.013	2.095	1.534 ± 0.013	2.104	1.515 ± 0.013
2.113	1.508 ± 0.013	2.122	1.535 ± 0.013	2.131	1.511 ± 0.014	2.139	1.501 ± 0.014
2.148	1.497 ± 0.014	2.157	1.493 ± 0.014	2.166	1.512 ± 0.015	2.174	1.514 ± 0.015
2.183	1.504 ± 0.016	2.191	1.517 ± 0.016	2.200	1.491 ± 0.016	2.208	1.454 ± 0.017
2.217	1.493 ± 0.017	2.225	1.465 ± 0.017	2.234	1.460 ± 0.017	2.242	1.498 ± 0.018
2.250	1.457 ± 0.018	2.259	1.475 ± 0.018	2.267	1.475 ± 0.018	2.275	1.455 ± 0.019
2.283	1.455 ± 0.019	2.292	1.467 ± 0.020	2.300	1.435 ± 0.020	2.308	1.440 ± 0.020
2.316	1.470 ± 0.021	2.324	1.403 ± 0.020	2.332	1.410 ± 0.020	2.340	1.454 ± 0.021
2.348	1.445 ± 0.021	2.356	1.411 ± 0.020	2.364	1.436 ± 0.021	2.372	1.428 ± 0.021
2.380	1.417 ± 0.020	2.388	1.435 ± 0.021	2.396	1.457 ± 0.021	2.403	1.408 ± 0.021
2.411	1.407 ± 0.022	2.419	1.388 ± 0.022	2.427	1.439 ± 0.024	2.434	1.448 ± 0.025
2.442	1.394 ± 0.027	2.450	1.398 ± 0.028	2.457	1.361 ± 0.028	2.465	1.377 ± 0.029
2.473	1.369 ± 0.031	2.480	1.379 ± 0.032	2.488	1.360 ± 0.033	2.500	1.371 ± 0.008
2.749	1.228 ± 0.006	2.999	1.095 ± 0.007	3.249	0.968 ± 0.007	3.499	0.855 ± 0.006
3.749	0.771 ± 0.006	3.999	0.690 ± 0.005	4.249	0.615 ± 0.010	4.499	0.580 ± 0.009
4.749	0.537 ± 0.009	4.999	0.519 ± 0.010	5.249	0.530 ± 0.007	5.500	0.492 ± 0.010